THE UNIVERSITY OF NEW SOUTH WALES

An Investigation of Flowability and Compaction of Iron Ore Fines

A Thesis

by

Zi Wang

March 2015

Submitted in Partial Fulfillment of the

Requirements for the Degree

of

Master of Engineering

in

Materials Science and Engineering

ORIGINALITY STATEMENT

‘I hereby declare that this submission is my own work and to the best of my knowledge it contains no materials previously published or written by another person, or substantial proportions of material which have been accepted for the award of any other degree or diploma at UNSW or any other educational institution, except where due acknowledgement is made in the thesis. Any contribution made to the research by others, with whom I have worked at UNSW or elsewhere, is explicitly acknowledged in the thesis. I also declare that the intellectual content of this thesis is the product of my own work, except to the extent that assistance from others in the project's design and conception or in style, presentation and linguistic expression is acknowledged.’

PLEASE TYPE

THE UNIVERSITY OF NEW SOUTH WALES
Thesis/Dissertation Sheet

Surname or Family name: Wang

First name: Zi Other name/s:

Abbreviation for degree as given in the University calendar: ME

School: School of Materials Science and Engineering Faculty: Faculty of Science

Title: An investigation of Flowability and Compaction of Iron Ore Fines

Abstract 350 words maximum: (PLEASE TYPE)

Iron ore is an important material for iron and steel making. About half of mined iron ores are fines which can cause many problems in handling and processing of iron ore. It is therefore important to understand the flow properties of iron ore fines and to increase their sizes.

The flowability of iron ore fines is measured by the shear testing method. The yield locus line is drawn based on the measured shear stress and compression stress. The unconfined yield stress, cohesion and flow function are then obtained from the yield locus line using the Mohr circle method. Different types of iron ore fines are tested in the experiments. Compared with the goethite fines, the magnetite fines have higher cohesion, larger unconfined yield stress and flow function.

The compaction behaviour of different types of iron ore fines is conducted using a Universal Testing Machine, focusing on the effects of load pressure, particle size, particle mixture and moisture contents. It is found that larger loads and particle size increase the compact density. Also particles mixtures with different size ranges leads to higher relative density. The unconfined compression is used to measure the compressive or crushing strengths of compacts. It is observed that crushing strength of magnetite and goethite powders reach the highest strength with 5% moisture content and with 2.5% moisture content for hematite. Moreover, particle mixtures for magnetite and goethite powder also result in higher crushing strength. The diametrical compaction is used to measure the tensile strengths of compacts. Under the same experiment condition, a compact has much lower tensile strength than compressive strength. The consolidation pressure and particle size have similar effects on the tensile strength to those observed for the compressive strength.

The findings from the work will help us develop better understanding of the powders and lead to better design and control of the handling of iron ore fines.

FOR OFFICE USE ONLY Date of completion of requirements for Award:

THIS SHEET IS TO BE GLUED TO THE INSIDE FRONT COVER OF THE THESIS

Table of Content

Abstract

Iron ore is an important material for iron and steel making. Australia is one of the world's major iron ore producers and the largest iron ore exporter. But more than half of mined iron ores are fines, causing a number of problems such as inconvenience of transportation and negative health impact. It is therefore important to understand the flow properties of iron ore fine and to increase its size by compaction. This work studies the flowability of iron ore fines and investigates its compaction behaviour.

The flowability of iron ore fines was measured by the shear testing method using an FT4 rheometer. In the experiments, the maximum shear stress of the tested particles was measured by the point of incipient failure or the yield point which is the highest value of shear stress calculated from the measured torque of shear cells in each testing. The yield locus line was drawn based on the measured shear stress and compression stress. Other results, such as unconfined yield stress, cohesion and flow function, were also obtained from the yield locus line using the Mohr circle method. Magnetite and goethite particles were tested. Compared with the goethite fines, the magnetite fines had higher cohesion, larger unconfined yield stress and flow function. Larger particles had lower flow function than smaller particles. Increasing moisture content reduced the flowability of both magnetite and goethite particles but the flowability of magnetite particles was less affected by moisture content.

The compactions of iron ore fines including die compaction, unconfined compression and diametrical compression were conducted using a Universal Testing Machine (Instron 5566). The magnetite, goethite and hematite powders were tested in the experiments. In the die compaction, the effects of load pressure, particle size, particle mixture and moisture contents on the relative density of the compacts were investigated. It was observed that larger loads and particle size resulted in higher compact density. Also particles mixtures of different sizes led to higher relative density.

The compressive or crushing strengths of the compacts were tested using the unconfined compression. In the experiments, the compacted sample was crushed by upper pattern of the machine and the maximum load was recorded. It was observed that crushing strength of magnetite and goethite powders reached the highest strength with 5% moisture content and with 2.5% moisture content for hematite. Moreover, particle mixtures for magnetite

and goethite powder also resulted in higher crushing strength. The mixture of particles of different sizes had no visible effect on the compacts of goethite particles.

The tensile strengths of the compacts were tested using the diametrical compaction. The procedure of the diametrical compaction of magnetite powders was similar to those of die compaction and unconfined compression, and tensile strength was determined from the stress-strain curve. It was observed that the shapes of stress-strain curves in the diametrical compression were different from those in the uniaxial unconfined compression. In general, under the same experiment condition, a compact has much lower tensile strength than compressive strength. The consolidation pressure and particle size had similar effects on the tensile strength to those observed for the compressive strength. However, the tensile strengths of the compacts were not particularly influenced by moisture content.

In summary, this work has characterised the flow and compaction behaviour of different types of iron ore fines under various conditions. The findings will help develop better understanding of the powders and lead to better design and control of the handling of iron ore fines.

Chapter 1 Introduction

Iron ore is an important material for iron and steel production. Metallic iron can be produced from nature iron ore through the processes of crushing, grinding, magnetic separation, and gas and water purification. Iron ores are rich in iron oxides, and usually in form of magnetite (Fe_3O_4), hematite (Fe_2O_3), goethite (FeO(OH)), limonite (FeO(OH), n(H_2O)) or siderite ($FeCO_3$) (Dana and Dana, 1883). Australia is one of the major iron ore producers in world. In 2009, Australia produced 394 million tons of iron ore of which 362 million tons were exported valued at $30 billion (Garcıa-Flores et al., 2011). Western Australia produced 97% of the total production in 2009. Australia is also the largest iron ore exporter and ranks the second (with 17%) after China (39%) as producer (McKay et al., 2012).

However, about 50% of mined iron ore in Australia is iron ore fines, whose size is less than 6mm (O'Brien, 2009). As a consequence, the discharge of iron ore fines from silos or containers may result in many problems, such as flow obstructions, segregation, shocks and vibrations, or unsteady flow (Schulze, 2008). Iron ore fines also cause many problems, such as increasing the cost of handling, inconvenience of transport and negative health impact by inhalation (Schulze, 2008). Thus, in many processes, the lump ores with size larger than 10mm are preferred. The process of compaction or briquetting can be applied to enlarging the size of iron ore fines to solve those problems. Uniaxial die compaction is the most typical form of consolidation process. It is a process that decreasing the porosity of powders in a confined space. Die compaction is used in many industries, such as powder metallurgy, ceramics, hard metals, pharmaceutical tablets, detergent, magnets, and others.

Crushing strength and tensile strength of compacted particles are tested after die compaction. Both crushing strength and tensile strength of iron fine compact are influenced by a number of factors, including materials property, particle size and distribution, maximum load of compaction, mixed moisture and lubricant. Crushing strength can be measured by uniaxial compress of iron ore fine compact immediately. Comparing to crushing strength, experimental measurement of tensile stress of compacted particles is difficult to be conducted. However, the tensile stress can be transformed from the result of diametrical compress of iron ore fine compact by further calculation.

The purpose of the work is to characterize the properties of iron ore fines and promoting the capacity of iron ore packing and compaction process. Its outcomes can lead to better design and control of the process.

This thesis includes seven chapters as detailed below.

In Chapter 1, a brief introduction of the background of the work is given.

Chapter 2 is the literature review which introduces the previous work on flow and particle theories, experimental characterization of flowability and compaction.

Chapter 3 describes the procedure of the experiments, including experimental apparatus and types of iron fines as well as the analysis methods.

In Chapter 4, the experimental results of flowability of iron ore fine measured by FT4 rheometer are presented. Flow properties including unconfined yield stress, cohesion and flow function are calculated based on the Mohr circles. The effects of key parameters are also discussed..

Chapter 5 presents the results of crushing strength of iron ore fine compacts. The effects of experiment conditions such as maximum loading, particle size, moisture and lubricants are analysed.

In Chapter 6, the experimental results of diametrical compaction are presented. The tensile strength of the compacts are calculated. The effects of experimental conditions are investigated.

Chapter 7 concludes the whole thesis and discusses future work in this area.

Chapter 2 Literature Review

2.1 Introduction

Iron occupies about 5% of the earth crust and is the fourth most abundant element in the crust. Iron ores are rocks from which metallic iron can be economically extracted. The principal iron ores include magnetite (Fe_3O_4), hematite (Fe_2O_3) and goethite (FeO(OH)).

However, over half of mined iron ores is fine particles. This poses many issues in handling, transport and store processes of iron ore. The characterization of flowability and compaction of iron ore fines can contribute to alleviate those problems. Although the properties of iron ore fines are different to other powders, some experimental methods and compaction behaviours of particles are similar. Thus, previous works of flowability and compaction related to other powders should be reviewed to help understand the flowability and compaction behaviour of iron ore fines.

Therefore, this chapter will review previous work of characterization of material flowability, which contains dynamic flow energy, bulk properties and shear properties. Previous work on the characterization of compaction behaviour is also reviewed. This chapter is divided into three main sections. In the first section, characterisations of particle properties and characteristics, such as particle density and particle shape, are given. The second section is about the effect of particle size on compaction behaviour. The third section is about the effects of experiment conditions, such as die wall friction and compaction rate.

2.2 Types of iron ore and their properties

A large number of minerals contain iron. However, only a few are used commercially as the source of iron. Minerals containing important amounts of iron may be grouped according to their chemical composition into oxides, carbonates, sulphides and silicates. Table 2.1 shows the oxide and carbonate classes of iron minerals and indicates the mineral species commonly used as sources of iron. Oxide minerals are the most important sources of iron, with the carbonate, sulphides and silicates being of minor importance. In the descriptions of the important iron ore minerals or mineral groups that follow, the chemical compositions are for the pure minerals, the iron content of commercial ores or

concentrates generally is lower due to the presence of gangue and other impurities.

Table 2.1 Main iron materials (Poveromo, 1999)

Class and Mineralogical Name		Chemical Composition of Pure Mineral	Common Designation
Oxide			
Magnetite		Fe_3O_4	Ferrous-ferric oxide
Hematite		Fe_2O_3	Ferric oxide
Ilmentite		$FeTiO_3$	Iron-titanium oxide
Limonite	Goethite	$HFeO_2$	Hydrous iron oxides
	Lepiclocrocite	FeO(OH)	
Carbonate			
Siderite		$FeCO_3$	Iron carbonate

- **Magnetite**

Chemical composition of magnetite is Fe_3O_4, which has 72.36% iron and 27.64% oxygen. Magnetite always contains trace elements of Mg, Mn, Ti, V, Cr etc. In addition, Mg^{2+} and Mn^{2+} replace Fe^{2+} in magnetite. Magnetite contains titanium in small amounts as inclusions of ilmenite. The content of Ti in magnetite can reflect the origin of it. When the titanium content reaches 12-15% or more, magnetite is termed titaniferous magnetite. The content of Ti in Magnetite, which is contact metasomatic origin or hydrothermal origin, is markedly lower. The magnetic with lowest content of Ti is sedimentary-metamorphic origin (Li, 2008).

Magnetite is isometric, most commonly in octahedron, also in rhombic dodecahedron with faces striated and very rarely in cubic (Figure 2.1) (Dana and Dana, 1883). It has a colour of dark grey to black and density of 5.17 g/cm^3. Its other physical and optical properties are in listed in Table 2.2. Most magnetite has strong magnetism. The magnetic property of magnetite is important as it allows exploration by magnetic methods and makes possible the magnetic separation of magnetite from gangue materials to produce a high quality concentrate (Poveromo, 1999).

Magnetite occurs in igneous, metamorphic, and sedimentary rocks. It has become increasingly important as a source of iron as a consequence of the continued

improvements in magnetic concentration techniques and in the expanded use of high grade products (Poveromo, 1999).

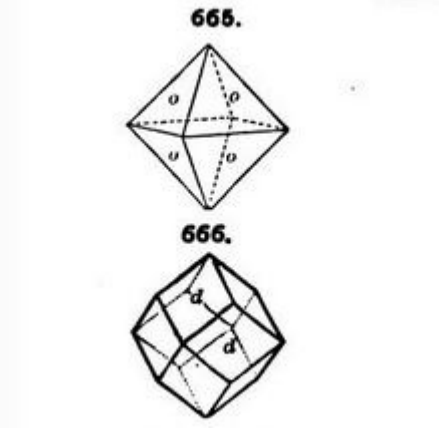

Figure 2.1 Crystal form of magnetite (Dana and Dana, 1883).

Table 2.2 Physical and optical properties of magnetite (Anthony et al., 2011)

Cleavage	Parting on {111}, very good
Fracture	Uneven
Tenacity	Brittle
Mohs Hardness	5.5-6.5
VHN (100g load)	681-792
Transparency	Opaque
Streak	Black
Luster	Metallic to submetallic and may be dull

- **Hematite**

Hematite has a chemical composition of Fe_2O_3 corresponding to 69.94% iron and 30.06% oxygen. Common varieties are termed crystalline, specular, martite (pseudomorphic after magnetite), maghemite (magnetic ferric oxide), earthy, ocherous, and compact. Hematite always contains Ti, Al, Mn, Fe^{3+}, Cu and a small amount of Ca and Co. Sometimes it includes mixing materials of TiO_2, SiO_2 and Al_2O_2 (Li, 2008).

Hematite has a hexagonal structure, commonly in complex rhombohedral, psudocubic, prismatic and rarely in scalenohedral. It usually shows in aggregates of rhombohedral and tabular (Figure 2.2) (Dana and Dana, 1883). It has colours including steel grey and maybe with iridescent tarnish, dull to bright red, white to grey-white with a bluish tint

(Anthony et al., 2011). The density of hematite is 5.26 g/cm^3. Its other physical and optical properties are in Table 2.3.

Hematite is one of the most important iron minerals. It has a wide occurrence in many types of rocks and is of varying origins. It occurs associated with vein deposits, igneous, metamorphic, and sedimentary rocks, and as a product of the weathering of magnetite. Some low-grade deposits of disseminated crystalline hematite have been successfully treated by both gravity and flotation techniques to produce high quality concentrates (Poveromo, 1999).

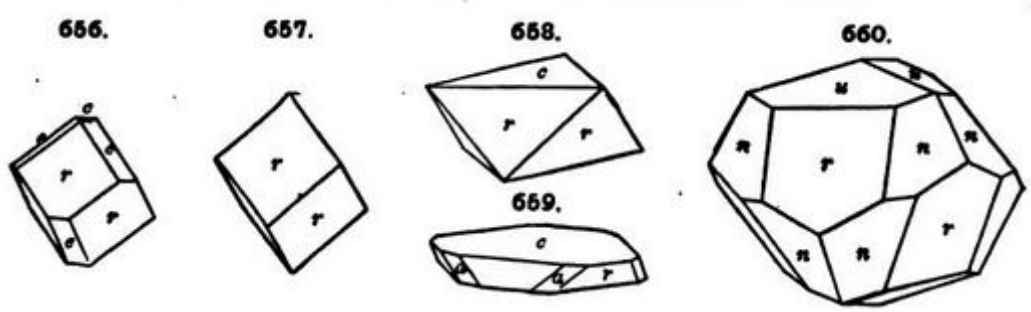

Figure 2.2 Crystal form of hematite (Dana and Dana, 1883)

Table 2.3 Physical and optical properties of hematite (Anthony et al., 2011)

Cleavage	Parting on {0001} and {10$\bar{1}$1}
Fracture	Uneven to subconchoidal
Tenacity	Brittle, elastic in thin laminae
Mohs Hardness	5-6
VHN (100g load)	1000-1100
Transparency	Opaque
Streak	Cherry-red or reddish brown
Luster	Metallic or submetallic to dull

- **Goethite**

Goethite (FeO(OH)) contains 62.85% iron, 27.01% oxygen, and 10.14% water. Due to different origin, its component is various. Goethite, which is hydrothermal origin, has higher purity. Exogenous origin leads to the components of Al_2O_3, SiO_2, MnO_2 and CaO. Goethite, which is formed in oxidation zone of metallic mineral deposit, contains Cu, Pb, Zn and Cd. Hydrogoethite (FeO(OH)·nH_2O) is the goethite contains adsorption water (Li,

2008)

Goethite is orthorhombic, rarely monocrystal, more commonly as aggregates of capillary to acicular crystals, or stalactitic masses with concentric or radial fibrous internal structure (Dana and Dana, 1883), this is shown in Figure 2.3. It also shows cryptocrysalline in “limonite”. Goethite is commonly yellow or brown to nearly black in color, and is compacted to earthy and ocherous. Its density is 3.3-4.0 and other physical and optical properties revealed in Table 2.4.

Goethite is a common weathering product derived from numerous iron-bearing minerals in oxygenated environments. It is an important component of ore in weathered iron deposits, and also a primary precipitate in hydrothermal, marine and bog environment upon oxidation of reduced iron-bearing waters (Anthony et al., 2011).

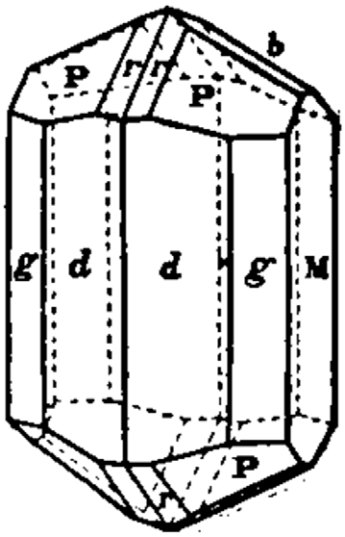

Figure 2.3 Crystal form of Goethite (Dana and Dana, 1883)

Table 2.4 Physical and optical properties of goethite (Anthony et al., 2011)

Cleavage	{010}, perfect; {100}, less perfect
Fracture	Uneven
Tenacity	Brittle
Mohs Hardness	5-5.5
VHN (100g load)	667
Transparency	Opaque

Streak	Brownish yellow, yellow-orange, ocher-yellow
Luster	Imperfect adamantine metallic to dull earthly; silky when fibrous

2.3 Characterization of flowability of powders

The flow properties of powders can be represented by dynamic flow energy, bulk properties and shear properties. Dynamic flow energy is the surface energy of the bulk material in dynamic conditions. Bulk property, which is affected by particle size and shape, is not a direct measure of flowability but provides a useful indicator as to whether a powder is cohesive or free flowing. Flow function, which is one of shear properties, is a numerical characterization of flowability. Flow function can be plotted from the values of major principal stress and unconfined yield stress, which can be found from yield loci figure obtained from shear testing. Other shear properties of tested materials, such as cohesion and internal friction angle, can be calculated by the yield locus figure though plotting Mohr circle.

2.3.1 Dynamic flow energy

- **Specific energy**

Specific energy is the flow energy per unit mass. It is a measure of how easily a powder will flow in an unconfined or low stress environment. It represents the relative cohesion level of the particle under low stress conditions. It is calculated from the energy requirement to establish a particular flow pattern in a conditioned volume of powder. Specific energy depends primarily on the shear forces acting between particles. Cohesion is often the most important property in low stress environment. Gravity also affects specific energy significantly. Thus, flow energy can be expressed in terms of specific energy (Freeman and Fu, 2008).

In the study of Fu et al. (Fu et al., 2012), three lactose particles including FlowLac 100 which is more spherical than other two, SpheroLac 100 which is less spherical than FlowLac 100 but has a similar size, and InhaLac 230 which has the same shape with SperoLac 100 but is larger than others, were used in their experiments. As shown in Figure

2.4 which plots means specific energy (SE) of different particles, the particles with larger sizes (i.e. InhaLac 230) have higher specific energy, which means lower flowability. The higher specific energy of this sample is a result of the higher cohesion between the particles. In addition, the particles which are more spherical are more free-flow. This is caused by lower morphological interaction.

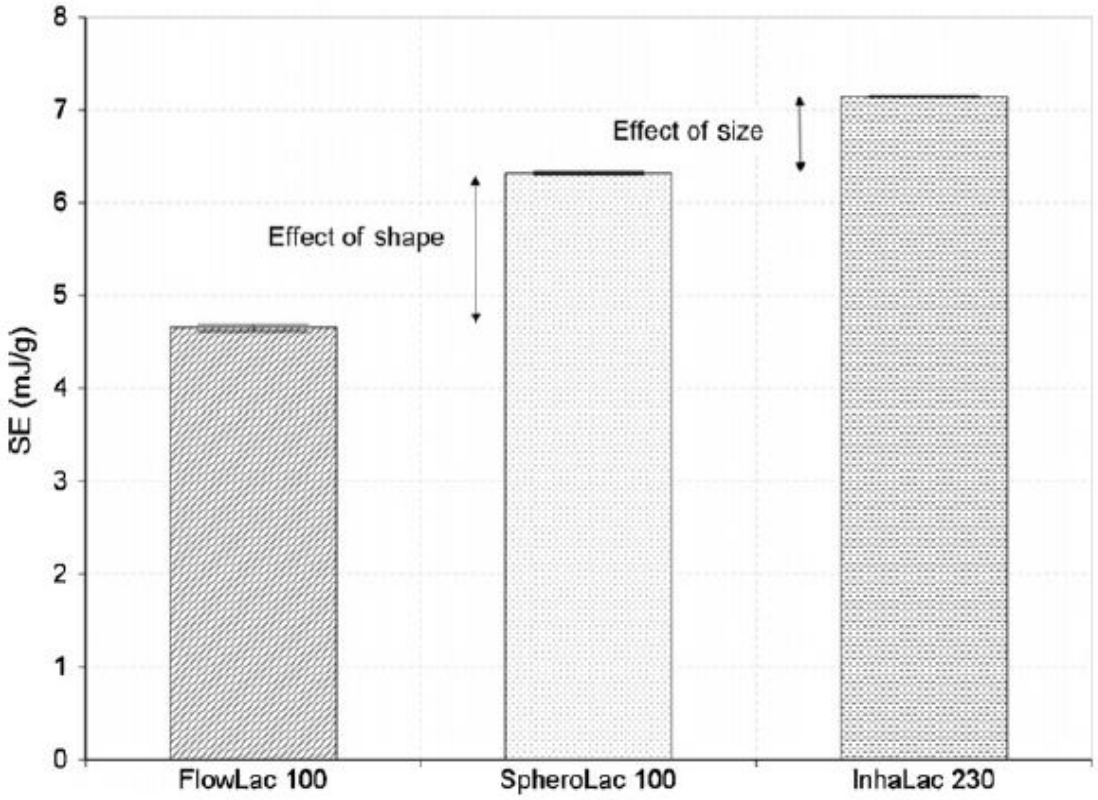

Figure 2.4 Specific energy of the three lactose powders (Fu et al., 2012)

- **Basic flowability energy**

The basic flowability energy is defined as the energy required to complete a standard test upon a conditioned powder. It is regarded as a measure of rheological properties of the powder when in a conditioned state. The maximum flow energy is demanded by non-cohesive powders, which have the lowest shear strength. Lindberg et al. (Lindberg et al., 2004) indicated that basic flowability energy is related with compaction behaviour of material. Higher basic flowability energy of particles reflects its higher packing density and the higher forces required to cause the powder to flow under compaction.

2.3.2 Bulk properties of particles

- **Compressibility**

Compressibility is a bulk property that examines the volume change of conditioned sample when it is slowly compressed so that air can escape (Freeman and Fu, 2008). Compressibility is not a direct measure of flowability, but it provides a useful indicator regarding cohesion. Low compressibility is often associated with low cohesion of particles.

In the study of Fu et al. (Fu et al., 2012), particle size and shape influence the compressibility. As revealed in Figure 2.5, the particles which are less spherical have higher compressibility. And the particles with larger particle size have lower compressibility, which is caused by the lower cohesion.

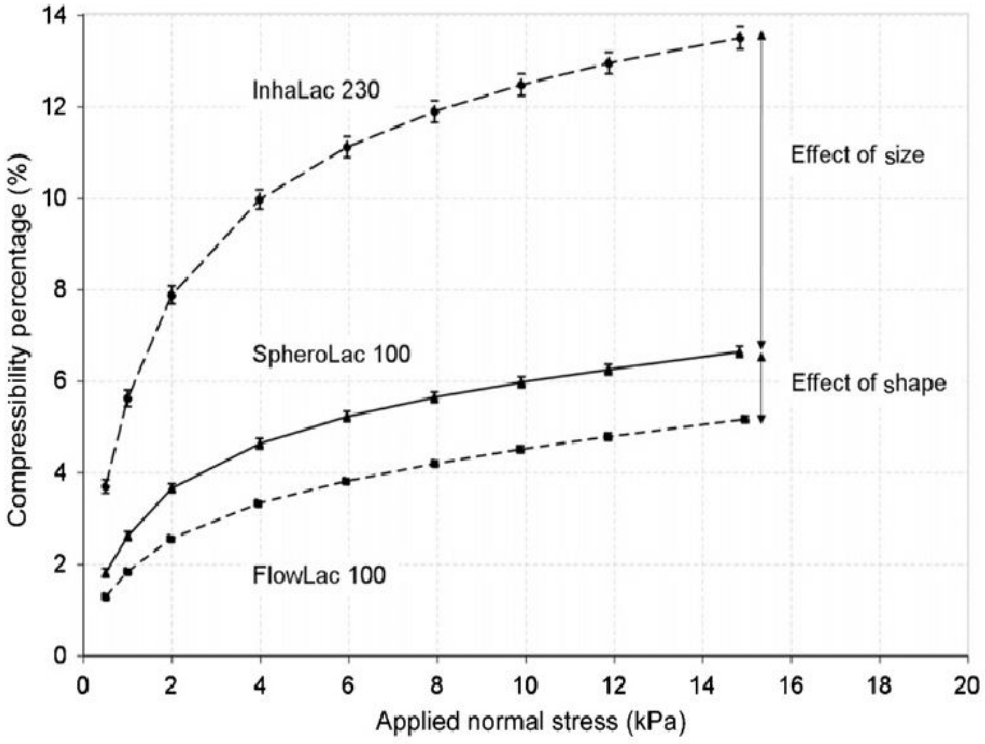

Figure 2.5 Compressibility versus normal stress (Fu et al., 2012).

- **Permeability**

Permeability describes how easily a powder compact can transmit a fluid through its bulk. Physical properties including cohesion, particle stiffness, surface texture and bulk density

influence permeability of the compact. External factors, such as consolidation stress, also have an influence by changing porosity and particle contact surface areas (Freeman and Fu, 2008). Permeability is affected by particle shape and particle size distribution (Fu et al., 2012). In a constant air flow (10 mm/s), as shown in Figure 2.6, SpheroLac 100 has lowest pressure drop and is the most permeable sample. This is caused by its relatively larger particle size and irregular shape, which leads to a relatively large void structure. In addition, smaller particles which are more cohesive has higher pressure drop and less permeable. In this case, the effect of particle size is more significant than particle shape. Freeman and Fu (Freeman and Fu, 2008) indicates that cohesive particles consisting mainly of sub-30 μm particles are the least permeable, granular powders are typically most permeable. Particles with large particles and fines can form a tight packing structure, with fines filling the spaces between particles, thus decreasing the permeability of the powder bulk.

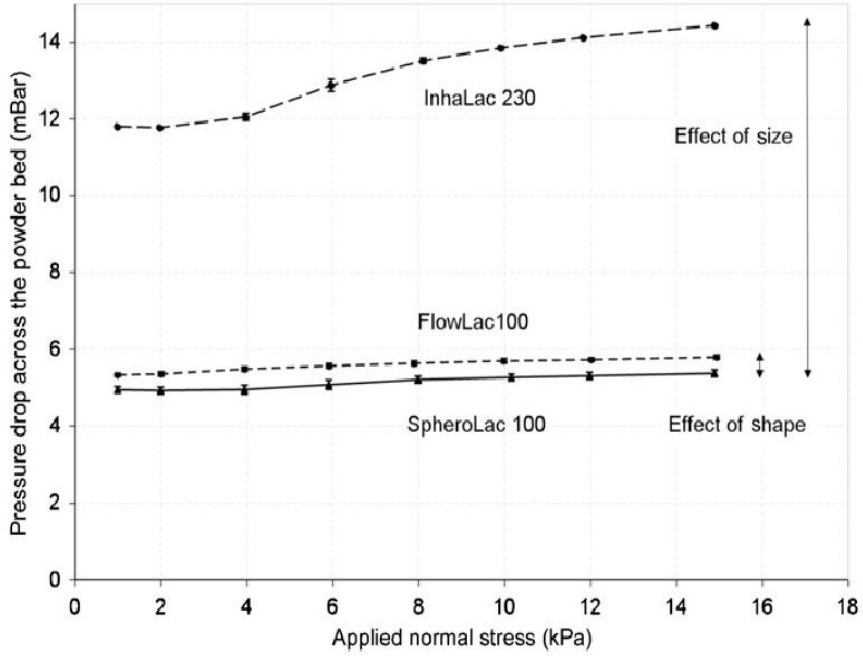

Figure 2.6 Permeability as a function of normal stress at constant air velocity (Fu et al., 2012).

2.3.3 Shear testing

Shear testers are used in advanced bulk solid technology. The first shear tester designed for bulk solids was the traditional shear tester developed by Jenike in 1960 so was called Jenike shear tester. Some years later ring shear testers designed for bulk solids were developed (Schulze, 2008).

The shear testing includes two steps: first the bulk solid specimen is consolidated, which is called “pre-shear”. Subsequently a point on the yield limit is measured, which is called “shear to failure”. The yield limit of a consolidated bulk solid is called a yield locus. A yield locus is valid for only one normal stress at pre-shear, σ_{pre}. For one well-defined state of consolidation, this has been attained by pre-shearing until steady-state flow prevails. If a different normal stress is applied at pre-shear, one will obtain a different yield locus. Since one can choose an infinite number of normal stresses at pre-shear, an infinite number of yield loci can be attained.

A yield locus is usually a slightly convex curve, as shown in Figure 2.7, with the curvature increasing toward smaller normal stress. With free-flowing, cohesionless bulk solids usually obtain a nearly straight-lined yield locus that goes through the origin. A yield locus is valid for one specific bulk density, namely that bulk density prevails at the end of pre-shear when steady-state flow is attained. If the yield locus is known, various parameters associated with flow properties can be determined, including consolidation stress, unconfined yield strength, flowability and internal angle of friction.

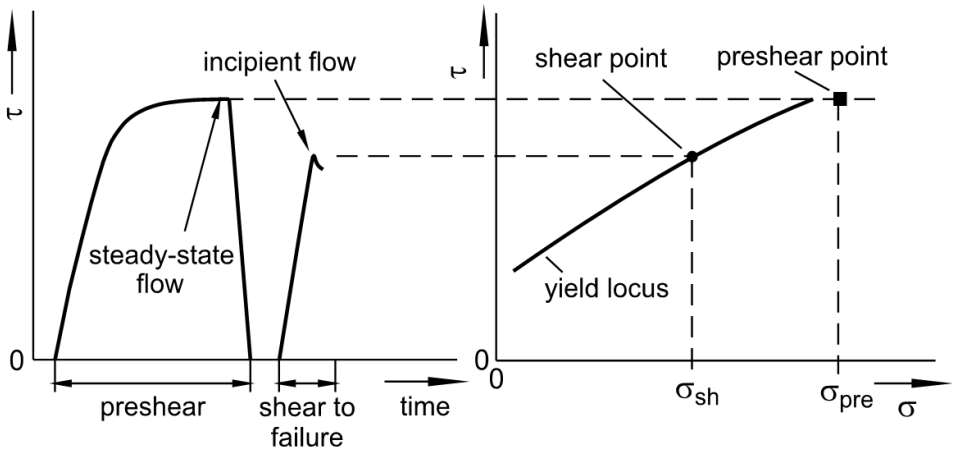

Figure 2.7 Measurement of the yield locus (shear point) by pre-shear and shear to failure (Schulze, 2008).

Consolidation stress and unconfined yield strength can be determined by constructing a Mohr circle. Each point on a Mohr stress circle represents the normal and shear stress on one particular cutting plane of a bulk solid specimen. For each yield locus there is a Mohr stress circle that represents the stress state at the end of consolidation. From the shear test one knows one point on this Mohr stress circle: the pre-shear point. It represents the

normal and shear stress acting in horizontal cutting plane at steady-state flow. The value of cohesion of tested materials is the intersection of yield locus line and y axis, and the value of tensile stress of materials is the intersection of yield locus line and x axis. As shown in Figure 2.8, σ_1 is major principal stress, σ_c is the unconfined yield stress, σ_t is the tensile stress and τ_c is the cohesion.

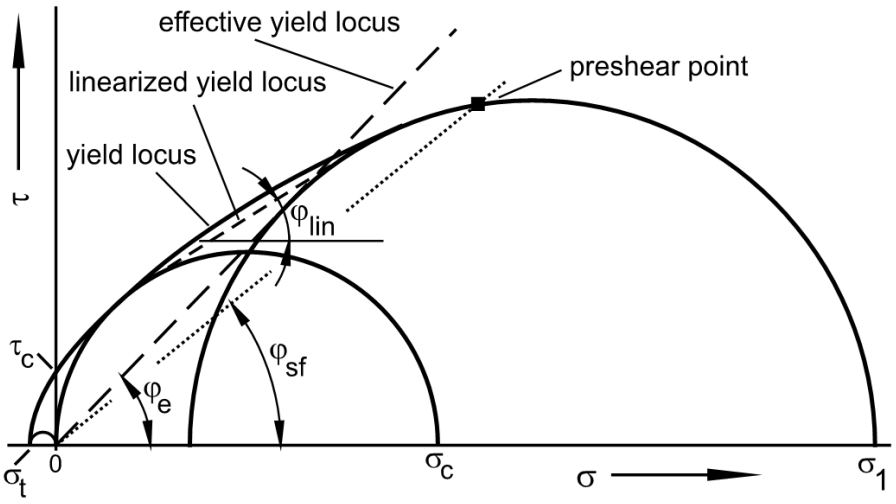

Figure 2.8 Yield locus and Mohr circle (Schulze, 2008).

2.4 Characterization of compaction

Although compaction of large particles can only increase bulk density slightly, compaction of fine or wet powders increases compact density significantly (Schulze, 2008). In addition, increasing bulk density also increases the strength of the compact. Under confined compaction, the bulk solid begins to flow near the failure point and there exists one particular yield limit for the bulk solid. In addition, compaction behaviour of fine particles is influenced by its materials properties, particle size distribution and experimental conditions.

2.4.1 Effects of materials properties

Poquilon et al. (Poquillon et al., 2002) identified the effect of morphological parameters on the compaction of iron ore powders. Green strength (strength of compacts before sintering) has found to be related to the contact area between particles, which is related to the shape of the particle. The spherical powder S (average size is 15μm, main composition is Fe_2O_3, density is 1.169 g/cm3), and spongy powder E (average size is 30 μm, main composition is Fe_2O_3, density is 1.173 g/cm^3) were prepared to do the uniaxial

compaction testing, the range of compaction pressure was from 100Mpa to 390Mpa. Green strength was an ability of compacted particles to withstand pressure. Zinc stearate was used to reduce die wall friction as lubricant. Figure 2.9 shows that powder E had better compressibility than powder S, especially at low pressure (Poquillon et al., 2002). In the SEM analysis, interparticle porosity was reduced and the contact area between particles was increased with increasing pressure. In addition, plastic deformation of spongy particles was larger than spherical particles because the sliding of the particles was easier between spherical particles.

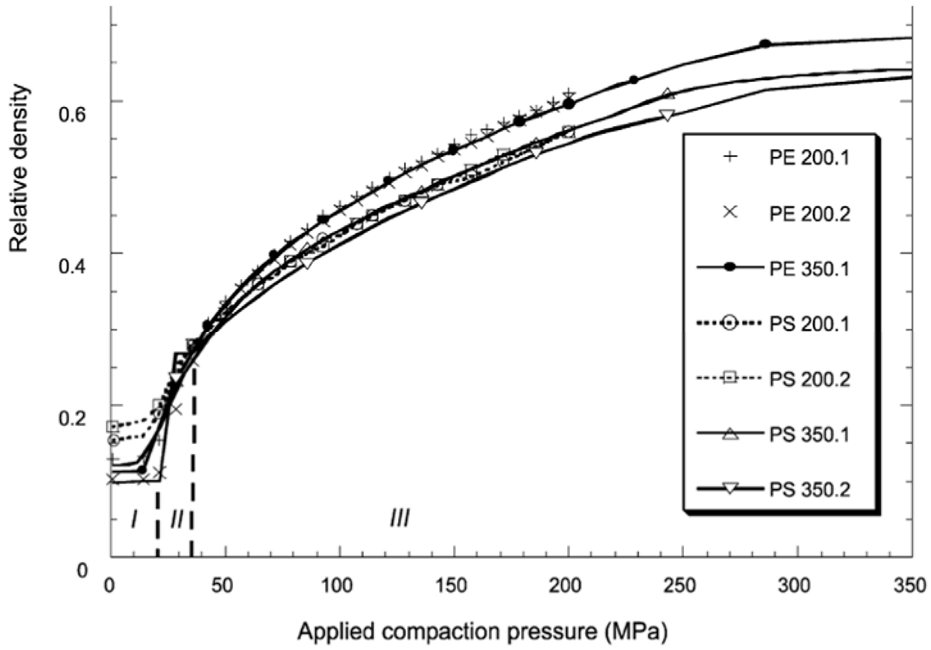

Figure 2.9 Relative density of the compacts vs. the applied compaction pressure
PE 200.1 is test 1 of spongy particles with 200 MPa maximum load; PS 350.2 is test 2 of spherical particles with 350 MPa maximum load (Poquillon et al., 2002).

2.4.2 Effect of particle size distribution

McKenna and McCafferty (McKenna and McCafferty, 1982) studied the influence of particle size variation on the tensile strength of compacts forms from three different materials: spray-dried lactose, Sta-Rx 1500 and Avicel PH-101. The tool surface was lubricated by magnesium stearate with the compaction rate of 0.1 cm/s. In this study, tensile strength is used to examine the strength of samples, because the tensile strength is independent of tablet dimensions.

As shown in Figure 2.10, in term of spray-lactose tablets, which was mainly deformed brittle fracture (Hardman and Lilley, 1970), the particle size had a significant influence on compact tensile strength. An increase of compaction strength was caused by a decrease of particle size. In addition, Sta-Rx 1500, which is compacted by plastic flow (Rue and Rees, 1978), had a similar trend with spray-dried lactose. The smallest particle size range (-45μm) had a significant increase in tablet tensile strength over the whole compression range. Finally, Avicel PH-101 was a plastically deforming material (David and Augsburger, 1977), so particle size variation had little effect on the tensile strengths of the compaction.

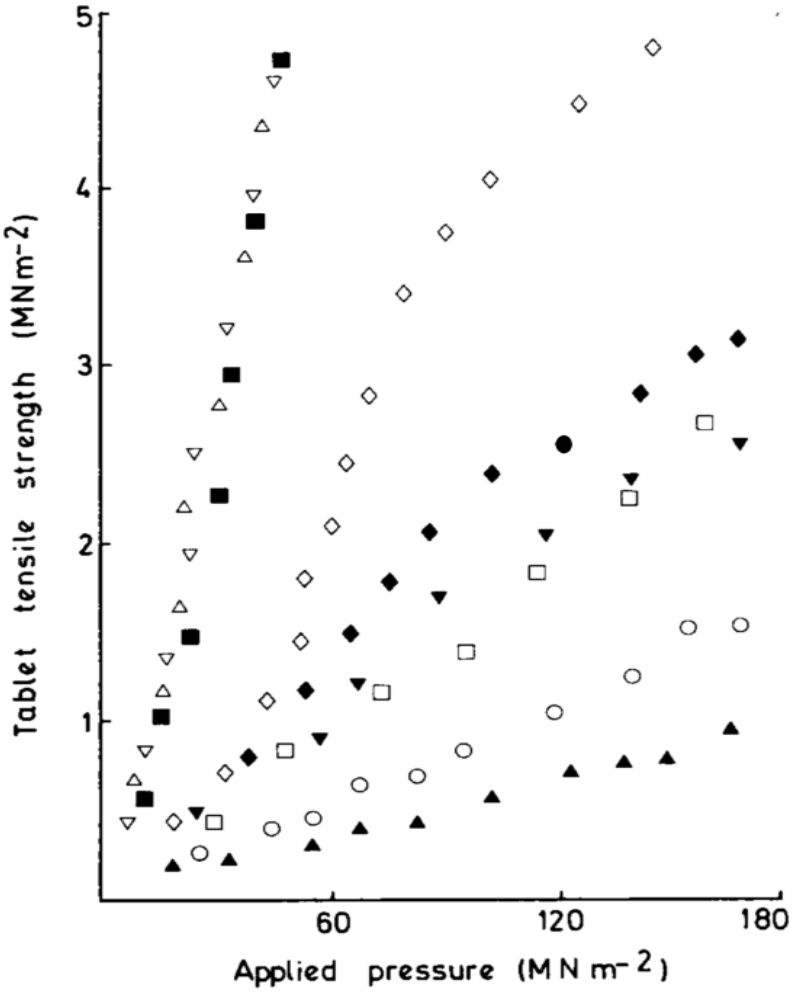

Figure 2.10 Relation between applied pressure and tensile strength of tablets prepared from different size fraction of spray-dried lactose, Sta-Rx 1500 and Avicel PH-101. □=0-45μm. ○=90-125μm. ▲=180-250 μm Spray-dried lactose; =0-45μm =80-125μm ▼=180-250μm Sta-Rx 1500; ■=0-45μm =90-125μm ▵=180-250μm Avicel PH101 (McKenna and McCafferty, 1982).

However, Almaya and Aburub (Almaya and Aburub, 2008) indicated that the relationship of strength of sample and particle size was related with lubricant. Their work used a brittle deforming material (Dibasic calcium phosphate dehydrate), a plastically deforming material (Microcrystalline cellulose) and a viscoelastic material (Starch 1500). The results showed that powder size affects compact strength only with added lubricant in plastically deforming material (MMC), which means these particles are sensitive to lubricant. Moreover, powder size influenced the compact strength with and without added lubricant in viscoelastic material (starch). Finally, powder size had no significant influence on compact strength with and without added lubricant in brittle material (dibasic calcium phophate dihydrate).

The hardness of compacted particles is another parameter to affect its strength. Hardness is a measure of resistance of materials to deformation when a force is applied. Katikaneni et al. (Katikaneni et al., 1995) used ethylcellulose to analysis the hardness-compression force profiles. Hardness increases with the decrease of particle size (Figure 2.11). This is consistent with the theory that smaller particles allow a greater packing density and a greater number of contact points for inter-particulate boding (Seelig, 1947).

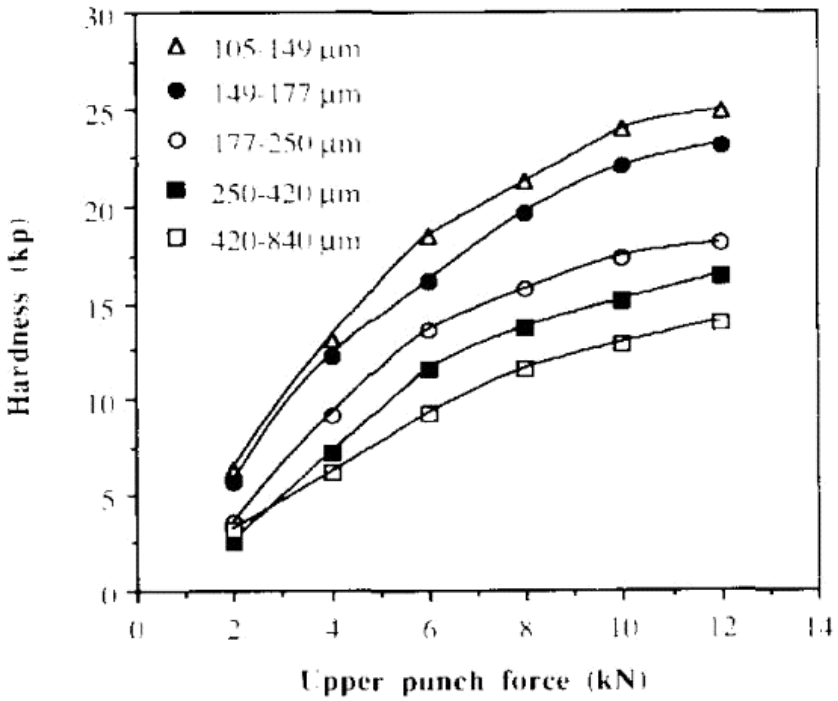

Figure 2.11 Compressional force effects on ethylcellulose tablet hardness using different particle size fractions (Katikaneni et al., 1995).

Fell and Newton (Fell and Newton, 1971) indicated that the smaller particle size causes lower packing density at the same pressures. In other part, for tablet volumes determined after ejection from the die, the difference in relative volume between the two larger particle-size fractions was considerably reduced, as shown in Table 2.5.

Table 2.5 Values of D_A, D_B and D_0 as described by Heckel (D_0=initial apparent relative density of powder; D_A=densification due to die filling and particle rearrangement; and D_B=densification due to particle rearrangement.) (Fell and Newton, 1971).

Density Determined	Particle-Size Fraction, μm.	Crystalline			Spray Dried		
		D_0	D_A	D_B	D_0	D_A	D_B
At pressure	0–32	0.322	0.728	0.406	0.285	0.703	0.418
	75–104	0.587	0.760	0.173	0.538	0.748	0.210
	180–210	0.618	0.764	0.146	0.527	0.754	0.227
Released after slow compaction	0–32	0.322	0.728	0.406	0.285	0.696	0.411
	75–104	0.587	0.761	0.174	0.538	0.754	0.218
	180–210	0.618	0.769	0.151	0.527	0.754	0.227
Released after fast compaction	0–32	0.322	0.773	0.451	0.285	0.668	0.383
	75–104	0.587	0.731	0.144	0.538	0.728	0.190
	180–210	0.618	0.711	0.997	0.527	0.741	0.214

2.4.3 Effects of operation conditions

2.4.3.1 Effect of die wall friction

Die wall friction causes compact density inhomogeneity in compaction. The inhomogeneity in compact may also lead to non-uniform stress distribution that may cause capping and lamination and thus affects the strength of the compact.

Abdel-Hamid and Betz (Abdel-Hamid and Betz, 2011) introduced a definition of radial tensile strength (RTS) of a compact, given by

$$\sigma = \frac{2F}{\pi dh} \qquad 2.1$$

where F is the force required to cause failure in tension, d is the diameter of the compact and h is the compact thickness.

Fig. 2.12 shows the effect of compaction pressure on radial die-wall parameters for different powders, including Microcrystalline cellulose, directly compressible mannitol, calcium hydrogen phosphate dihydrate, pre-gelatinized starch, spray-dried lactose monohydrate, and magnesium stearate (Abdel-Hamid and Betz, 2011). It was shown that increasing compaction pressure increased significantly both residual die-wall pressure (RDP) and maximum die-wall pressure (MDP) but reduced both RDP/MDP ratio and SR (radial stress ratio). In addition, Pre-compaction pressure had no influence on RDP and SR for micro-crystalline cellulose, pre-gelatinized starch and calcium hydrogen phoshate dihydrate.

Increasing speed decreased MDP for all materials but also led to the increase in RDP for mannitol and the decrease of RDP of microcrystalline cellulose lactose and pre-gelatinized starch, and no effect for Ecompress. On the other hand, the increase in speed led to the increase in radial recovery for mannitol. There was no influence of speed on the radial recovery of materials with brittle behaviour. In addition, the authors also indicated that with the increase in RDP, the RTS also increased which means the strength of the samples increased.

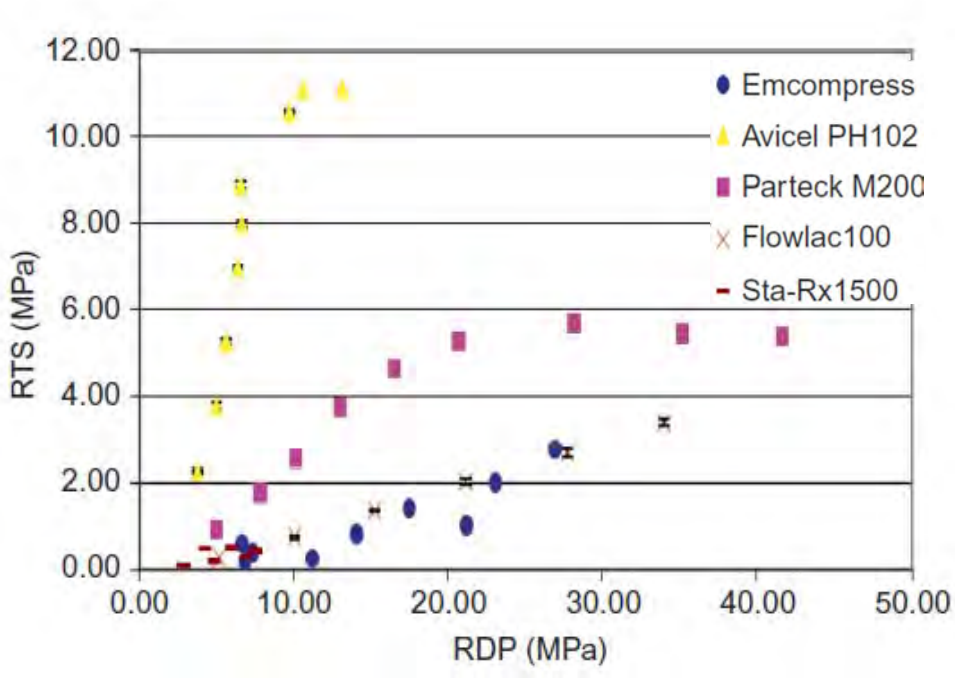

Figure 2.12 Change of RDP with RTS at compaction speed 0.5 m/s (Abdel-Hamid and Betz, 2011).

2.4.3.2 Effect of compaction rate

Fell and Newton (Fell and Newton, 1971) indicated that the relative volumes of tablets prepared at slow compaction rates were lower than those of two larger particle-size fractions, but the opposite was true for tablets prepared at higher rates of compaction, as shown in Fig. 2.13. The Heckel plot showed that the densification due to particle rearrangement indicates the smallest size fraction underwent the greatest rearrangement at both slow and fast compactions. Particle rearrangement was generally greater for the spray-dried lactose.

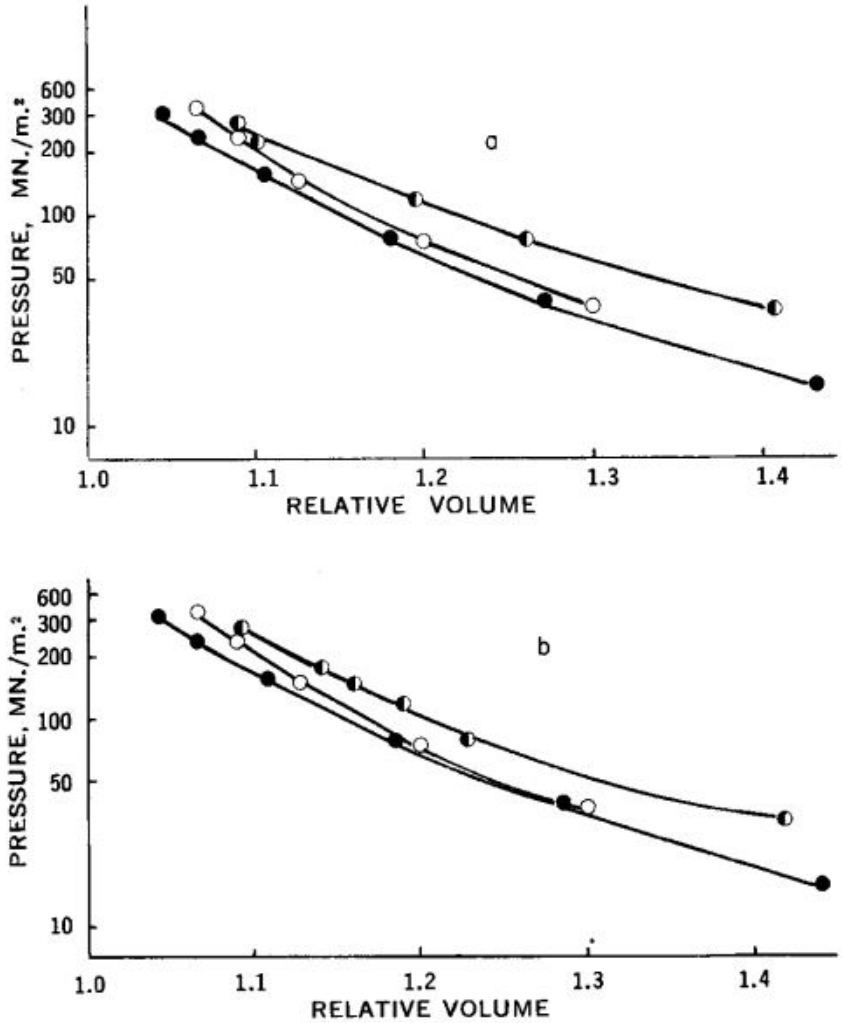

Figure 2.13 Relative volumes of tablets compacted at known pressures for (a) 75-104 μm crystalline lactose, and (b) 75-104 μm spray-dried lactose. ● relative volume determined at pressure, slow compaction; ○ relative volume determined after release of pressure, slow compaction; ◐ relative volume determined after release of pressure, fast compaction (Fell and Newton, 1971).

2.4.3.3 Effect of lubricants

The lubricant of die compaction can be divided into internal lubricant and external lubricant. Internal lubricant is a lubricant to mix with particles while external lubricant is to apply on the inner surface of dies. Both lubricants can increase the relative density of compacts, but it is found that internal lubricant is more effective than external lubricant (Zhornyak and Oliker, 1981). External lubricant only has little impact on final density, as shown in Figure 2.14. However, lubricant leads to a more uniform distribution of inter-granular pore size (Figure 2.15), which can reduce the critical flaw size variability (Uppalapati and Green, 2005). However, internal lubricant will decrease its strength, especially in the particles, which has poor compatibility. In the study of Enneti et al. (Enneti et al., 2013), The compacted particles with no internal lubricant showed the highest green strength at all compaction pressures and the green strength decreased with the increasing amount of the lubricant (Figure 2.16).

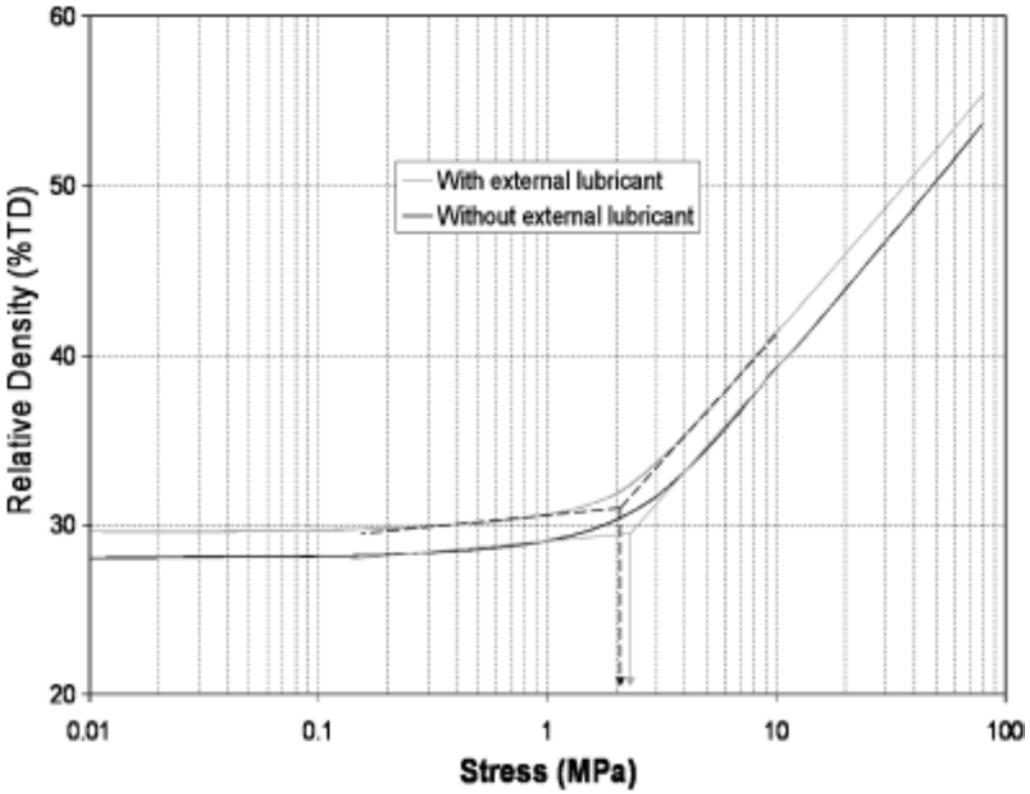

Figure 2.14 Compaction Curve of powders with and without external lubricant (Uppalapati and Green, 2005).

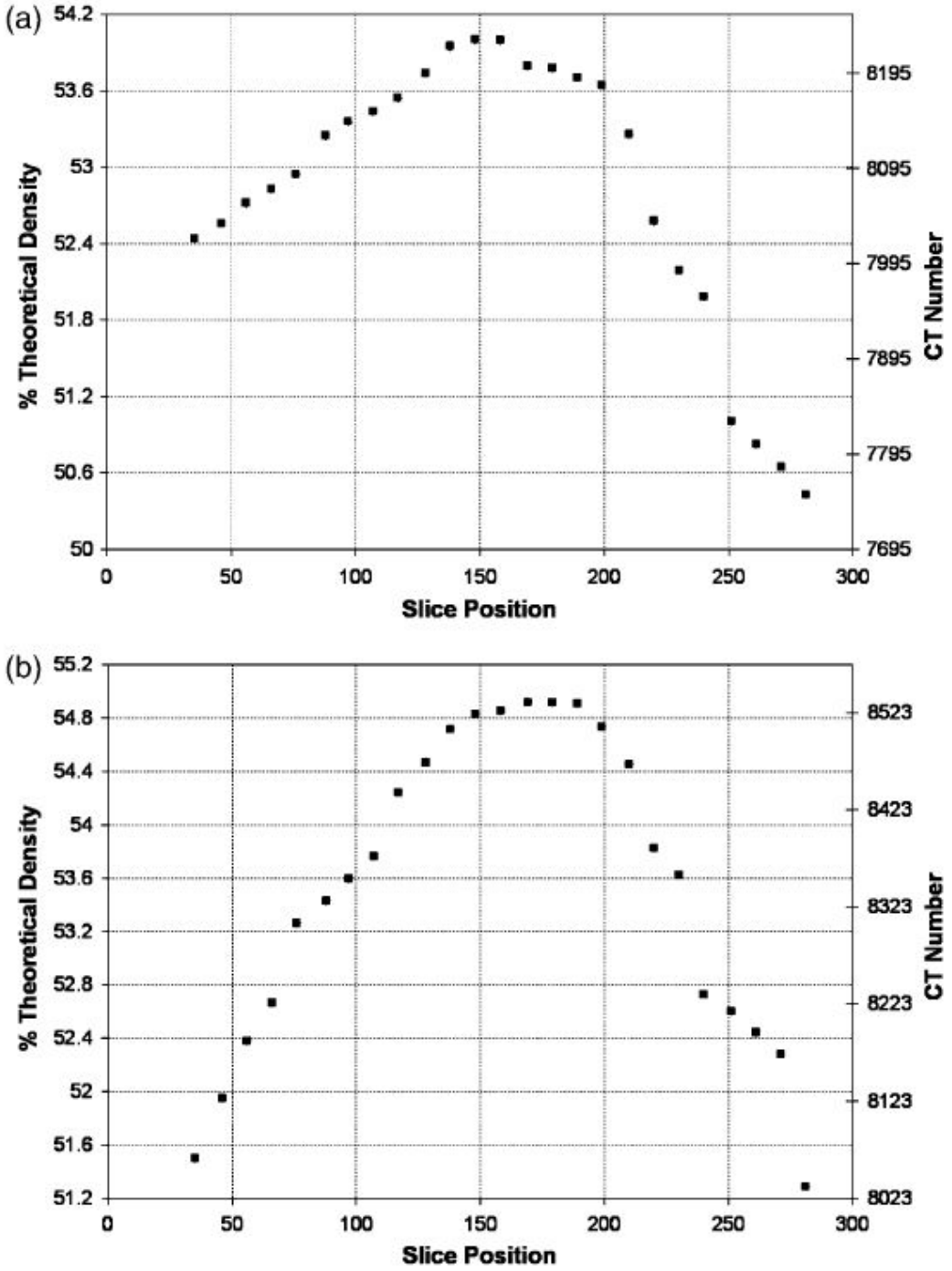

Figure 2.15 CT number plotted against slice position for powder (a) with external lubricant and (b) without external lubricant (each slice is 17.5μm thick) (Uppalapati and Green, 2005).

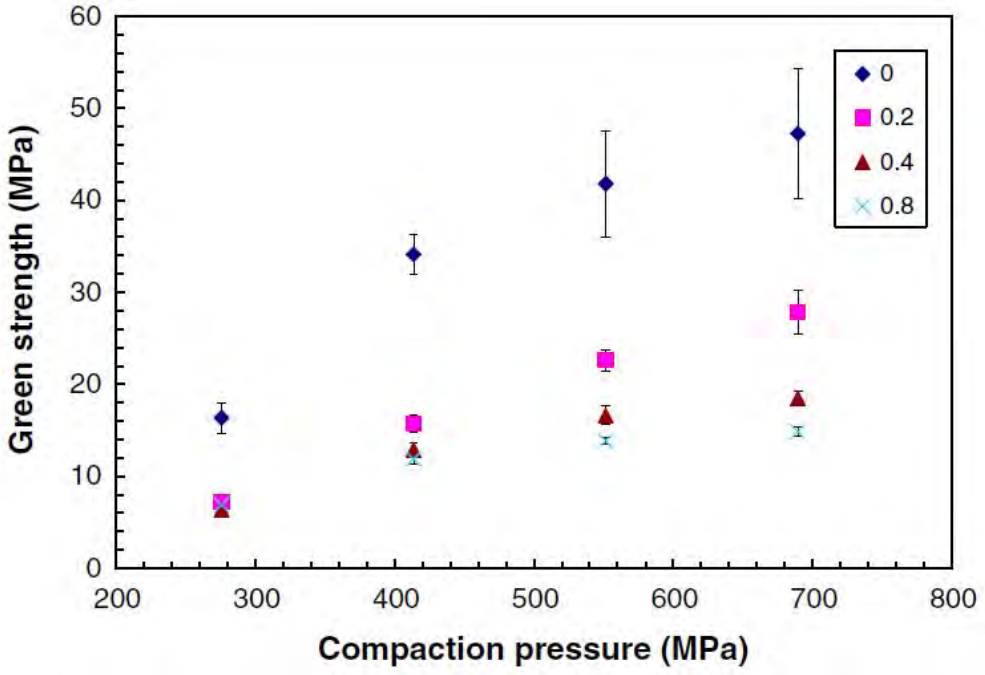

Figure 2.16 Variation in green strength with compaction pressure for powders mixed with varying % amounts of EBS (L) (Enneti et al., 2013).

Internal lubricant can form an adsorbed lubricant film around particles. As a result, solid-solid contact including contact between particles and die wall, this will reduce die wall friction. Thus, this would accelerate the rearrangement of the powders and accelerate the rise in density of the compact, which means that lower load is required for the same specified displacement, as shown in Figure 2.17 (Nor et al., 2008). However, the lubricant film also interferes with the bonding properties of particles by acting as a physical barrier, which will cause a reduction in compact strength (Almaya and Aburub, 2008).

Hirai and Okada (Hirai and Okada, 1982) claimed that in an unlubricated condition, the coefficient of wall friction increases significantly at low range of compaction pressure of two testing materials (lactose and sucrose), and then achieves a constant value. In addition, the coefficient of wall friction of Sodium bicarbonate almost maintains a constant and the coefficient of wall friction of sodium chloride decreased slowly.

For the lubricated powders, the wall friction decreases significantly. For example, lubricated lactose powders show nearly constant which is lower than the unlubricated lactose.

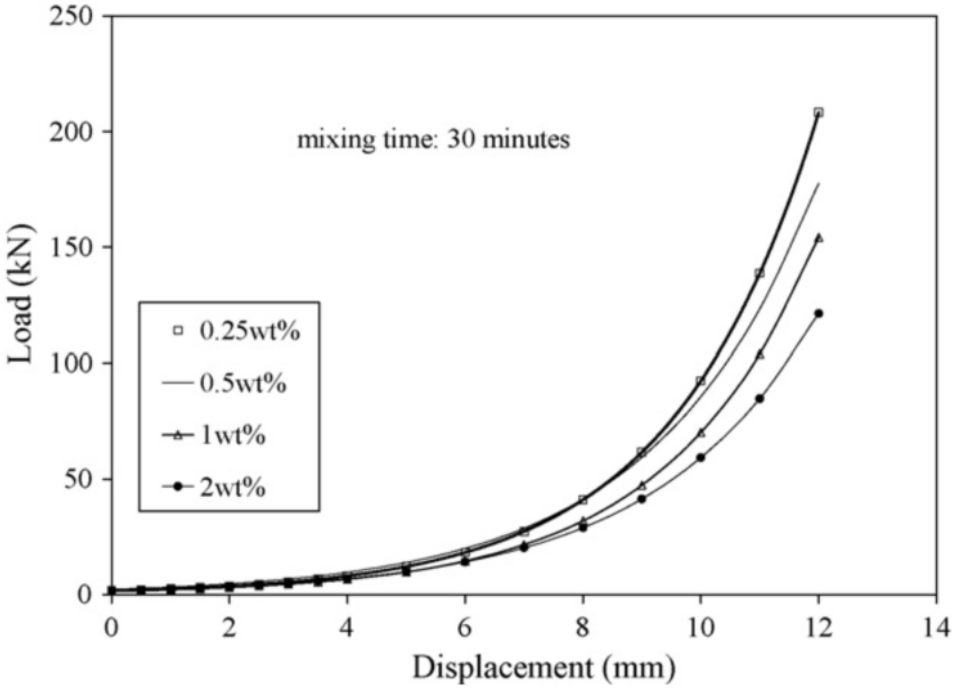

Figure 2.17 Load vs. displacement for the compaction (Nor et al., 2008).

In some studies (Ward and Billington, 1979, Zhornyak and Oliker, 1981, Nor et al., 2008), zinc stearate was also selected as an internal lubricant. Ward and Billington (Ward and Billington, 1979) indicated that 0.05-0.2 wt% of zinc stearate as internal lubrication was essential to compaction of iron powder to reduce die wall friction to generate higher relative density (Figure 2.18), but is has a negative impact of health.

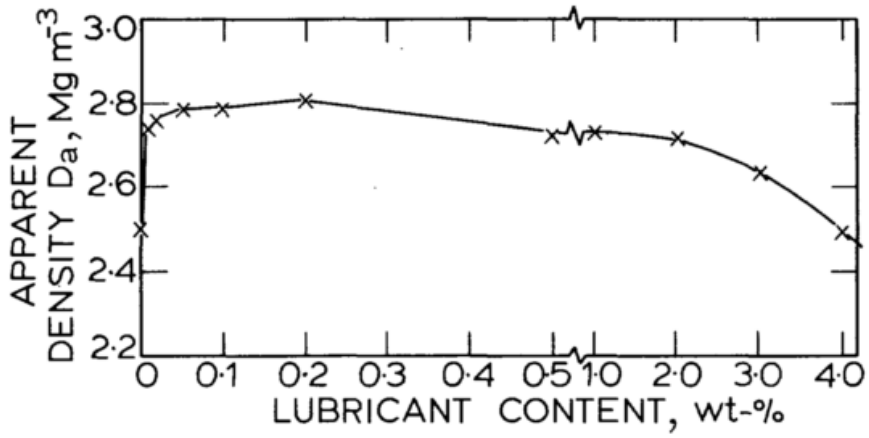

Figure 2.18 Effect of deposited zinc stearate on apparent density of iron powder (Ward and Billington, 1979).

2.4.3.4 Effect of moisture content

The compact density varies with moisture content. The material property affects the density on a range of moisture content. It has been tested on MCC powders (Sun, 2008) (Figure 2.19) showing that the density increased as moisture content increased until 3.3%. Between 3.3% and 5.1%, the density stayed constant at around 1.46 g/cm^3. It was manifest that the further increasing of moisture content will lead to decreasing of density. Because cellulose is not all crystalline, so the initial increase of density may be due to the anti-plasticization effects of water on amorphous polymer (Dlubek et al., 2002).

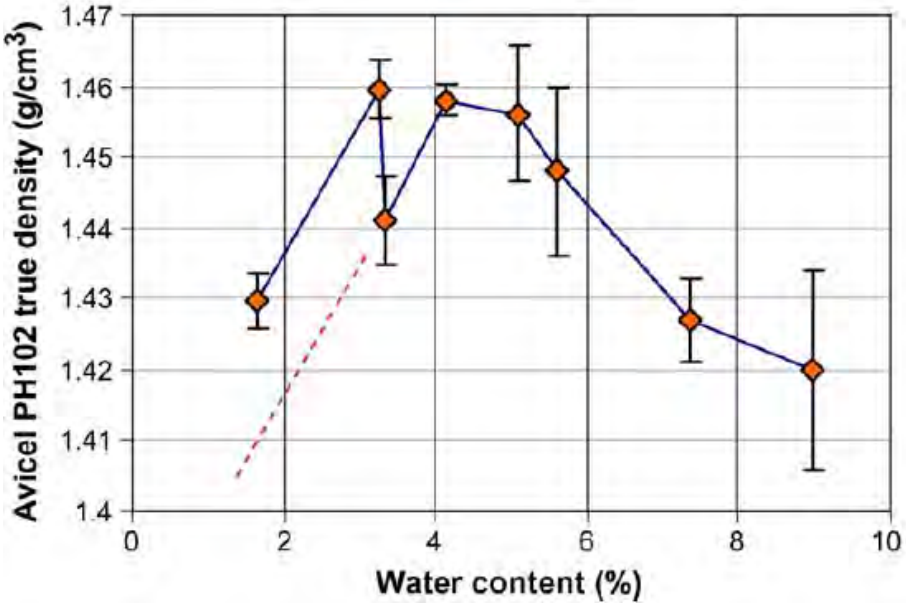

Figure 2.19 True density of MCC as a function of water content. The broken line indicates the expected true density of MCC free from moisture exchange between MCC and air (Sun, 2008).

2.4.3.5 Effect of compliance of system

The compliance of the compaction system may cause some errors in die compaction. This is because that the samples in the instrumented die cannot be accessed directly. The recorded punch displacement includes the deformation of the samples and the elastic deformation of various elements of the testing frame, such as punches, load cells, adaptors, and spacers. In light of this, correction for elastic compliance is needed to generate an accurate stress strain curve (Shang et al., 2012)

The compliance of the system was determined by pressing together the top and bottom punches (no powder in the die). The force-displacement response of the system is presented in Figure 2.20, where the force is measured by the upper load cell. It can be observed that the curve is non-linear during the early stages and becomes linear at higher loads. There is a small difference between the loading and unloading curve, which is assumed due to the initial settling of the components (Shang et al., 2012).

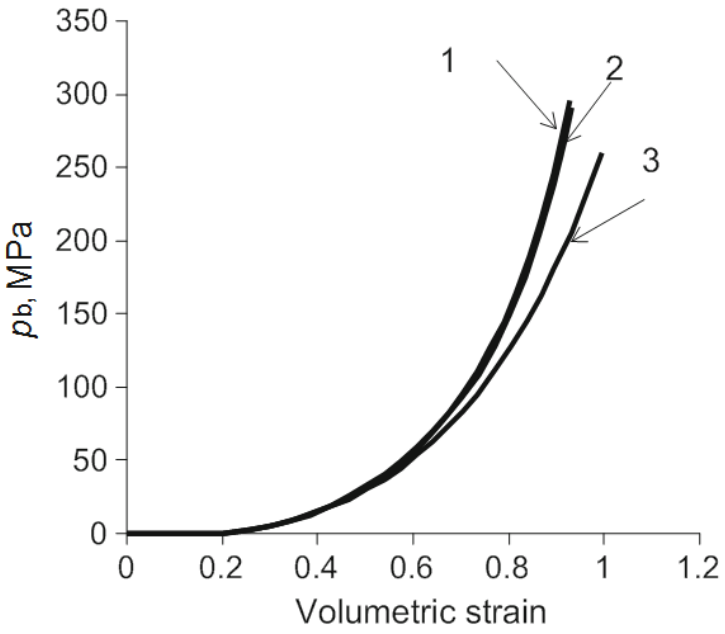

Figure 2.20 Correction using non-linear (1) and linear (2) system compliance and raw data (3) (Shang et al., 2012).

2.5 Summary

Iron ore fines are the products of ore mining and treatment processes and may cause problems in handling and transportation of ore. It is therefore important to understand iron ore behaviour in these processes. Among iron ores, magnetite, hematite and goethite are the main resources of iron. Magnetite and hematite have similar physical properties of relatively high density and hardness. However, goethite is much softer and has lower hardness. All those three types of iron ores are brittle in tenacity and have uneven fracture, although they have different direction of cleavage. In light of this, magnetite, hematite and goethite are more valuable to be tested to measure their properties and record related behaviour in compaction.

The flowability of fine particles can be represented by its dynamic flow energy, which is a measure of how easily a powder will flow in an unconfined or low stress environment, bulk properties, which is an indicator of regarding cohesion, and shear properties including cohesion and flow function. The sharp and size of particles influence the flow energy and bulk properties of fine particles. In addition, the effect of particle size is more important than particle shape. The shear testing can measure the yield locus of tested fine particles. From the yield locus line, the cohesion, unconfined yield stress and flow function can be calculated by plotting a Mohr circle. This type of testing can get more information than single flow energy testing and compressibility testing, and thus is preferred to measuring particle flowability.

In the compaction and strength testing including compression strength and tensile strength, there are some factors influencing behaviour of particles. In regards of morphology, spongy has better compressibility than spherical particles, especially at a low pressure. In the study of different particle size, different types of materials have different trend with increasing the particle size in its strength. And the effect of particle size in compact strength also is related to the lubricant. In relative density part, smaller the original particle size, the greater is the relative volume at all applied pressures. Die wall friction is a significant factor in particle compaction. Increasing compaction pressure increases the die wall friction which has negative impact on both density and strength of tablet. In order to eliminate or reduce the die wall friction as well as inter-particles friction, lubricant is required. Compaction rate also affects the relative density of compacted particles. The relative density shows a positive relationship with compaction rate. Form the literature, moisture content influences the relative density, the relative density of compacted particles increase with increasing moisture content before reach the peak value, and then it shows a negative relationship. Thus, for iron ore fines, the effect of particle size distribution, moisture content and lubricant should be tested in both relative density and strength studies. And both crushing strength testing and tensile strength testing are necessary. In order to increase both the relative density and strength of sample, external lubricant is more appropriate. And the compaction rate should be relatively fast.

Chapter 3 Experimental Procedure

3.1 Introduction

This work consists of three components: characterization of particles flowability, compressive strength of iron ore fine compacts and tensile strength of iron ore fine compacts. Flowability of a type of powders is how easily consolidated powders begin to flow (Schulze, 2008). Fine particles may result in many problems in transporting, storing and handling due to their poor flowability. In order to avoid those problems, solutions have to be found which should consider the flowability of iron ore fines.

In addition, the process of compaction or briquetting can be applied to enlarge the size of iron ore fines to solve problems of iron ore fines, such as low efficiency of transport, high cost of handling and inhalation issue. The properties of compacted iron particles can be found by the experiments of uniaxial unconfined compression and diametrical compression.

This chapter is to describe the preparation of iron ore fine samples and the procedure for each experiment.

3.2 Sample preparation

- ***Characterisation of materials properties***

Three types of iron ore fines were used in this work, magnetite, goethite and hematite.

The densities of three types of iron ore particles were measured in hydrostatic weighing method. Hydrostatic weighing method is a method using weight of sample in air (m_a) and its weight in water (m_w) to calculate the density of sample (ρ_s) by:

$$\rho_s = \frac{m_a}{m_a - m_w}\rho_w \qquad 3.1$$

where ρ_w is the density of water. The uncrushed iron ores, which were about 1 to 5 gram, were selected to be measured to minimize the errors. The results are also shown in Table 3.1 for comparison. The results of all types of iron ore are similar to the results in the literature (Anthony et al., 2011).

Table 3.1 Densities of different types of iron ores (Anthony et al., 2011)

Iron ore	Measured density (g/cm^3)	Mohs Hardness	VHN (100g load)
Magnetite	5.17 (5.17)	5.5-6.5	681-792
Goethite	3.3-3.4 (3.50)	5-5.5	667
Hematite	5.26 (5.31)	5-6	1000-1100

- ***Crushing***

The tested iron ore was supplied by Rio Tinto. The as received ore had a size ranging from approximately 1 cm to 2 cm. To prepare iron ore fines, those raw iron ore have to be crushed first. The crushing was conducted using a Fritsch impact mill (Figure 3.1). The raw iron ores were first put into the feeding entrance on the top of the mill. Then, the raw iron ores were crushed inside the mill by high speed rotating impactors. The pre-crushed and crushed iron ore powders are shown in Figure 3.2.

Figure 3.1 Fritsch crusher

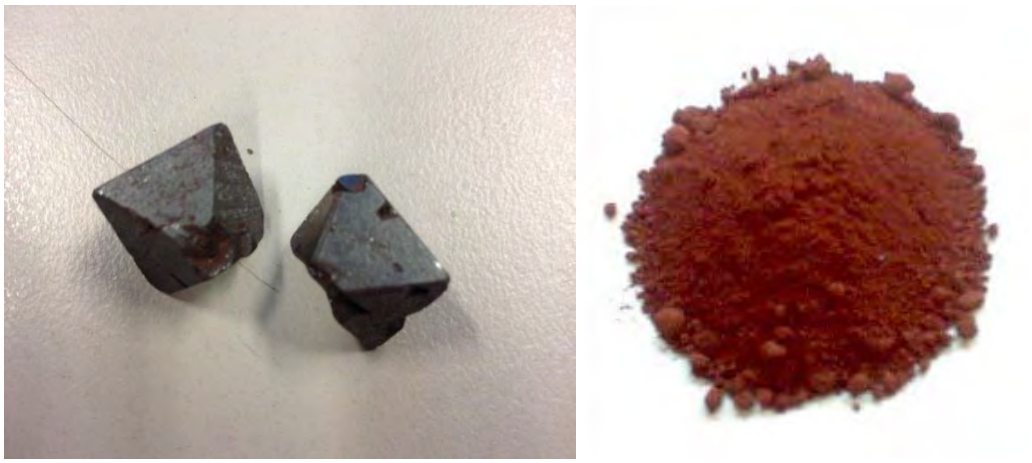

(a) (b)

Figure 3.2 (a) Pre-crushed iron ore crystal and (b) crushed iron ore powders

- ***Sieving and size classification***

The crushed iron ore fine was classified to various sets of different diameters by sieves. In order to classify the iron ore particles completely, a sieve shaker conducts the procedure of sieving for 60 minutes (Figure 3.3). The diameters of the sieves contain 25μm, 75μm, 200μm and 280μm. Thus, three sets of iron ore fines can be sieved including 25-75μm, 75-200μm, and 200-280μm.

Figure 3.3 Sieve shaker

- ***Adding water***

To investigate the effect of moisture, water was added to the particles. The iron ore particles were weighed in a glass container by using electronic balance, and the weight of

added water was calculated by the required percentage of moisture. Required amount of water was then added by a dropper into the glass container and the electronic balance was used to measure the weight of added water and ensured the added amount of water was equivalent to the calculated amount. Then the sample and water were well mixed by using the glass container and stick for 10 minutes. The mass ratio between iron ore and moisture was 2.5%-10% for different experiments.

In addition, before the testing, all samples were dried in the oven to ensure no moisture left in the samples. The classified samples were then stored in glass bottles to prevent the particle to be mixed with moisture and other powders.

3.3 Procedure of characterization of flowability

Flowability of powders was measured by shear testing using Freeman Technology FT4 Rheometer (Figure 3.4). In the FT4 rheometer, the maximum shear stress of tested particles is measured by the point of incipient failure or the yield point. This is the highest value of shear stress, which is calculated by the measured torque of shear cell, in each test.

Figure 3.4 Freeman Technology FT4 Rheometer

The correct testing mode was selected from the software of computer. From the results of shear testing, major principal stress (σ_1), minor principal stress (σ_2), unconfined yield stress (σ_c), cohesion (τ_c) and flow function (FF) of iron ore fines were determined.

During the testing, iron ore fines were consolidated by a bull-dozing blade action that pushed the powders downwards towards the bottom of the containing vessel (Figure 3.5), then a porous piston was used to apply levels of normal stress to iron ore fines. The shear testing was conducted by a shear cell, which was to measure shear stress at a certain compression pressure. The shear stress and compression stress were recorded by the computer (Figure 3.6). Based on the figure of shear stress and compression pressure, the yield locus line of tested particles can be plotted by FT4 rheometer (Figure 3.7).

Figure 3.5 Assembled 25mm×25ml Split Vessel

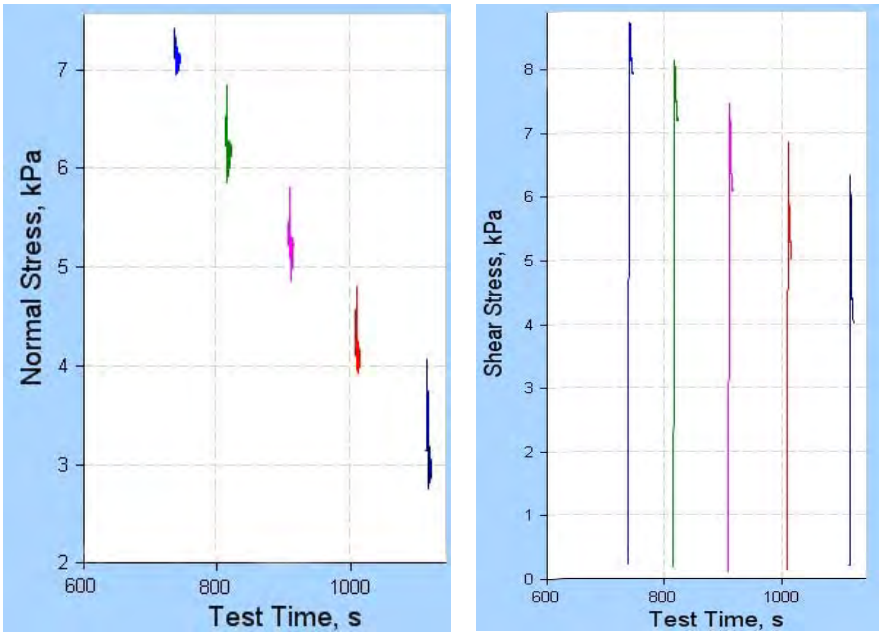

(a) (b)

Figure 3.6 Recorded (a) normal stress, and (b) shear stress. (Magnetite, 25-75μm, 5% moisture, 9KPa pre-consolidation pressure)

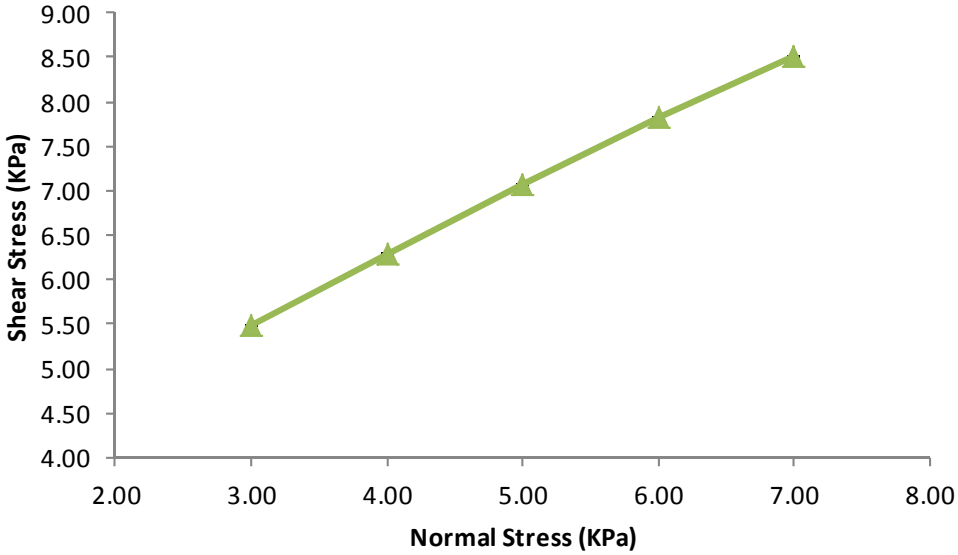

Figure 3.7 Yield locus line (magnetite, 25-75μm, 5% moisture, 9KPa pre-consolidation pressure).

3.4 Procedure of uniaxial compression

After the particles were sieved and mixed with water in the sample preparation, the next step of the testing was die compaction. Silicone oil was chosen as a lubricant to reduce the friction between the iron ore particles and the die wall. The inner wall of the die and the surface of both upper and lower piston were lubricated uniformly by the silicone oil. Although shown significant influence on increasing the density of compacted samples, internal lubricants were not used in this experiment to avoid contamination of iron ore particles.

The weight of samples in the die was about 5 grams that resulted in a height-diameter ration of 2:1 after applying an initial load of 227g, which was the weight of the upper die platen. The initial weight of the particles was measured by an electronic balance and the height between the upper surface of upper piston and the upper surface of the die h_0 were measured by the calliper. Those data were recorded to calculate the initial density of the sample ρ_i. The die is shown in Figure 3.8. The dimensions of the die were measured by the calliper with the height of 50.25 mm and the inner diameter of 12.74 mm. The length of the upper and lower pistons were 49 mm and 11.00 mm, respectively.

Figure 3.8 Compaction die

The compaction machine in this experiment was Universal Testing Machine Instron 5566 with maximum load 5 kN (Figure 3.9). Two flat round platens were installed on the machine, one was installed on the crosshead and the other was installed on base adapter. Those two platens were fixed with two steel column pins to reduce the shake of two platens during testing. The load cell, which was in the crosshead, recorded the change of the compaction force. The computer, which was connected with the machine, recorded those data and plotted the graph. Control panel of the machine and the Instron application software in the computer controlled the testing.

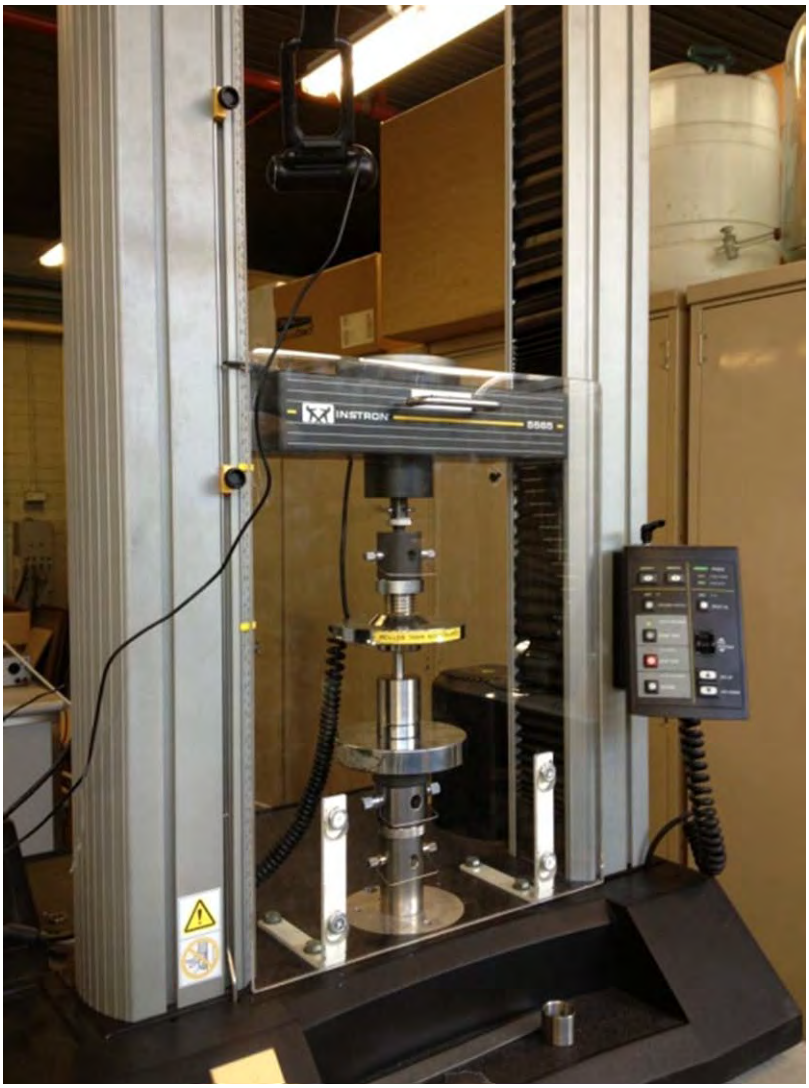

Figure 3.9 Universal Testing Machine Instron 5566

In the compaction, the compaction die was placed at the centre of bottom flat platen which was attached to the base adapter. After that, the upper flat platen, which was attached to the crosshead, was adjusted to touch the upper flat platen of the die accurately by using the control panel. Then the compaction testing was conducted under the control of pre-established compaction model in the software. The extension of the crosshead was recorded by computer, which could determine the relative density change of the samples. The experiment stopped at the pre-set load and then load moved upwards. After compaction, the compacted sample was ejected from the die. In order to calculate the final relative density and the strain in the unconfined compression, the weight and height of the sample were measured again.

The computer plotted load-extension graph is shown in Figure 3.10. The different curves

in the graph have different starting point. The difference is about 0.5 between two close curves. However, the purpose of the difference is to show the curves more clearly, the starting point in the raw data which are provided by computer is still all in zero. In addition, the graph is plotted by two parameters, load and extension, which should be transformed to stress and relative density respectively by further calculation in the data analysis part. The calculation will be discussed in the following section.

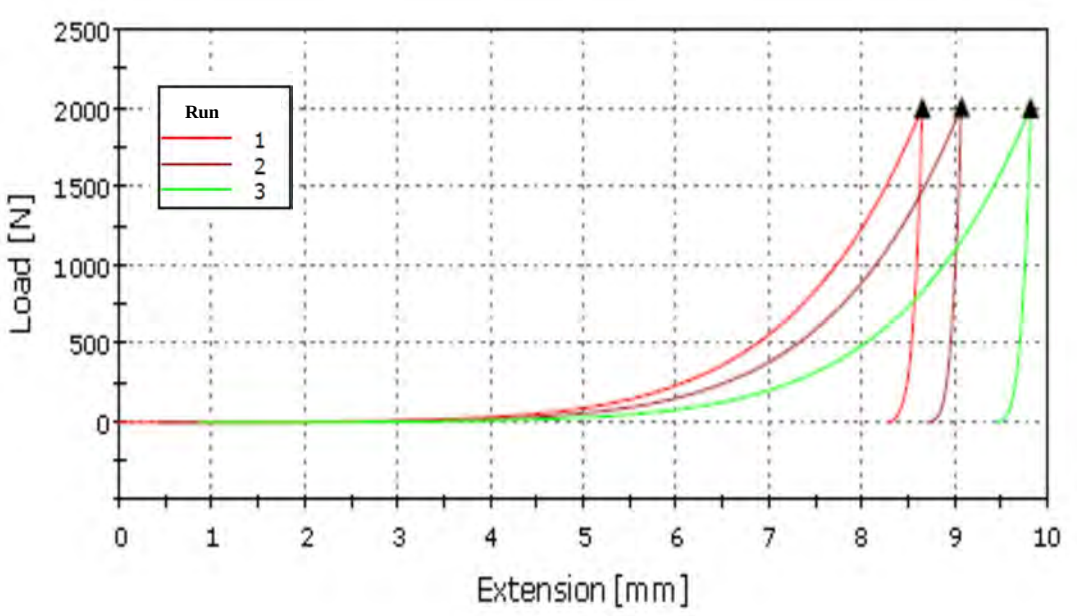

Figure 3.10 Load-extension graph of the die compaction testing

The unconfined uniaxial compression was conducted to exam the compressive strength of compacts. The compacted sample was placed onto the centre of the bottom flat platen, which was installed on the base adapter, and then a rigid plastic plate was added on the compacted sample as a top lid. The upper flat platen, which is installed on crosshead, was adjusted to touch the top lid accurately by the control panel. The compression procedure was controlled by the pre-established compression model of the software. The load was then added by the crosshead at a constant speed until the compacted sample fractured (Figure 3.11b).

Figure 3.11a shows a typical force-displacement curve obtained from a unconfined uniaxial compression. After reaching the peak load, the load decreases with displacement. Unlike the sudden drop on the load which is often observed for the compression of brittle materials, the decrease for the compact is relatively slow and smooth, indicating the

compact behaves more like a ductile materials in compression. This can also be observed in Fig. 3.11b which shows while the compact fractured, it was not crushed completely.

The different curves in the graph also have different starting point for same reason in the die compaction part. The force-displacement graph will be transformed to stress and strain in next chapter.

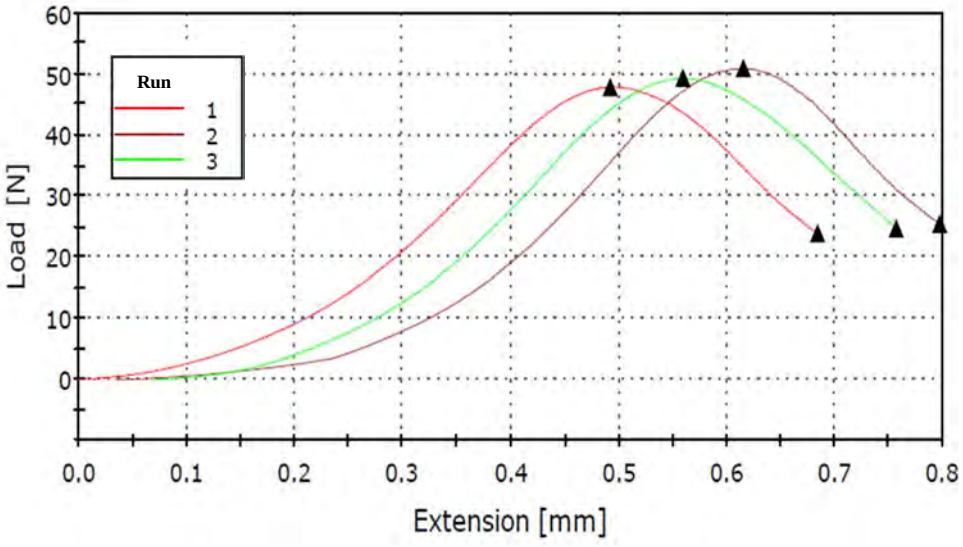

(a)

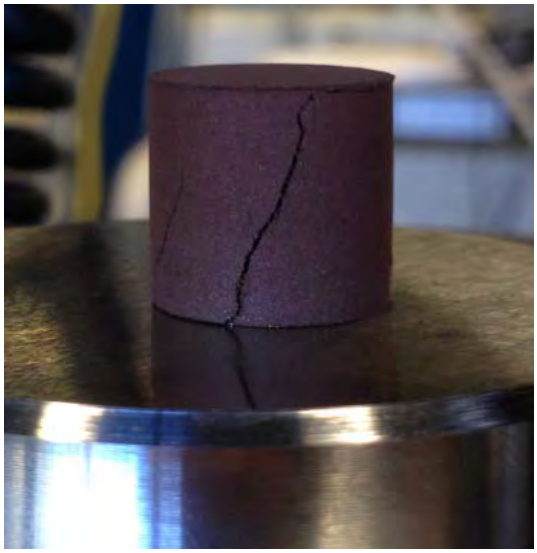

(b)

Figure 3.11 (a) Load-extension graph of the unconfined compression testing; and (b) a fractured sample after unconfined compression.

3.5 Procedure of diametrical compaction

In order to measure the tensile stress of compacts, the experiment of diametrical compaction was conducted. The tensile stress (σ_0) of the tablet can be obtained from its breakage stress of diametric compaction (Fell and Newton, 1970), given by

$$\sigma_0=\frac{2P}{\pi Dt} \qquad 3.2$$

where P is the applied load, D and t are, respectively, the diameter and thickness of the sample.

The experiment procedure of diametrical compaction also consisted of two main steps, die compaction and diametrical compaction. The procedure of die compaction was almost the same as what was used in the uniaxial compaction except the weight of the particles was the half of the weight in the uniaxial compaction. This was because the final height-diameter of the compact was 2:1.

The procedure of diametrical compaction was similar to the procedure of the unconfined uniaxial compression. The compacted tablet was placed onto the centre of the bottom flat platen in horizontal direction. The rigid plastic plate was also placed on the top of the tablet to protect the machine. The upper flat platen was adjusted to touch the plate accurately by using the control panel. The whole behaviour of compression was controlled by the pre-established compression model of the software. The load was added by the crosshead at a constant speed until the compacted sample was fractured. Figure 3.12a shows a typical force-displacement plot obtained in the diametrical compression and Figure 3.12b shows the compact broke into two parts after the compaction.

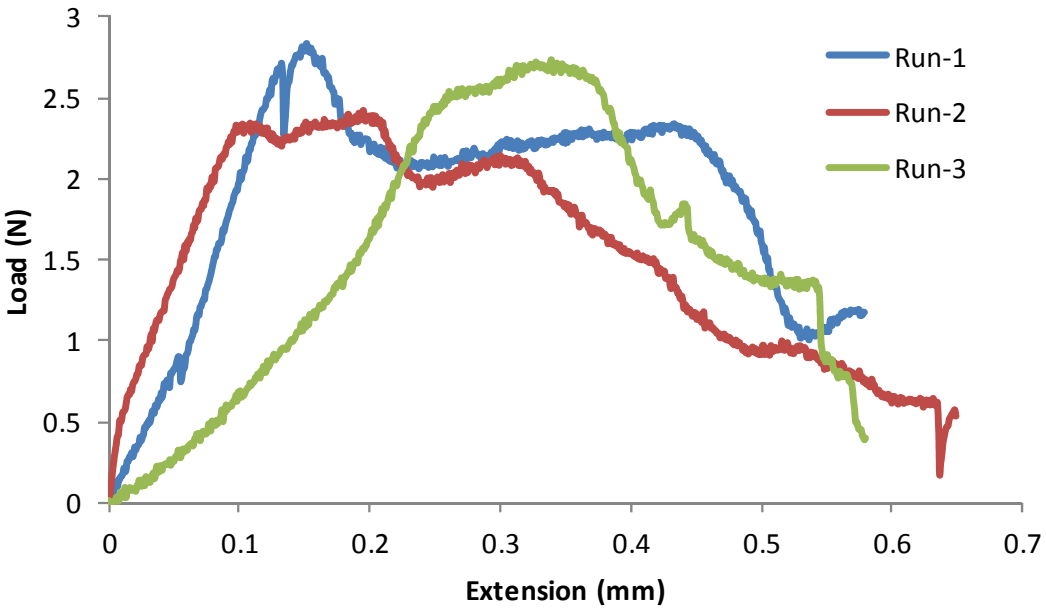

(a)

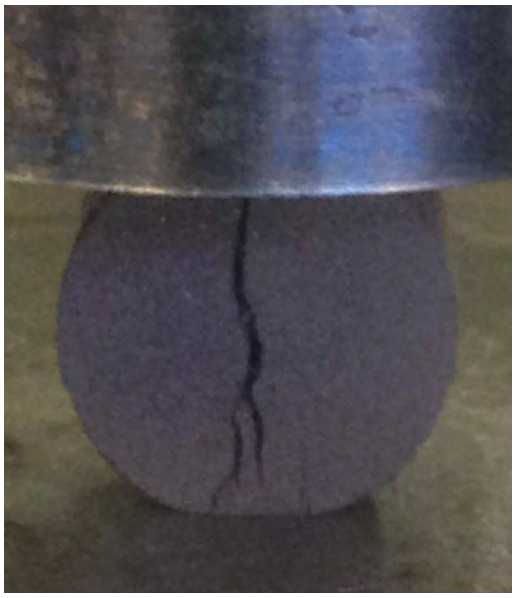

(b)

Figure 3.12 (a) Load-extension graph of the diametrical compression testing, and (b) a fractured tablet after diametrical compression.

3.6 Summary

This chapter describes the experimental procedures of the work. Firstly, the experiment of characterization of the flowability of iron ore fines was done using the Freeman FT4 Rheometer. The particle size range and moisture content were varied in the experiments. In the unconfined uniaxial compression and diametrical compression processes, the compacts were tested under the pre-established model which controlled compression

speed and maximum load of the experiment and recorded the information of force on and displacement of the upper punch. Key parameters such as particle size, maximum load, moisture content, were varied to study their effects on the structure and strength of the compacts.

Chapter 4 Characterization of flowability of particles

4.1 Introduction

Flowability is an important property of particles (Schulze, 2008). Characterisation of flowability of fine particles can help alleviate problems on handling, storing and transporting of particles.

There are many ways to characterise the flowability of particles. Shear testing is the most common method among them. The yield locus lines can be plotted from the testing and the Mohr circle can then be drawn based on those results. And the parameters of cohesion, major principal stress, minor consolidating stress and unconfined yield stress can be calculated from the Mohr circle. To conduct the shear testing of those iron ore particles, Freeman Technology FT4 Rheometer was used. Two types of iron ores (magnetite and goethite) were used to undergo the shear testing.

This chapter is divided to four sections. The first part is to analyse the result from FT4 based on a single case. The other three parts are to investigate the effects of powder material size and moisture content on particle flowability.

4.2 Flowability of particles

The analysis of particle flowability is based on the magnetite particles. The particles have size of 25-75 μm and was mixed with 5% (mass ratio) moisture content. The particles were pre-consolidated using a 9KPa load. During the shear testing, the shear stress and normal stress were recorded by FT4 rheometer. Figure 4.1 shows the normal and shear stresses of the magnetite particles from FT4 rheometer. Fig. 4.1a shows the normal stress (compression stress) is fluctuated during each point. However, when the compression stress coincides with the pre-set stress, the shear stress was recorded, which is the peak of each curve in Figure 4.1a. And then, based on the value of recorded compression stress and shear stress, a yield locus line can be drawn (Figure 4.2) along with the pre-shear point.

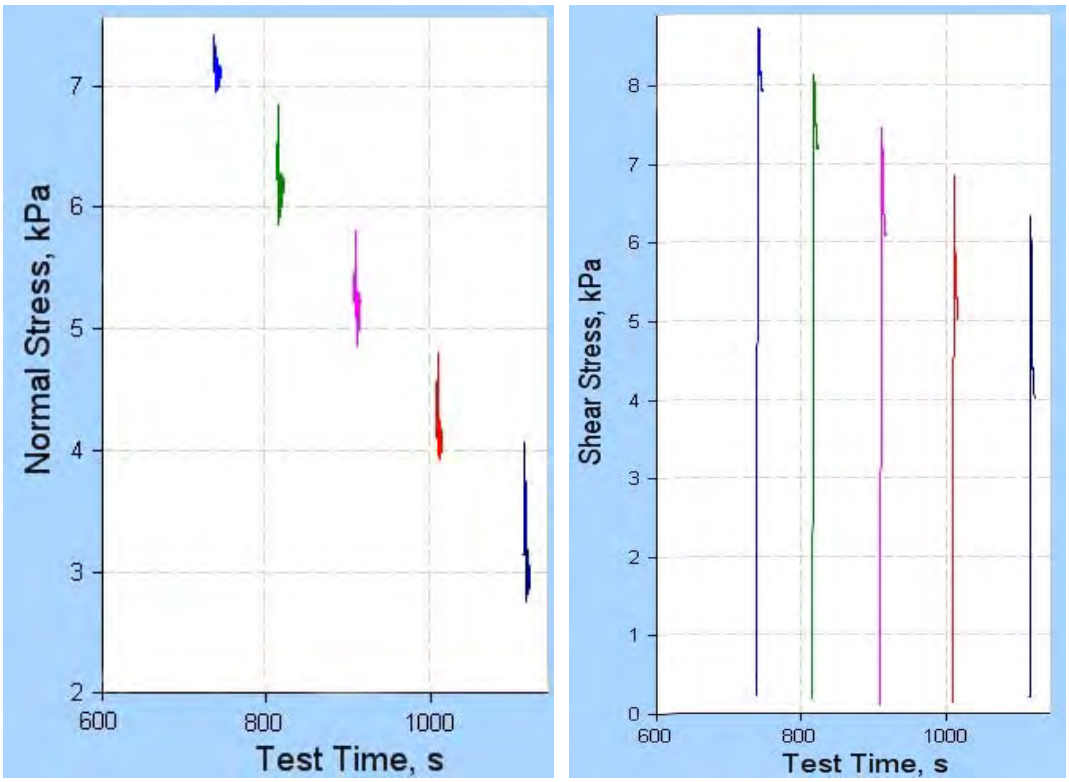

(a) (b)

Figure 4.1 Recorded (a) normal stress and (b) shear stress (magnetite, 25-75µm, 5% moisture, 9KPa pre-consolidation pressure).

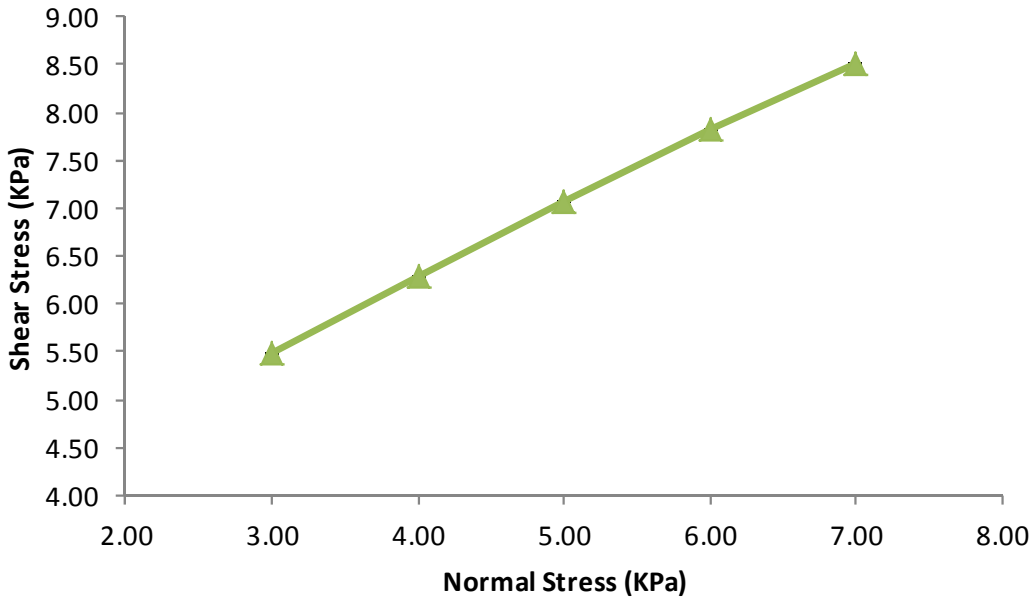

Figure 4.2 Yield locus line (magnetite, 25-75µm, 5% moisture, 9KPa pre-consolidation pressure)

For yield locus, there is a small Mohr stress circle that represents the stress state at the

end of consolidation. From the shear test, the pre-shear point was obtained. By this point and yield locus there is a large Mohr stress circle. It represents the normal and shear stress acting in the horizontal cutting plane at steady-state flow. The major and minor consolidation pressures can be obtained from the large Mohr stress circle and unconfined yield stress can be found from the small Mohr stress circle.

Thus, based on the recorded yield locus line and pre-shear point, two Mohr circle can be plotted. The large Mohr circle intersects the pre-shear point and tangency the yield locus, the small Mohr circle intersects the zero point and tangency the yield locus (Figure 4.3).

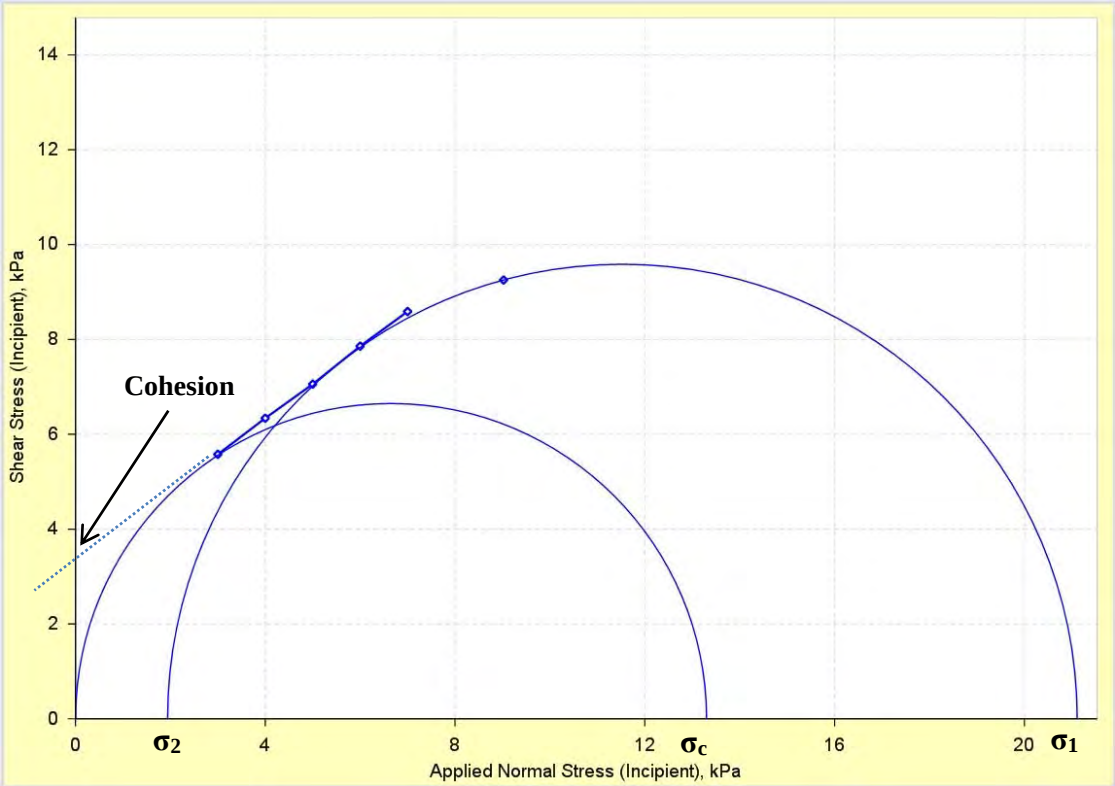

Figure 4.3 Mohr circles based on yield locus line and pre-shear-point.

As shown in Figure 4.3, each Mohr circle has two intersections with the x axis. The major consolidation stress (σ_1) is the intersection between the large Mohr circle and x axis which has a larger value. The minor consolidation stress (σ_2) is the intersection between the large Mohr circle and x axis which has a smaller value. The unconfined yield stress (σ_c) is the intersection between the small Mohr circle and x axis which is not zero. The value of cohesion (τ_c) can be obtained by the coinciding point of y axis and the extension of yield locus line. In addition, the flow function (FF) of tested materials can be calculated from

the values of the major principal stress and the unconfined yield stress, given by:

$$FF=\frac{\sigma_1}{\sigma_c} \qquad 4.1$$

This is based on the 9KPa pre-consolidation pressure. In the experiments most samples were conducted by four different compression pressures, 3KPa, 6KPa, 9KPa and 15KPa. Thus, a series of results of flowability can be obtained, such as unconfined yield stress (Figure 4.4), cohesion (Figure 4.5) and flow function (Figure 4.6) as the functions of major principal stress (MPS). Each sample with the same condition was tested three times and the average value was calculated. The error bar in the figure shows the standard deviation of each condition.

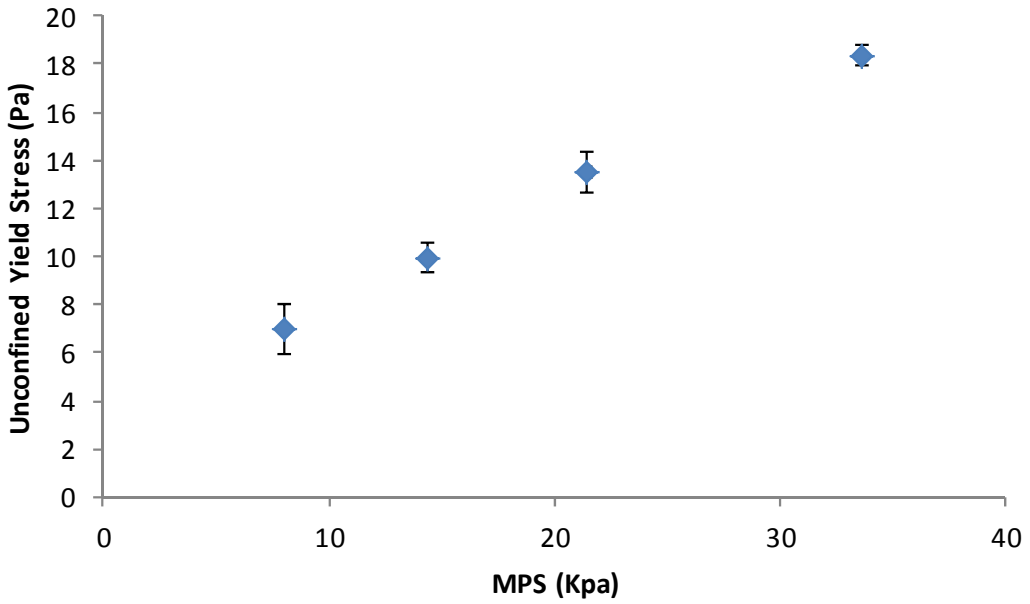

Figure 4.4 Unconfined yield stress (magnetite, 25-75μm, 5% moisture).

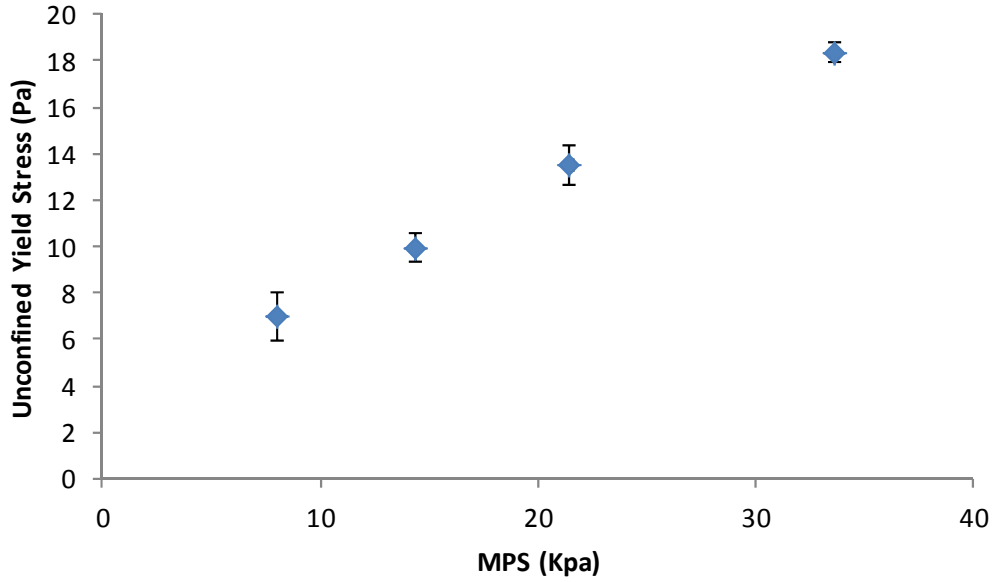

Figure 4.5 Cohesion (magnetite, 25-75μm, 5% moisture).

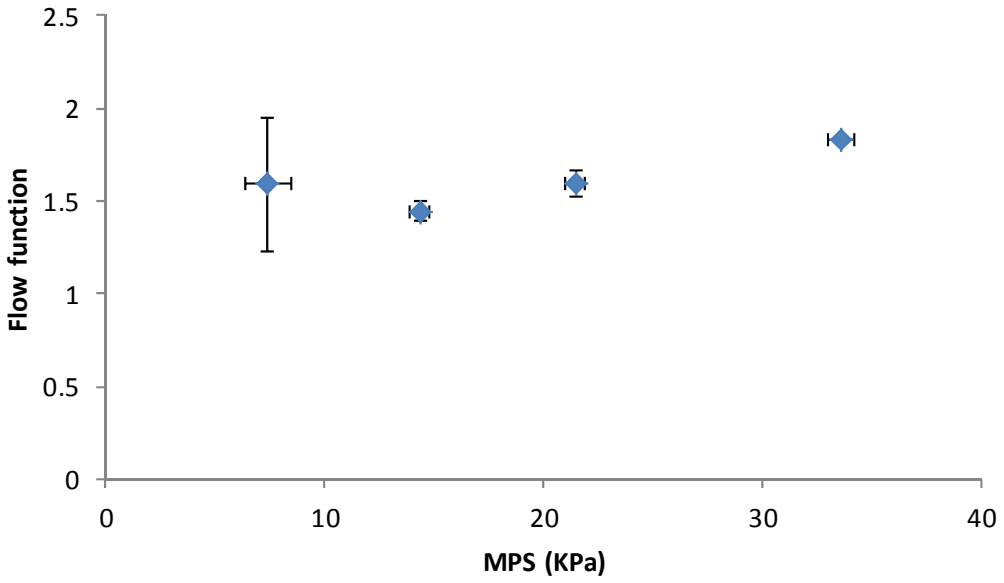

Figure 4.6 Flow function (magnetite, 25-75μm, 5% moisture).

4.3 Effects of iron ore properties

Different types of ores may have different flowabilities. In the experiments, two types of iron fines, magnetite and goethite, were tested with moisture content 5% (mass ratio) and the particle size 25-75μm. The flowability was tested under four different compression pressures from 3KPa to 15KPa.

Figure 4.7 shows the results of unconfined yield stress (σ_c) of two ore fines obtained under

different major principal stresses, which were caused by different pre-consolidation pressures. It is obvious that the magnetite particles have much higher unconfined yield stress under the same major principal stress than the goethite particles. In addition, the unconfined yield stress of magnetite increases sharply with the major principal stress. On the other hand, the unconfined yield stress of goethite compacts are much lower and its increase with MPS is slow from 0.8 KPa to 1.9 KPa when MPS increases from 9 KPa to 27 KPa.

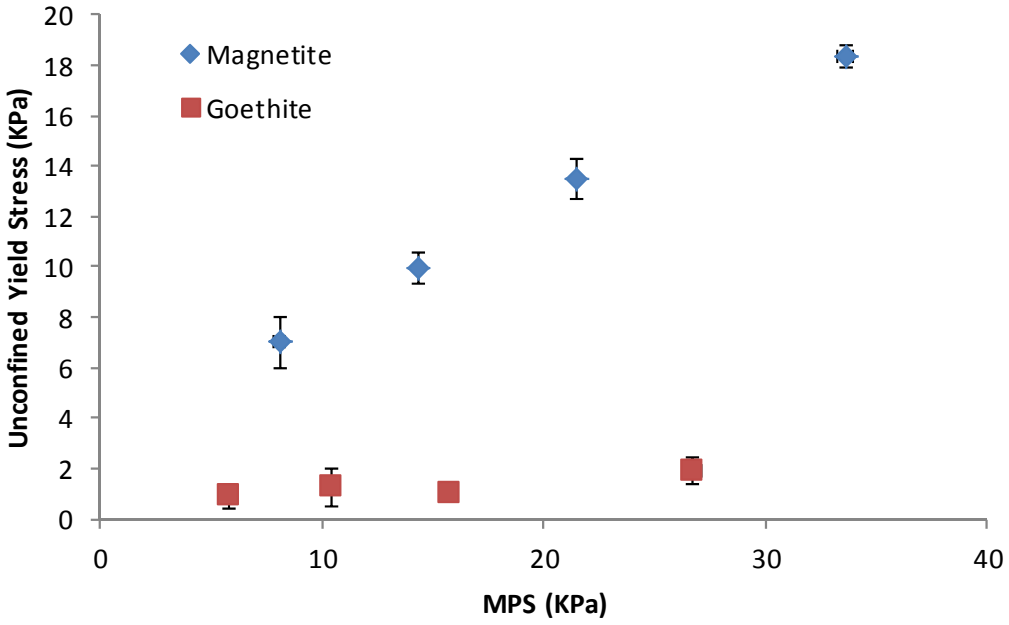

Figure 4.7 Relationship of major principal stress and unconfined yield stress of magnetite and goethite (5% moisture, 25-75μm)

Figure 4.8 shows the variation of cohesion with MPS. The magnetite particles are more cohesive than the goethite particles. This is the reason that the magnetite compacts have higher unconfined yield stress under the same major principal stress. And the cohesion of magnetite increases sharply with the increase of major principal stress. However, the goethite is fluctuated in a small range with the rise of major principal stress. It is because of the larger error of FT4's results on testing relatively free-flowing particles.

The results of flow function are shown in Figure 4.9. A larger flow function means more free-flowing of materials. The flow function of magnetite is relatively small and only increases slightly with increasing major principal stress, except with the 3KPa pre-consolidation stress. This may be caused by the unstable state of particles at low pre-

consolidation pressure. And the flow function of goethite increases sharply with the increasing major principal stress. In addition, the varying range of results of goethite is larger. This is because FT4 is hard to measure the parameters of non-cohesive particles. Therefore, the goethite particles is more free-flowing than the magnetite particles.

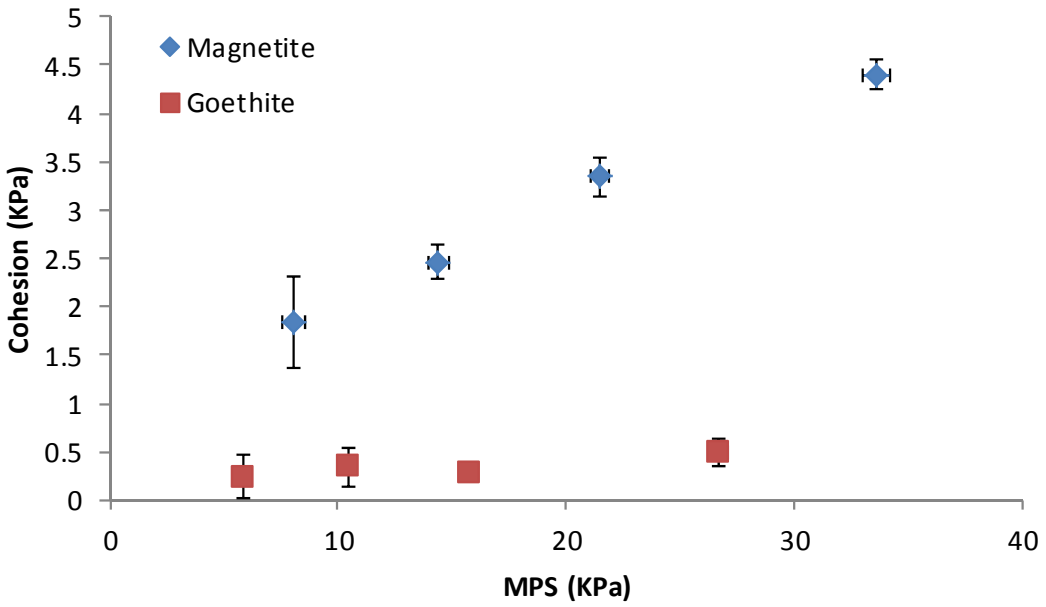

Figure 4.8 Relationship of major principal stress and cohesion of magnetite and goethite (5% moisture, 25-75μm).

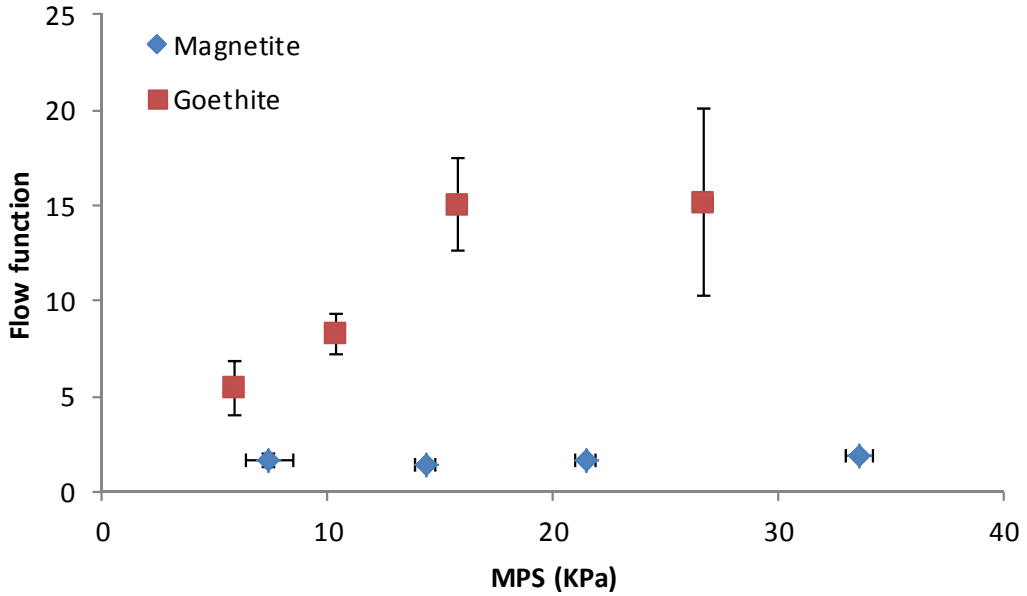

Figure 4.9 Flow functions of magnetite and goethite (5% moisture, 25-75μm).

4.4 Effect of particle size

The flowability of particles is also affected by the size of the particles. In the section, the moisture content was 5% (mass ratio) and the tested material was magnetite. The particle size ranges were 25-75μm and 200-280μm. The material was also tested under four different compression pressures, including 3KPa (only 25-75μm), 6KPa, 9KPa and 15KPa. Different compression pressures generated each major principal stress of two different sized particles.

Figure 4.10 shows the results of cohesion of two sized particles. The curve of the 200-280 μm particles is more fluctuated and has relatively large experimental variations. The relatively larger error bars for the large particles are due to the reduced cohesion of the compact of large particles. It is well known the inter-particle cohesion decreases with increasing particle size and therefore the measured values are more affected by other parameters, such as compact structure and sensitivity of the facility, causing poorer reproducibility for larger particles than for smaller particles. On the other hand, the cohesion of the 25-75μm particles increases steady with increasing major principal stress.

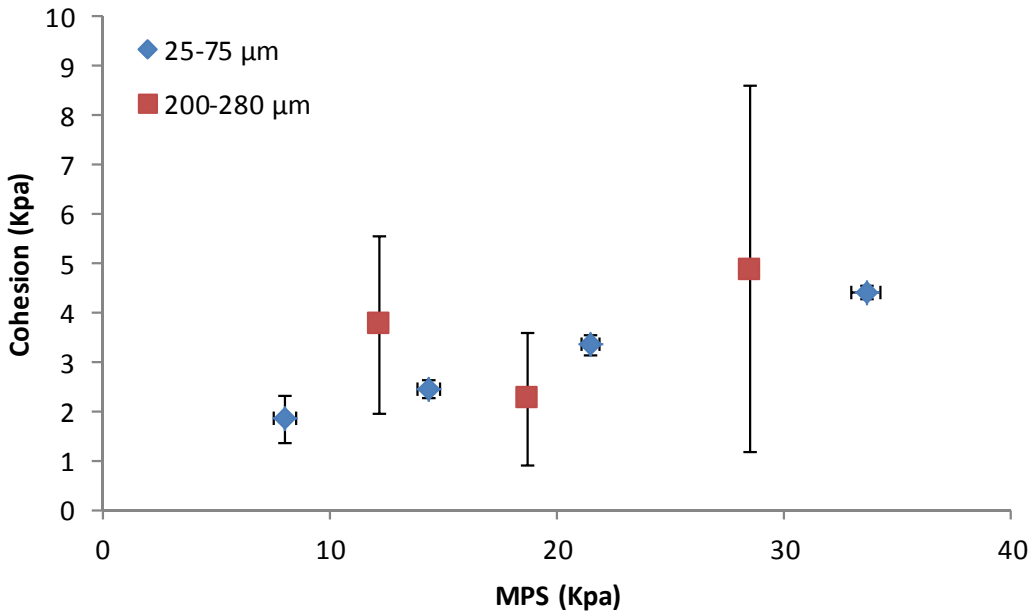

Figure 4.10 Relationship of cohesion and minor consolidating stress of particles with 25-75μm and 200-280μm (magnetite, 5% moisture).

Figure 4.11 shows the variation of the unconfined yield stress with MPS. The cohesion of the 25-75μm particles increases steadily while the curve of 200-280 follows a similar

trend. The unconfined yield stress of two sizes are similar with the same major principal stress. The larger experimental variation of the lager particles is because FT4 has difficulty measuring the parameters of non-cohesive particles.

The flow functions of two sizes of particles can also be obtained. From the Figure 4.12, the smaller particle are more cohesive than the larger particles. And the larger particles shows a more upward trend. The results indicate that the small particles are difficult to flow while but the large particles are more free-flowing.

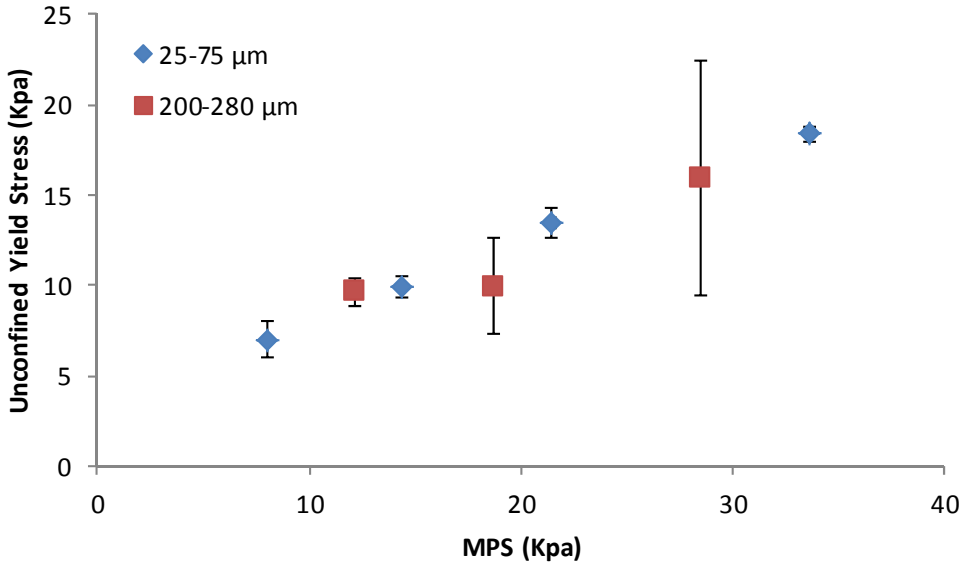

Figure 4.11 Relationship of major principal stress and unconfined yield stress of particles with 25-75µm and 200-280µm (magnetite, 5% moisture).

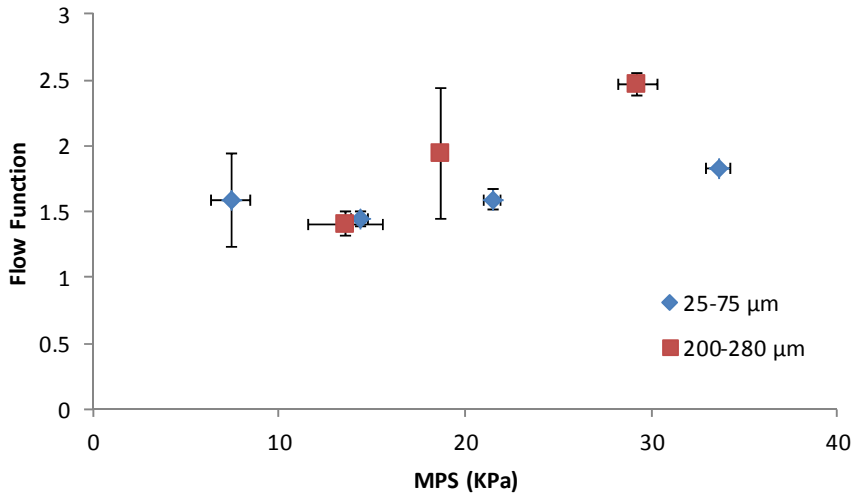

Figure 4.12 Flow functions of particles with 25-75µm and 200-280µm (magnetite, 5% moisture).

4.5 Effect of moisture content

Moisture content also influences the flowability of particles. In this section, the experimental conditions were as follows: the particle size range was 25-75μm, and the tested iron ore fines were magnetite and goethite. Three moisture contents, 2.5%, 5%, and 7.5% (mass ratio), were adopted in the experiments. The materials were tested under four different compression pressures including 3KPa, 6KPa, 9KPa and 15KPa. This section will be divided to two sections to discuss the effect of moisture content on the magnetite and goethite particles, respectively.

4.5.1 Effect of moisture content on magnetite particles

Figure 4.13 shows the variation of cohesion with different moisture contents. The cohesion of the particles with 2.5% moisture contents is lower than those with 5% and 7.5% moisture contents which are almost the same. This means moisture content plays an important role in the early stage but its role is getting smaller with increaing moisture content. In fact, adding too much water may actually decreases cohesion due to its lubricating effect.

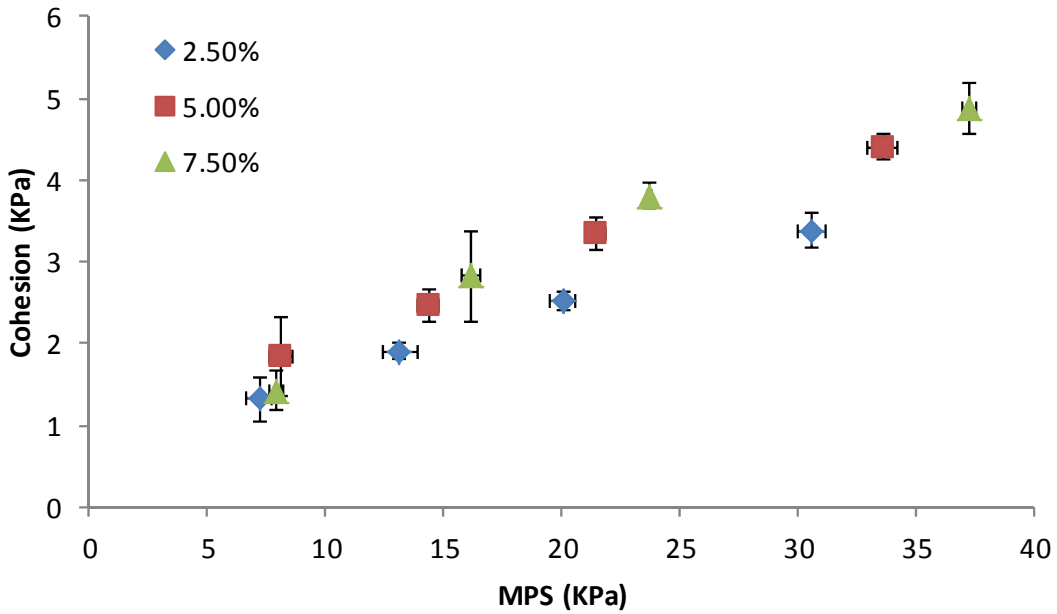

Figure 4.13 Relationship of cohesion and minor consolidating stress of particles with 2.5%, 5% and 7.5% moisture contents (magnetite, 25-75μm).

Figure 4.14 indicates that the unconfined yield stress also shows a similar trend to those

of cohesion. The unconfined yield stress with 2.5% moisture content is lower than those with 5% and 7.5% moisture contents and the unconfined yield stress with 7.5% is slightly higher that with 5% moisture content.

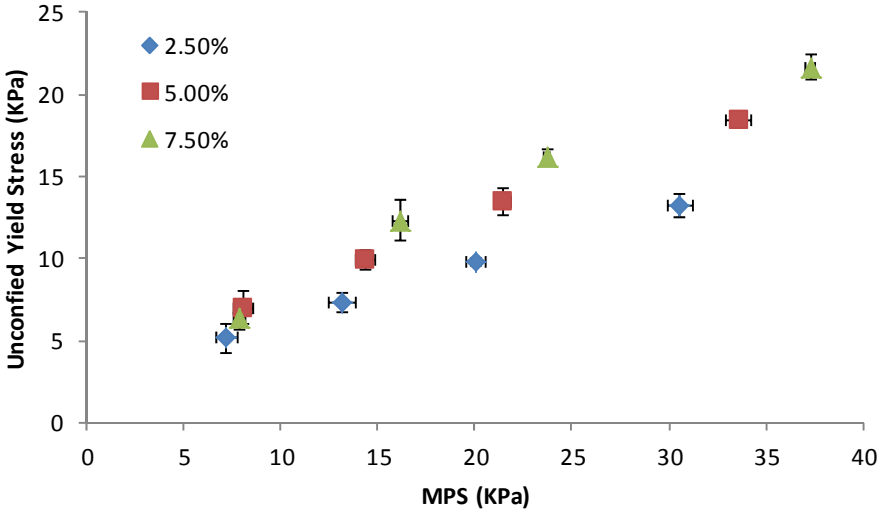

Figure 4.14 Relationship of major principal stress and unconfined yield stress of particles with 2.5%, 5% and 7.5% moisture contents (magnetite, 25-75μm).

Figure 4.15 shows that the particles with 7.5% moisture content are the most cohesive, followed by the particles with 5% and 2.5% moisture contents, respectively. The dry particles have the largest flow function. This means that the flowability of magnetite particles decreases with increasing moisture content.

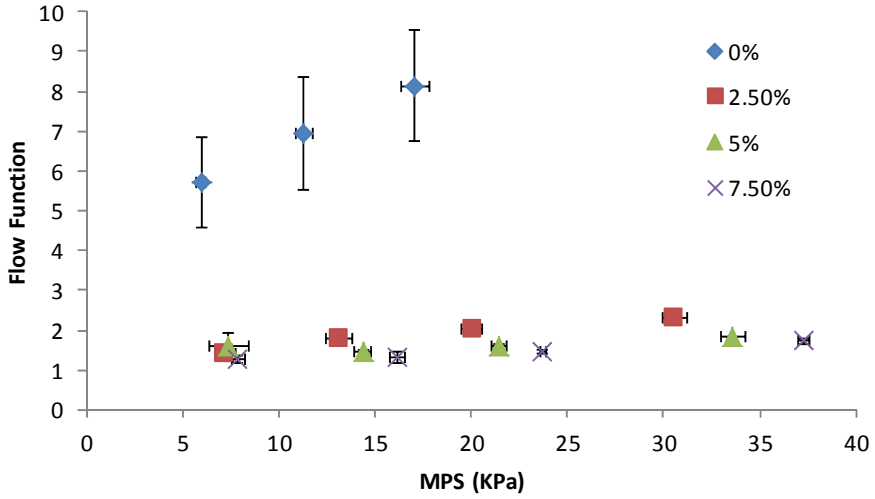

Figure 4.15 Flow functions of particles with 0%, 2.5%, 5% and 7.5% moisture contents (magnetite, 25-75μm).

4.5.2 Effect of moisture content on goethite particles

Figure 4.16 shows the change of the cohesion of goethite particles with different moisture contents. The cohesions with 2.5% and 5% moisture content are very low, but the particles with 7.5% moisture content have much higher cohesion. In addition, the inter-particle cohesion with 2.5% and 5% moisture content only increases slightly with the major principal stress but the cohesion with 7.5% moisture content has a dramatic increase sharply with the major principal stress. The results are very different from those of the magnetite particles. This means moisture has no much influence on cohesion at relatively low content. However, when the moisture content is larger than 5%, its effect on cohesion is more significant, particular at large major principal stress.

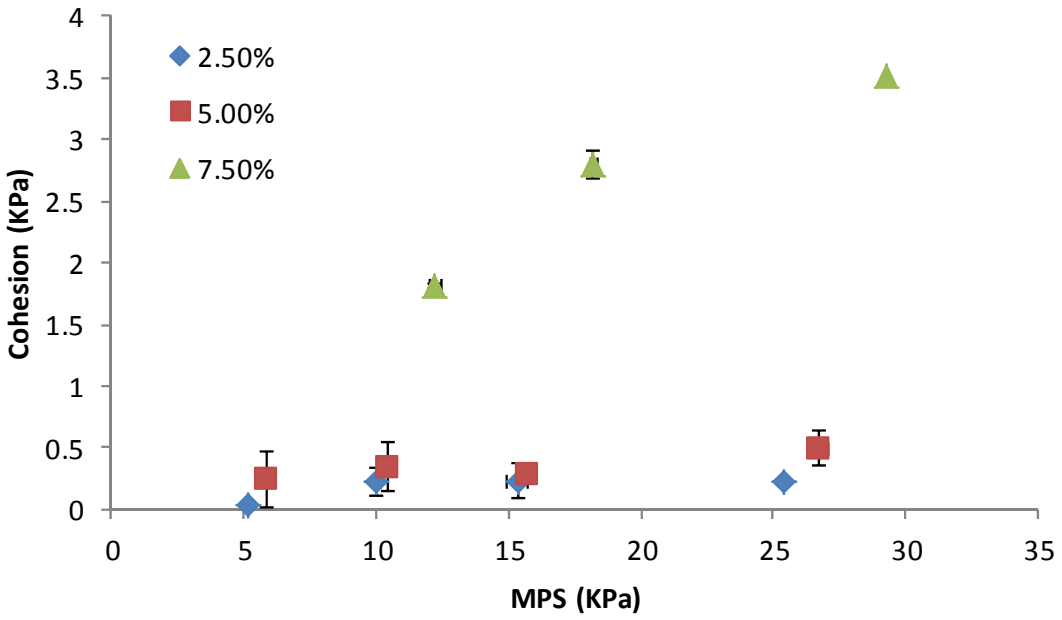

Figure 4.16 Relationship of cohesion and minor consolidating stress of particles with 2.5%, 5% and 7.5% moisture contents (goethite, 25-75μm).

Figure 4.17 indicates that the unconfined yield stress of the goethite compacts with moisture content shows a similar trend to that of cohesion: the unconfined yield stresses with 2.5% and 5% moisture contents are lower and increase slower with load, while the unconfined yield stresses with 7.5% moisture content is relatively higher and increases sharply with the major principal stress. This means that higher moisture content is more effective in increasing unconfined strength of the goethite compacts.

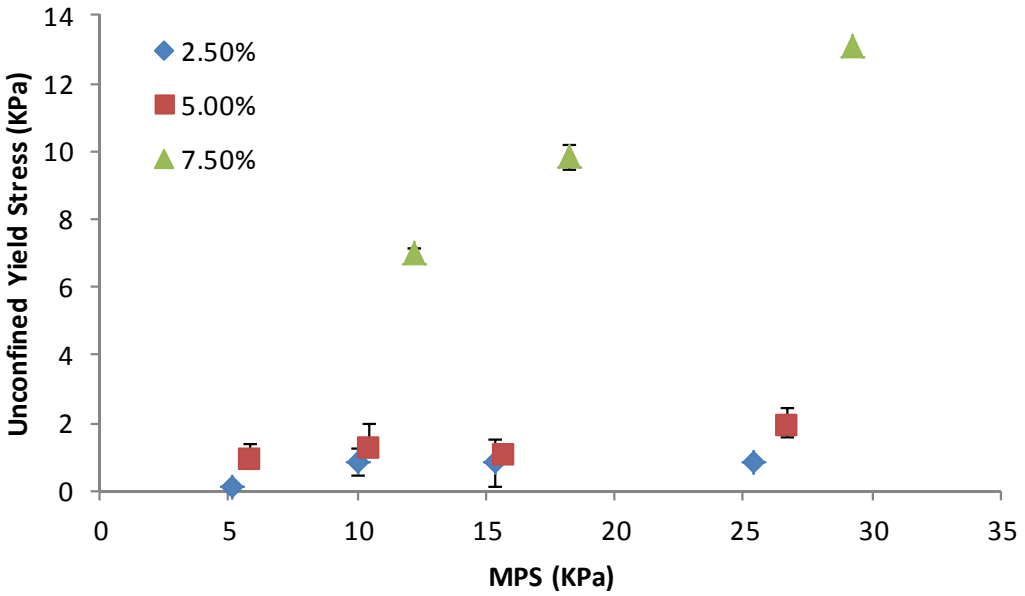

Figure 4.17 Relationship of major principal stress and unconfined yield stress of particles with 2.5%, 5% and 7.5% moisture contents (goethite, 25-75μm).

Figure 4.18 shows that the flow function of goethite is much higher than that of magnetite particles. The flow functions of goethite compacts with 2.5% and 5% moisture content are higher and increase with the major principal stress. However, the flow function with 7.5% moisture content is much lower and is almost unchanged with the major principal stress.

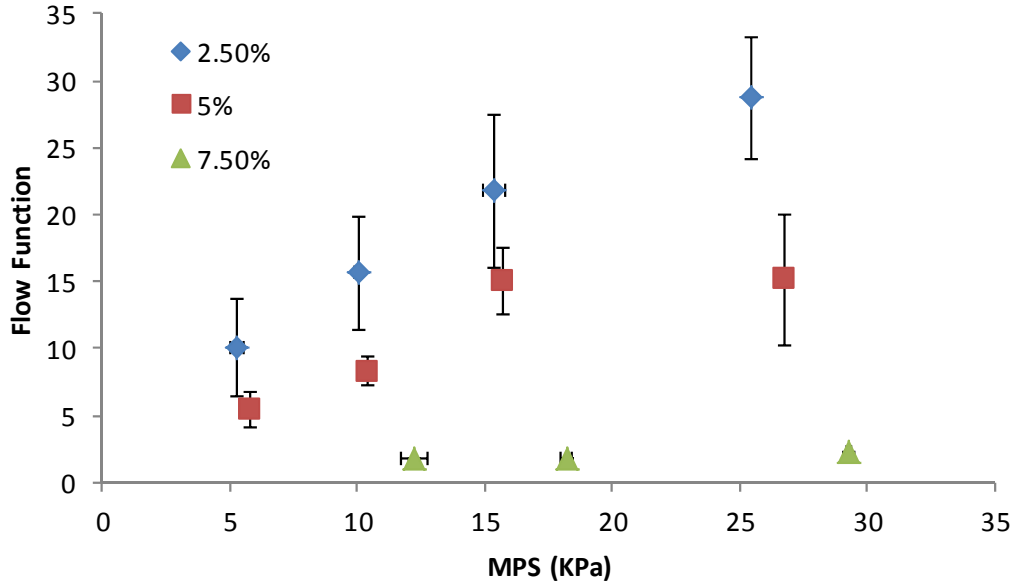

Figure 4.18 Flow functions of particles with 2.5%, 5% and 7.5% moisture contents (goethite, 25-75μm).

4.6 Summary

In this chapter, the shear testing experiments were conducted to analyse the flowability and compactability of magnetite and goethite particles. By plotting the yield locus from the experiments, unconfined yield stress, cohesion and flow function were calculated. The effects of materials, particle size and moisture contents were investigated.

The results showed that the magnetite compacts have higher cohesion, unconfined yield stress and lower flow function than the goethite compacts, suggesting the magnetite particles are more cohesive than the goethite particles. Also larger particles has lower flow function than smaller particles, therefore are more free-flowing.

Moisture content shows similar effect to both magnetite and goethite particles: particles with higher moisture content have higher unconfined yield stress, cohesion and flow function. However, the effect of moisture is relatively smaller on magnetite particles and goethite particles when the content was less than 5%, but its influence on goethite particles is much higher when the moisture content is higher than 5%.

Chapter 5 Crushing strength of iron ore fine compacts

5.1 Introduction

The presence of iron ore fines raises the cost of handling, inconvenience of transport and may result in negative health impact, such as inhalation (Schulze, 2008). The compaction or briquetting process can be applied to enlarging the size of iron ore fines to solve those problems. The crushing strength and relative density of compacted particles are affected by many factors, including materials properties, particle size, moisture content and lubricant. This work is to identify the influence of these parameters.

5.2 Pressure, relative density and compact strength

In the die compaction experiments, the magnetite powders, which has the size of 25-75μm and 5% moisture, is compacted under the compaction force of 2000N. The loading speed and unloading speed in the experiments are 3mm/min. The compacted sample is shown in Figure 5.1.

The load-displacement data obtained from the experiments are shown in Figure 5.2a. For comparison, it is necessary to convert the load (F) and displacement (L) to pressure (P) and relative density of the compacts (ρ_r). Compaction pressure is the average force per unit area. And the relative density is the packing density of particles. As a consequence, Figure 5.2a can be transformed to Figure 5.2b.

The rising part of the die compaction curve in Fig. 5.2b is the loading part. The peak value of die compaction curve is the pre-set compaction pressure. In addition, the decreasing part is the unloading part, which also reflects the elastic deformation of particles. The end point of the unloading part of the curve is the final relative density. Each experiment is repeated three times to minimize the error. Three curves are almost the same, which means the experiment are robust and reproducible. The average value is revealed in the relative density and compaction pressure figure. The error bar of standard deviation is also shown.

Figure 5.1 Compacted particles

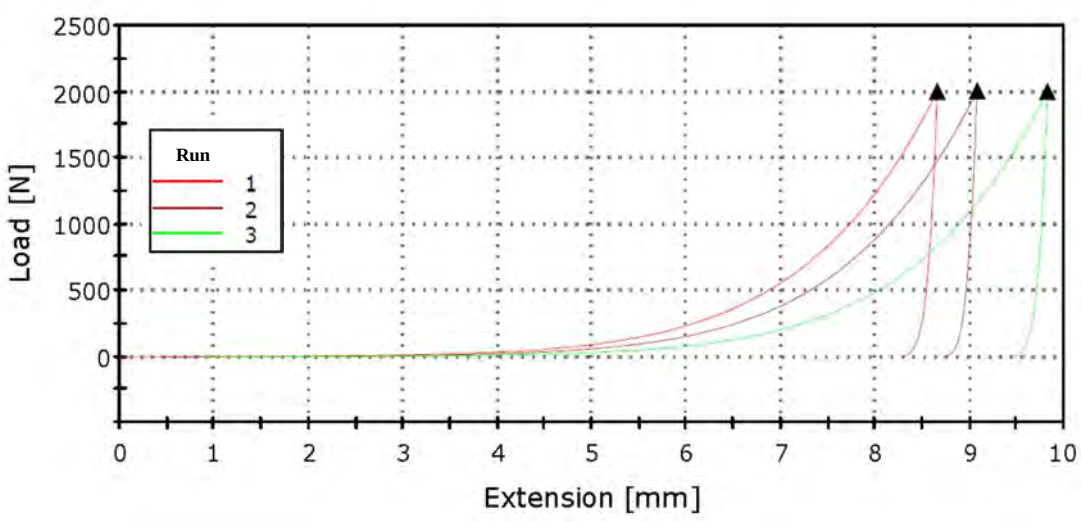

(a)

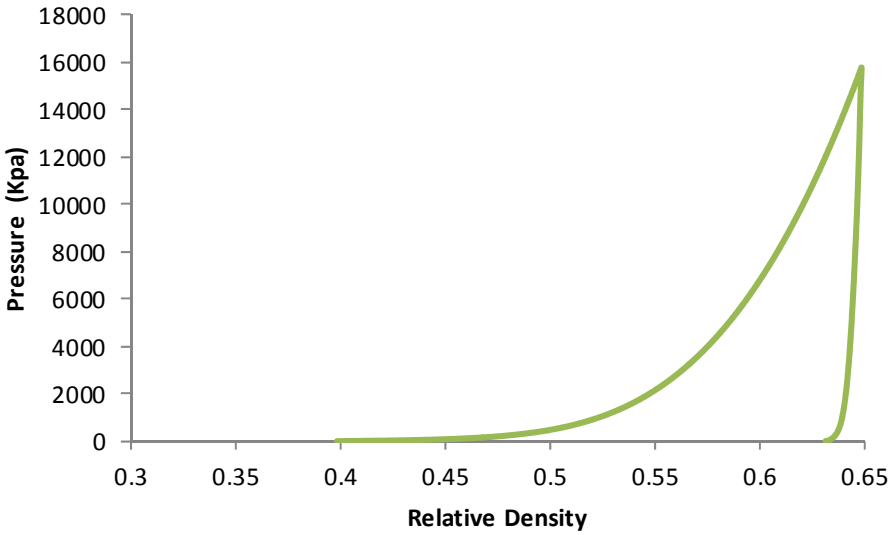

(b)

Figure 5.2. (a) Load-extension graph of the die compaction testing and (b) transformed die compaction curve (magnetite, 25-75μm, 5% moisture content, 2000N)

Heckel Equation can be used to analyse the compression parameters that are related to the deformability of the particle, which is given by

$$\ln \frac{1}{1-D} = KP + A \qquad 5.1$$

where D is the relative density of the compacted particles, K (Pa^{-1}) and A are constants. P is the compaction pressure (Pa). K is related to the plasticity of a compressed material and A is a measure of die filling and particle rearrangement before deformation and bonding of the discrete particles.

Based on Equation 5.1, Figure 5.2 can be converted to Figure 5.3. And the K and A can be found by the equation of the trend line. In addition, K is the reciprocal of the mean yield pressure, P_y, which is a measure of the ability of material to deform plastically. The results of A, K and P_y can be obtained from the trend line, which gives A of 0.85, K of 0.0112 Pa^{-1} and P_y of 84.75 Pa.

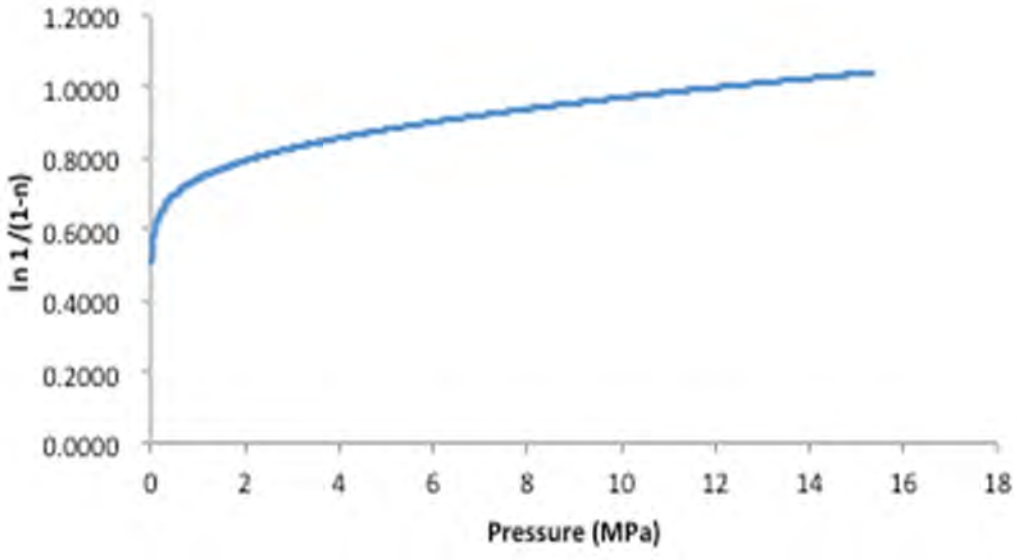

Figure 5.3 Relationship of ln 1/(1-D) and pressure by Heckel Equation (magnetite, 25-75μm, 5% moisture content, 2000N)

In the unconfined compression, the compact is compressed with the compression speed of 2mm/min. Fig. 5.4 shows the fractured compact which shows a shear fracture from top to bottom.

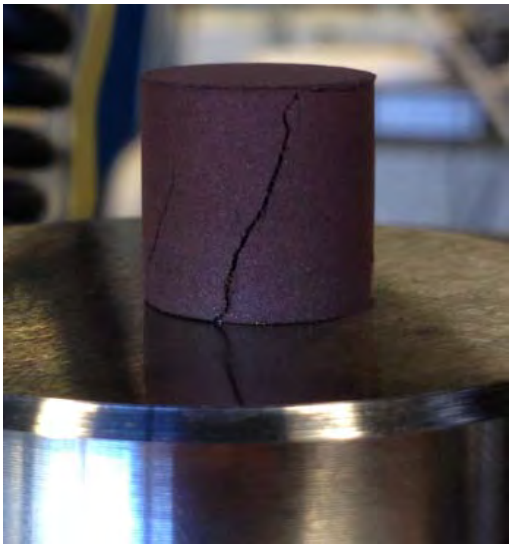

Figure 5.4 A fractured sample after the unconfined compression

The force-displacement plot is shown in the Figure 5.5a. The three curves are the three runs of experiments under the same experiment condition. As the graph is also plotted as load and punch displacement, it is required to change the load (F) and displacement (L) to compression pressure (P) and strain (a), as shown in Figure 5.5b. The unconfined compression increases until reaches the peak value, and then decreases. The peak value is defined as the crush strength of the compact.

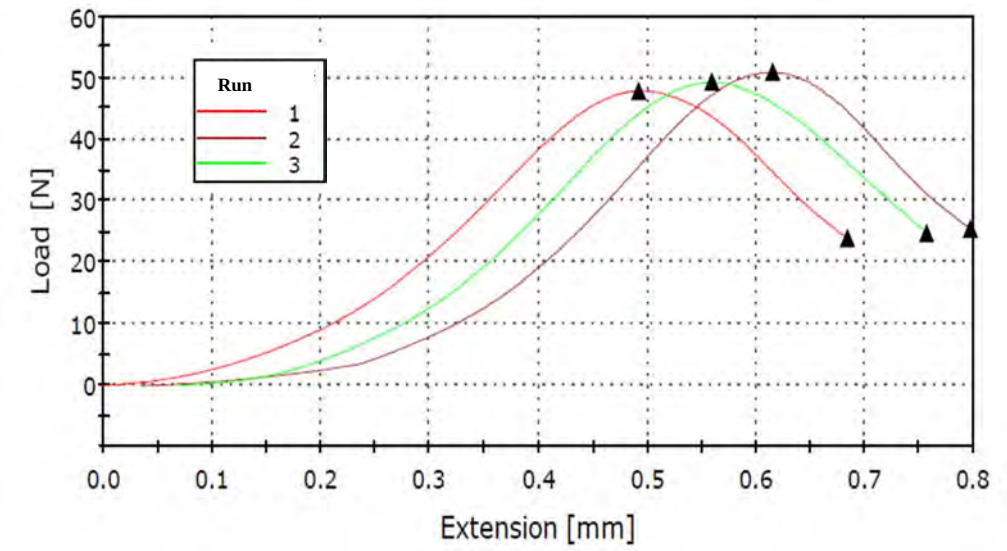

(a)

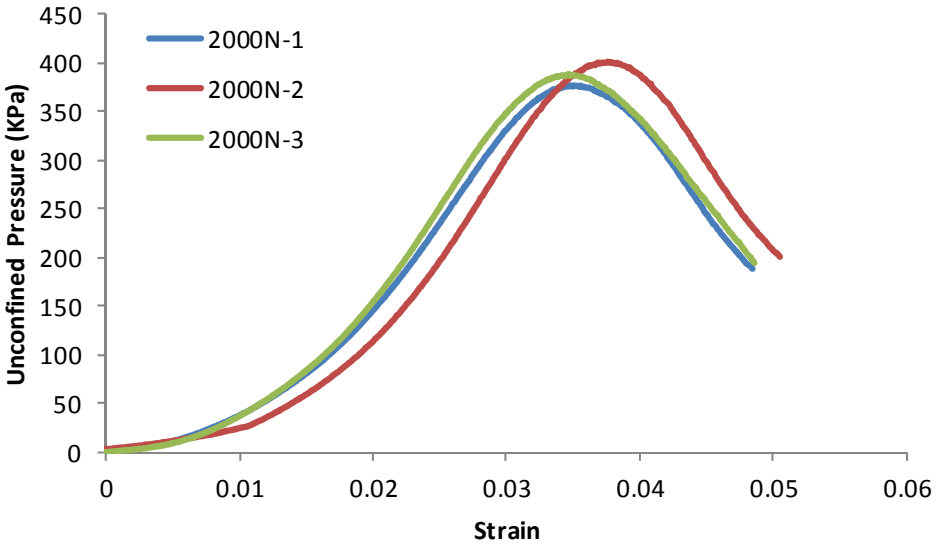

(b)

Figure 5.5. (a) Load-extension graph of the unconfined compression testing (b) transformed unconfined compression curve (magnetite, 25-75μm, 5% moisture content, 2000N)

5.3 Effects of material properties

Different iron ores may have different behaviour during compaction. In this work, the experiment conditions are as follows: the moisture content is 5% (mass ratio), the loading speed is 3mm/min and the lubricant is silicone oil. The load range is from 2500N to 4000N for the 200-280 μm magnetite particles and from 2000N to 4000N for others.

Figure 5.6 shows the compaction curves under different loads, which show similar trend in both loading and unloading part. Especially, the loading parts of all curves are almost overlapped. This means that the behaviours of iron ore particles are similar in different maximum load.

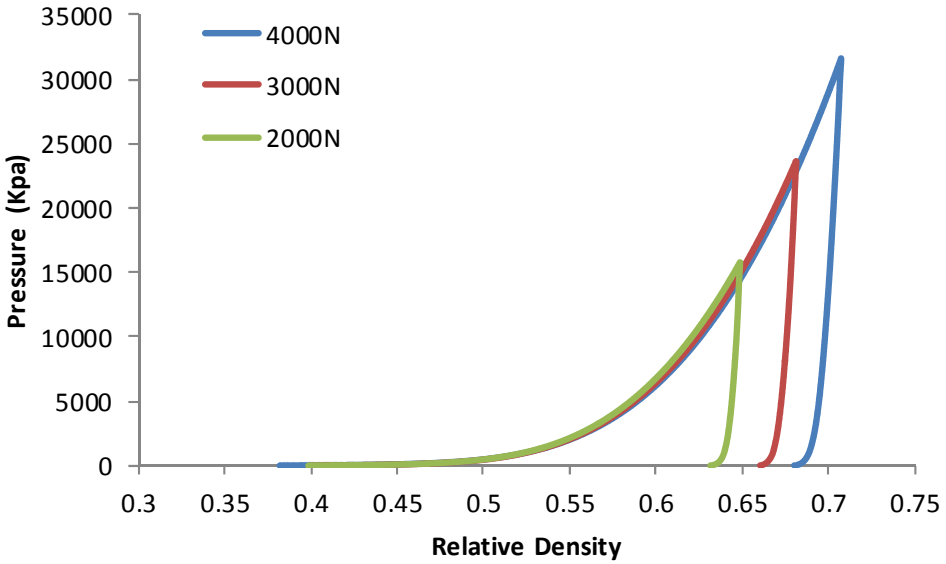

Figure 5.6 Die compaction curve of different maximum load (magnetite, 25-75μm, 5% moisture)

Based on Equation 5.1, K, P_y and A can be obtained. P_y is related to the plasticity of a compressed material and A describes the filling process and particle rearrangement before deformation and bonding of the discrete particles. All those parameters of all types of iron ore fines are given in Table 5.1. Form the figure, the hematite has highest value of P_y followed by the magnetite and goethite particles. The values of A are similar for three types of iron ore fines.

Table 5.1 K, A and P_y of iron ore fines

Material	Particle size	K (Pa^{-1})	P_y (Pa)	A
Magnetite	25-75μm	0.0066	151.52	0.91
	75-200μm	0.012	84.75	0.85
	200-280μm	0.015	65.36	0.85
Goethite	25-75μm	0.011	94.34	0.91
	75-200μm	0.012	81.97	1.01
	200-280μm	0.013	79.37	1.05
Hematite	25-75μm	0.0059	169.49	0.91
	75-200μm	0.0069	144.93	1.03
	200-280μm	0.0064	156.25	1.06

Figure 5.7 shows the compact density under different loads. The final relative density of all particles increases with increasing load. The goethite compact has a higher relative density compared to other two iron ores and the magnetite and hematite compacts have similar densities under the same load. This is because the hardness of goethite is much lower than those of magnetite and hematite. Thus, it is easier to be compacted. In addition, the highest relative density which can be achieved is about 0.77 under the load of 31.5MPa (4000N) when particle size range is 200-280 μm and material is goethite.

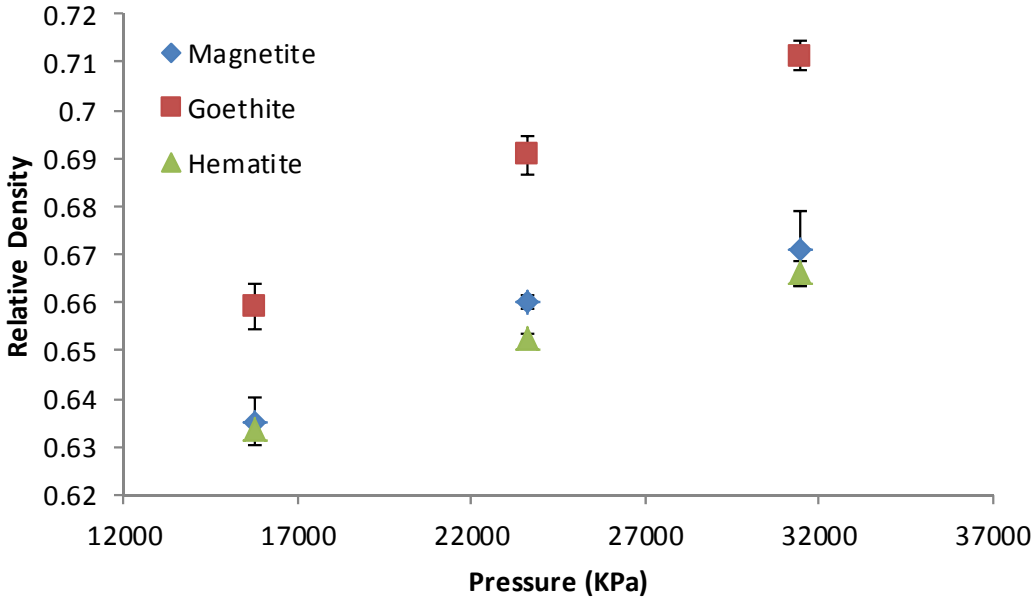

Figure 5.7 Relationship of relative density of maximum load and particle size (25-75μm, 5% moisture)

The unconfined compaction curve is shown in Figure 5.8. The results of crushing strength of all types of iron ore fines under different maximum load are shown in Figure 5.9. From the figure, although highest value of crushing strength is goethite, in same relative density, the strength of magnetite is greater than goethite and hematite. However, the trends of all types of iron ore fines are similar.

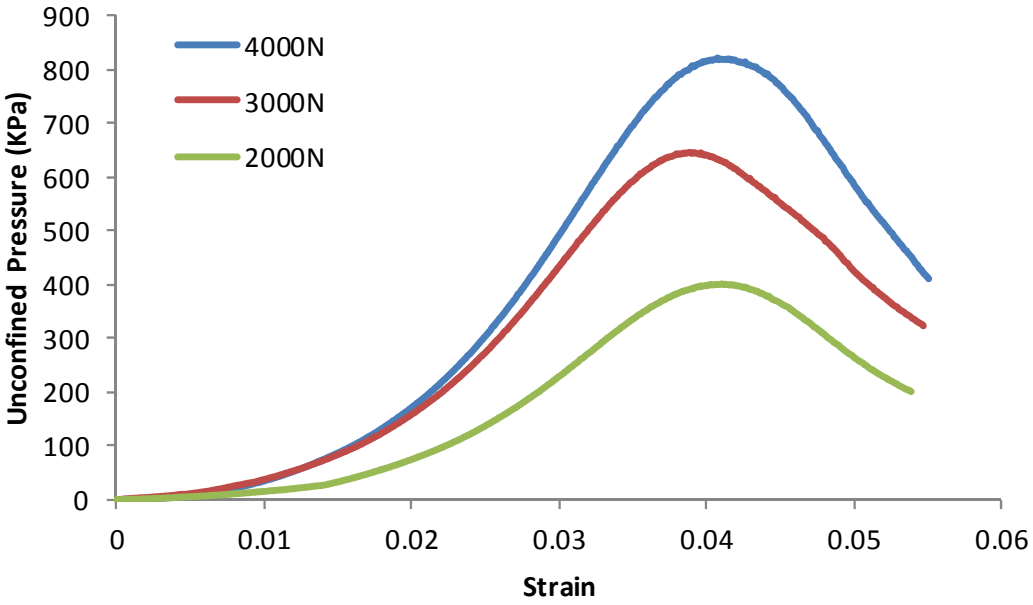

Figure 5.8 Unconfined compression curve of different maximum load (magnetite, 25-75μm, 5% moisture).

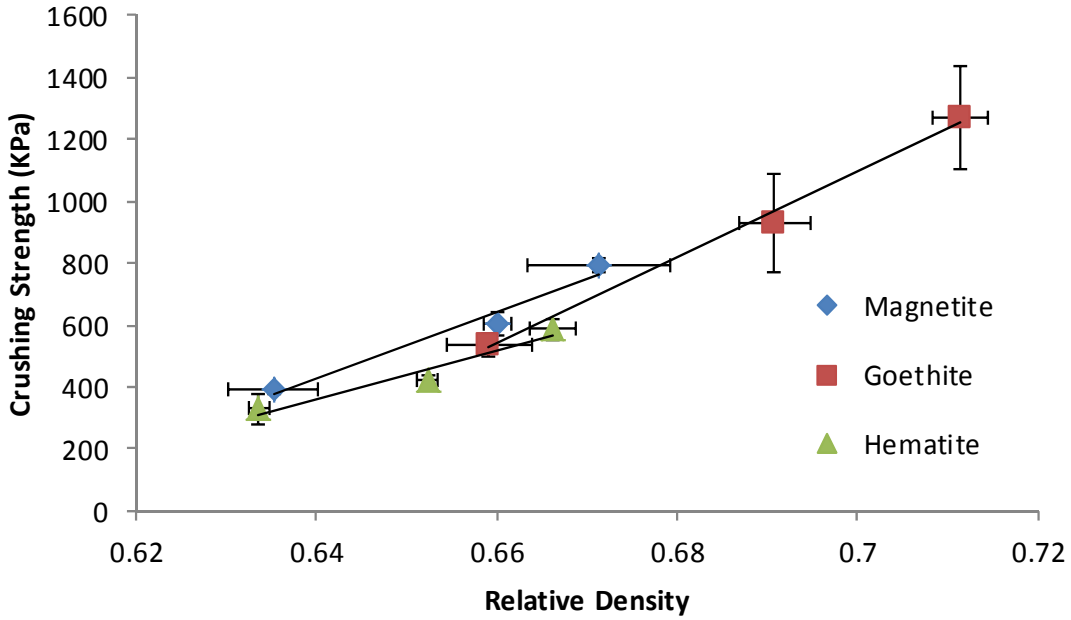

Figure 5.9 Relationship of crushing strength and relative density with different particle size (25-75μm, 5% moisture)

5.4 Effect of particle size

Particle size also influences the compaction of particles. In this section, the experimental conditions are as follows: the moisture content is 5% (mass ratio), the loading speed is 3mm/min and the lubricant is silicone oil. The ranges of particle size are 25-75μm, 75-

200μm and 200-280μm, respectively. The loading force in die compaction is 4000N

Fig. 5.10 shows the die compaction curves of different sized particles. It is obvious that different sized particles have different compaction response with the smaller particles have a faster increase in pressure with density, suggesting the smaller particles are more difficult to compact. The unloading curves, however, are similar for all the sized particles, indicating the compacts of different sized particles have similar elastic recovery.

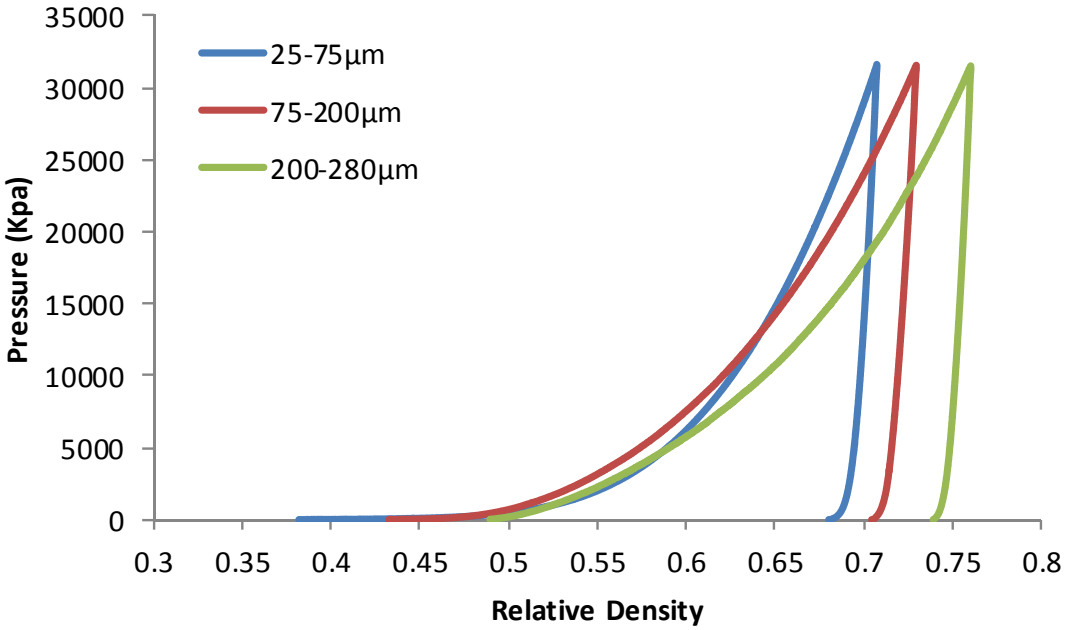

Figure 5.10 Die compaction curve of different particle size (magnetite, 5% moisture).

The variation of compact density are plotted in Figure 5.11. Larger particles lead to a greater relative density under the same loading for all types of iron ore fines, indicating they are easier to be compressed comparing with fine particles.

The unconfined compression curves of different sized particles are plotted in Figure 5.12. The compact of larger particles of 200-280 μm has a relatively smaller compressive strength of 150 KPa and a smaller strain of 1.7% when it is crushed. On the other hand, the compact of 25-75 μm particles has a compressive strength of 820 KPa and a critical strain of 3.6%. The increases in both compressive strength and strain for smaller particles are due to stronger bonding formed between the particles.

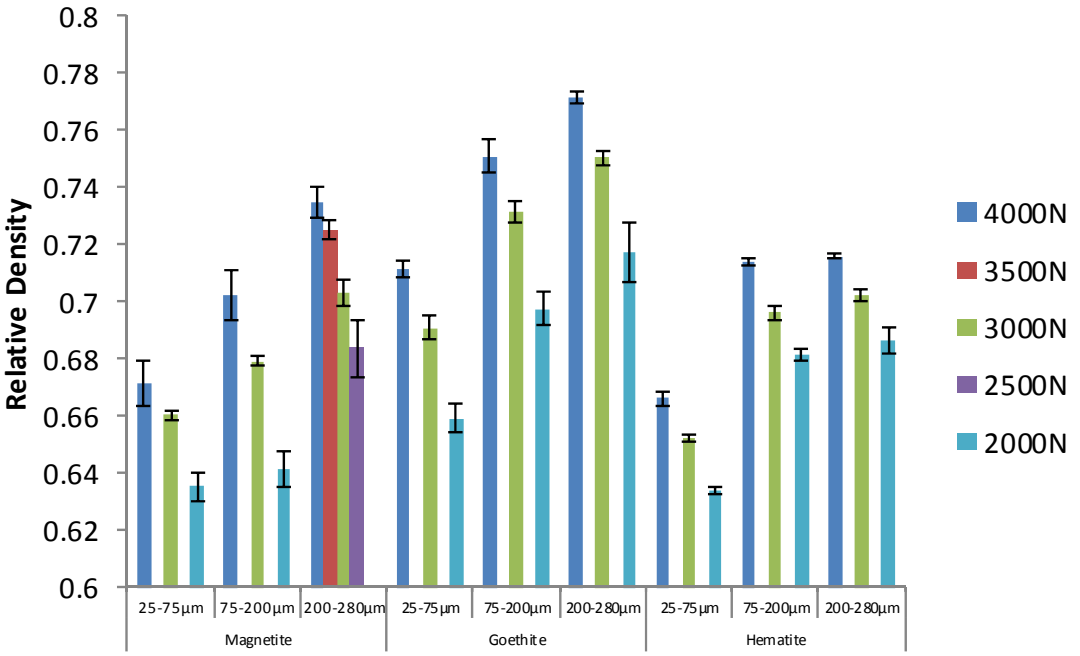

Figure 5.11 Relationship of relative density of maximum load and particle size (5% moisture).

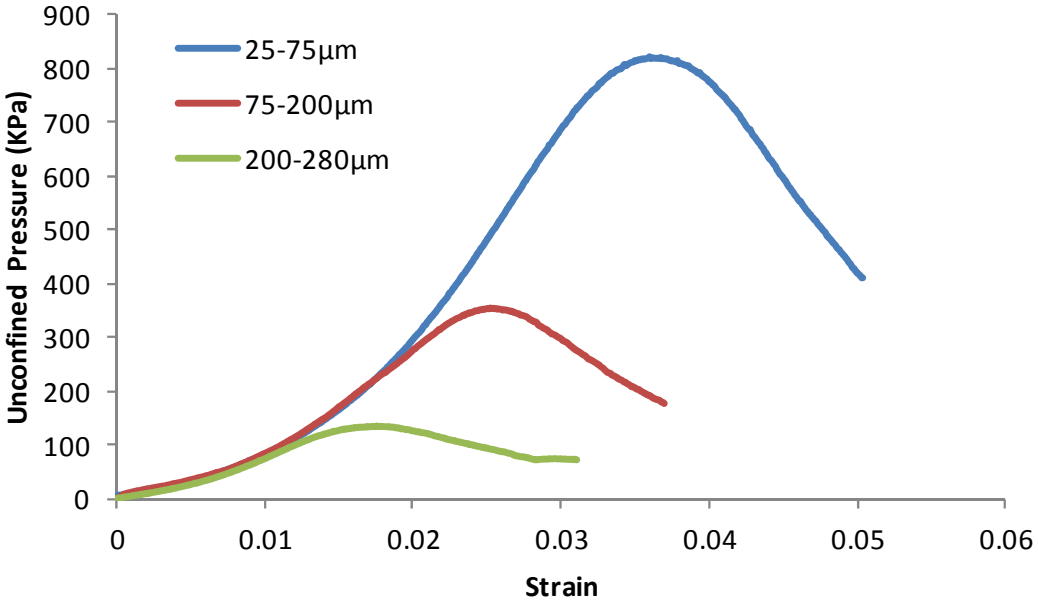

Figure 5.12 Unconfined compression curve of different particle size (magnetite, 4000N, 5% moisture).

Figure 5.13 shows the relationship between the compressive strength and compact density for different types of ore fines. For the magnetite powders (Fig. 5.13a), the crushing strength increase almost linearly with compact density with smaller particle compacts

have larger compressive strength which also increases faster. However, for the goethite and hematite particles (Fig. 5.13b and 5.13c), while the smaller particle compacts still have higher strength, the increase in the strength with compact density is similar.

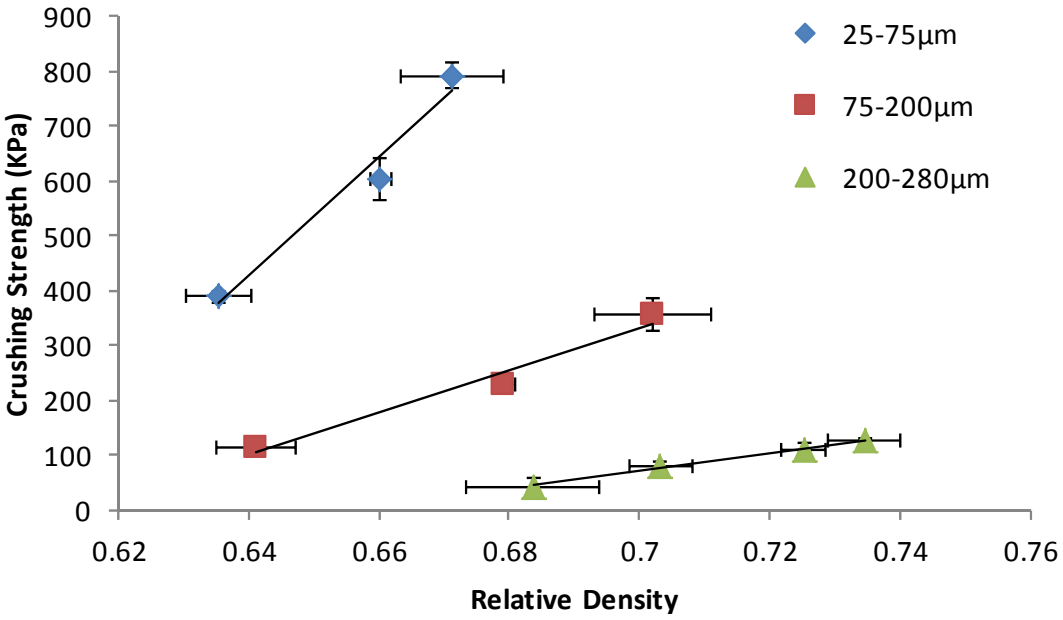

(a)

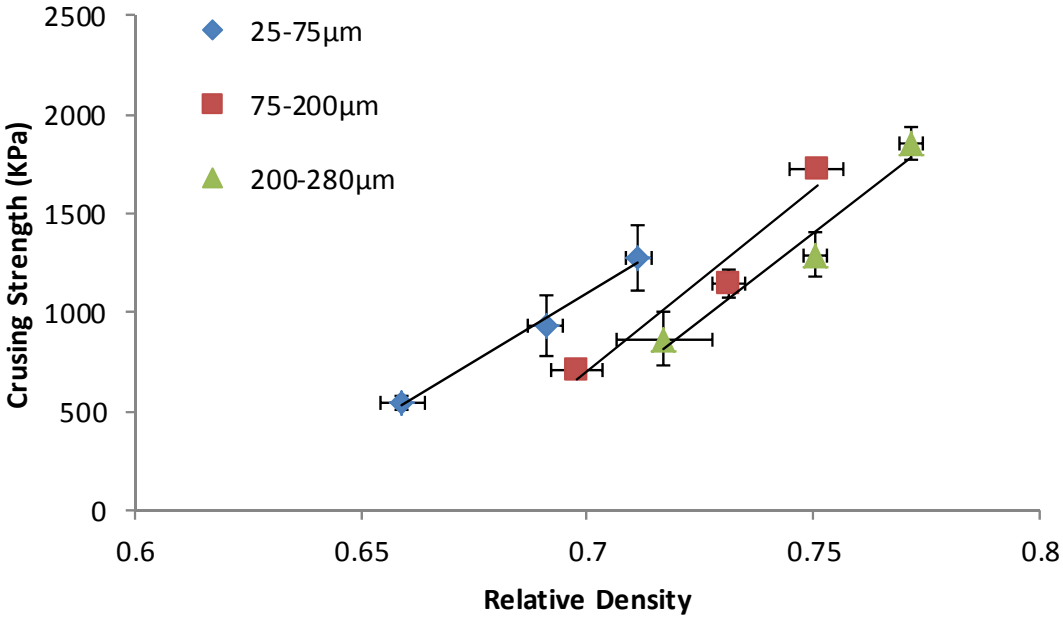

(b)

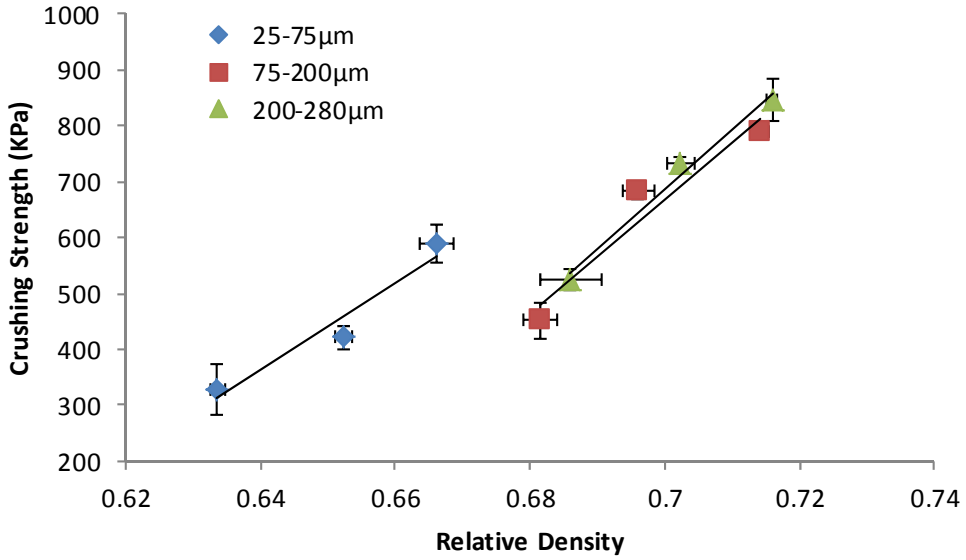

(c)

Figure 5.13 Relationship of crushing strength and relative density with different particle size (5% moisture): (a) magnetite; (b) goethite; and (c) hematite.

5.5 Effect of mixture of particles

The effect of the mixture of different sized particles on compact strength and structure is studied in this section. The experimental conditions are as follows: magnetite and goethite powers are tested with the moisture content 5% (mass ratio), the compaction speed 3mm/min and loading force 4000N. The particles of 25-75µm and 140-200µm are mixed with different portions.

Fig. 5.14 shows the die compaction curves of different particle mixtures. The compact consisting of 100% of small particles has a lowest initial density and the fasted increase of compaction pressure with density. On the other hand, the compact consisting of 100% of large particles has a higher initial density and a slower increase of compaction pressure with density. The results indicate that small particles are more difficult to compact. However, the mixture of 40% of small particles and 60% of large particles has the highest initial packing density and also a longer leading period before the pressure starts to increase rapidly. This means the mixture of large and small particles allows the largest degree of particle re-arrangement during packing and compaction. The increase of compaction pressure with compact density is similar to that of large particles, suggesting the densification of the compact is mainly due to the deformation of the large particles.

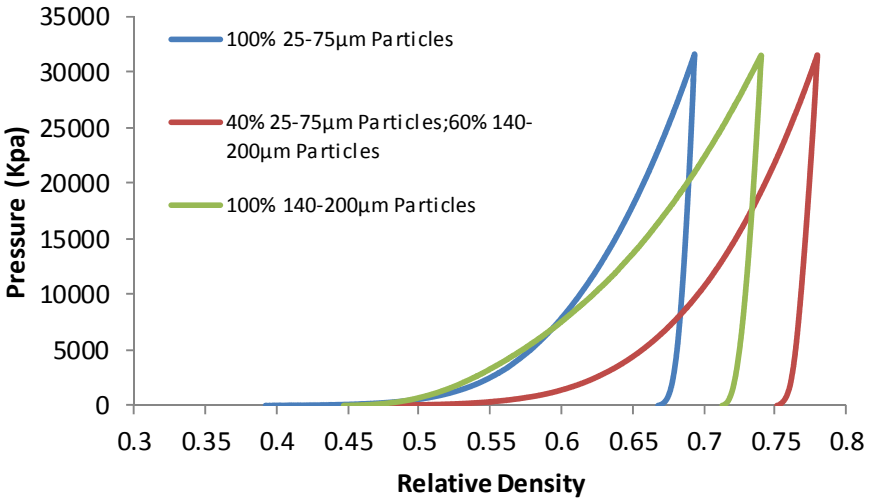

Figure 5.14 Die compaction curve of different percentages of 25-75µm particle and 140-200µm particle (magnetite, 4000N, 5% moisture).

Table 5.2 lists the values of K, Py and A obtained from the Heckel plot. As expected, the compact of 100% of small 25-75µm particles has a much higher Py than other two. The mixture of small and large particles has the largest A, indicating the largest particle re-arrangement.

Table 5.2 Values of K, A and P_y of magnetite of mixed particles

Percentage of 25-75µm particles	K (Pa^{-1})	P_y (Pa)	A
100%	0.0066	151.52	0.91
40%	0.017	59.88	1.01
0%	0.019	52.63	0.78

Figure 5.15 shows the relationship between compact density and the percentage of small particles in the mixture under the same compaction pressure. It is observed the compact density initially increased with increasing percentage of small particles. This is because the small particles can fill in the void among the large particles. However, with further increase in the percentage of small particles, the large particles start to be separated by the small particles, causing the decrease in compact density. The compact of the mixture consisting of 40% small particles and 60% large particles has the highest compact density. The trend applies both goethite and magnetite particles.

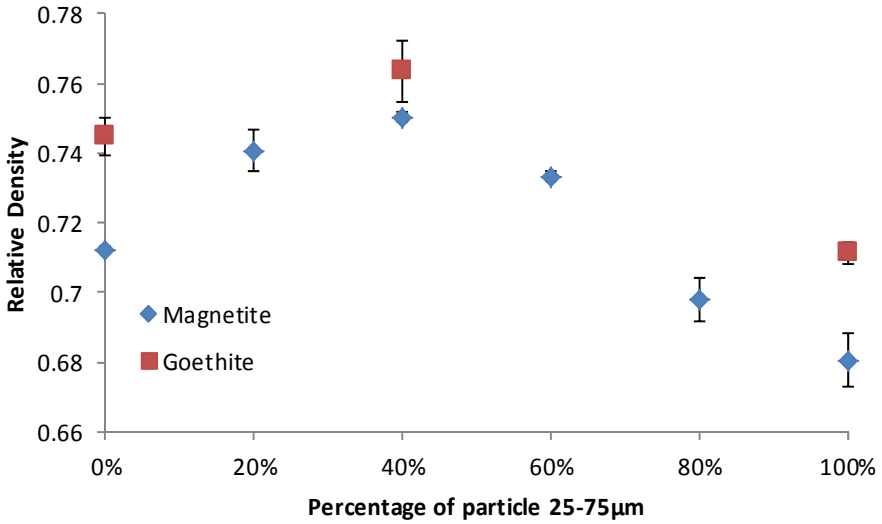

Figure 5.15 Relationship of relative density and different percentages of 25-75µm particle and 140-200µm particle (4000N, 5% moisture)

Fig. 5.16 shows the response of the compacts during unconfined compression. The compact of 100% large particles has the lowest strength while the responses of particle mixture and 100% small particles are similar.

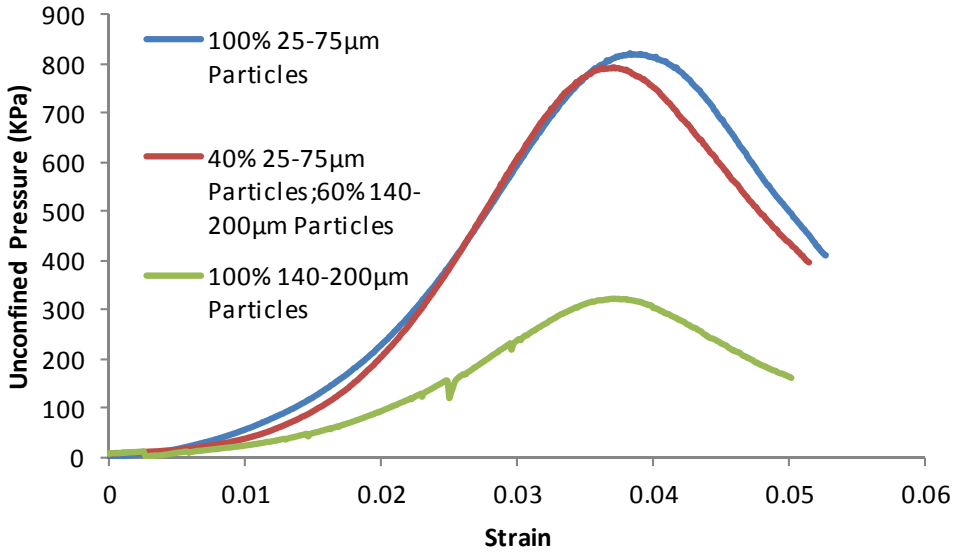

Figure 5.16 Unconfined compression curve of different percentages of 25-75µm particle and 140-200µm particle (magnetite, 4000N, 5% moisture).

Fig. 5.17 shows the variation of crushing strength with the percentage of small particles. The strength of magnetite compacts initially increases with the amount of small particles in the mixture till 40% and then becomes flat, indicating further increase in small particles

has no effect on compact strength. On the other hand, the percentage of small particles has no significant effect on the strength of goethite compacts.

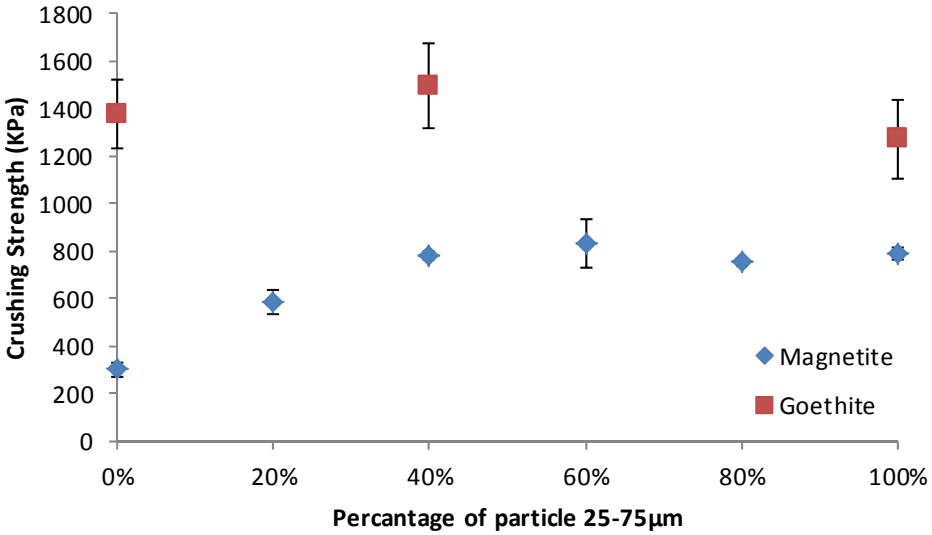

Figure 5.17 Relationship of crushing strength and different percentage of 25-75µm particle and 140-200µm particle (4000N, 5% moisture).

5.6 Effect of moisture content

The amount of water added to the powders also has a significant effect on compaction and compact strength. In this work, the moisture content was varied between 2.5% and 10% to study its effect.

Figure 5.18 shows the die compaction curve with different moisture contents. The compacts with smaller moisture content has lower initial compact densities, shorter particle re-arrangement period and faster increase in pressure with compact density. This indicates that more moisture can facilitate the compaction of powders. However, the unloading curves are similar for all the cases, suggesting the moisture content has no effect on the elastic response of the compacts.

Fig. 5.19 shows the variation of compact density with moisture content for different types of iron ore fines. The relationships between the compact density and moisture content show linear relationships for all types of particles. With the same moisture content, the goethite particles have the highest value of relative density among three types of iron ore fines while the relative densities of magnetite and hematite particles are similar.

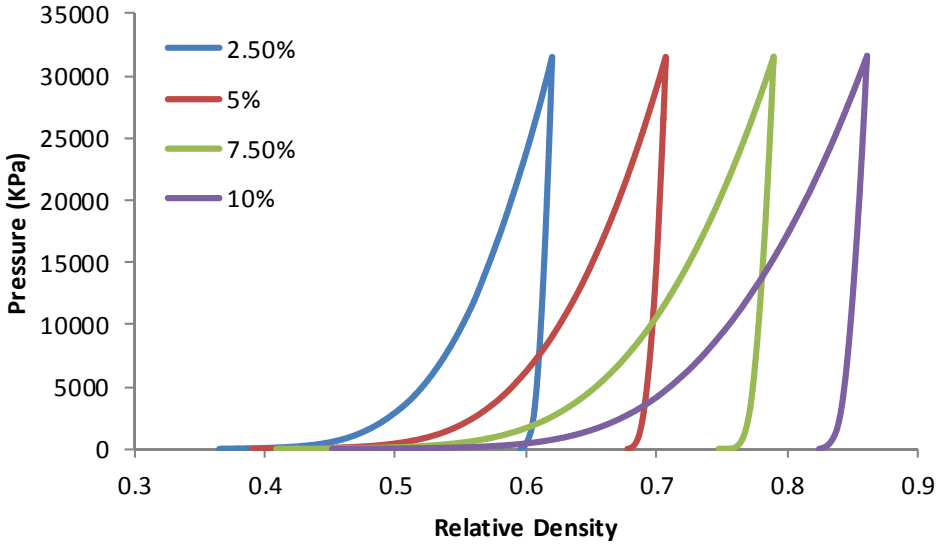

Figure 5.18 Die compaction curve of different moisture content (magnetite, 4000N, 25-75μm).

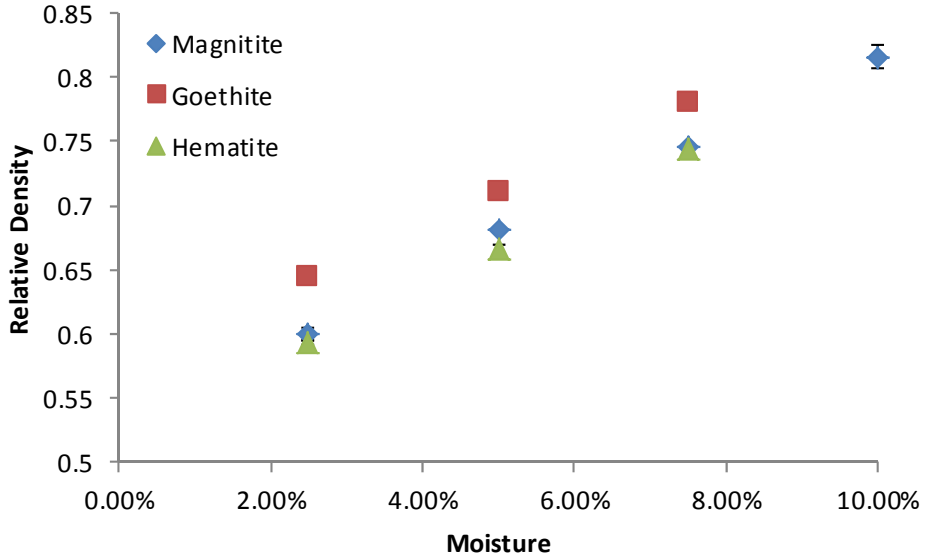

Figure 5.19 Relationship of relative density and different moisture (4000N, 25-75 μm).

Figure 5.20 shows the force-displacement relationship in unconfined compression for the compacts with different moisture contents. It is observed that compact strength increases initially with moisture content, reaches a maximum value with 5% moisture content and starts to decreases with further increase in moisture content. This is also confirmed in Fig. 5.21 which plots the variation of compact strength with moisture content. So the results suggest the moisture content should be controlled to achieve the optimal compact strength.

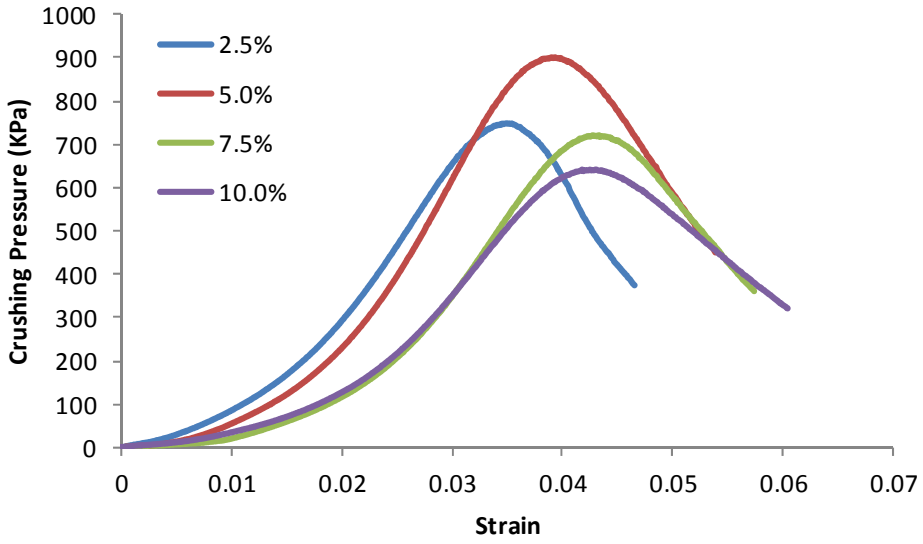

Figure 5.20 Unconfined compression curve of different moisture content (magnetite, 4000N, 25-75μm).

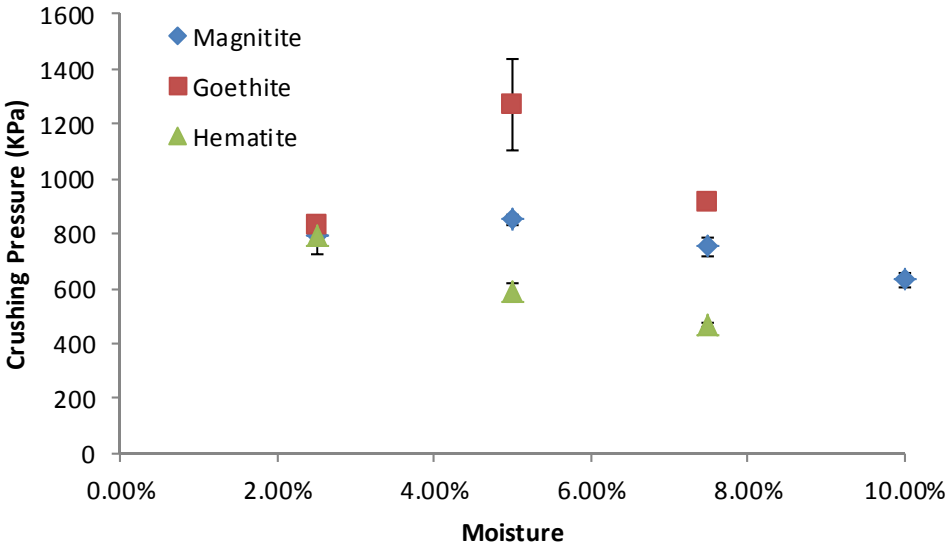

Figure 5.21 Relationship of crushing strength and different moisture (4000N, 25-75 μm).

5.7 Effect of lubricant

Lubricant also may affect the compaction process and compact properties. By reducing the friction between the compact and die surface, the formed compact has a more homogenous density distribution. It is therefore to study its effect on the compact of iron ore fines. The experiments were conducted under the following conditions: loading of 4000N (~32MPa) was applied to compact 25-75μm magnetite particles with 5% moisture

content (mass moisture) and 3mm/min compaction speed. Silicon oil was applied to the internal surface of the die.

Figure 5.22 shows that the compacts with the lubricant have a slightly higher density than those without the lubricant, but the difference is small. In terms of crushing strength, again the compacts with the lubricant have a slightly higher strength but the difference is even smaller. The results suggest the effectiveness of the silicone oil not significant.

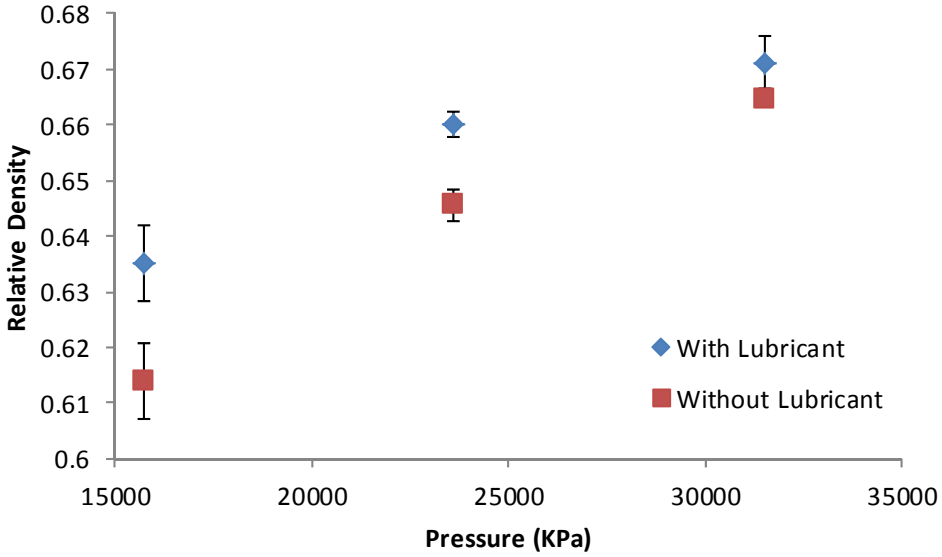

Figure 5.22 Effect of lubricant in relative density (magnetite, 25-75µm, 5% moisture).

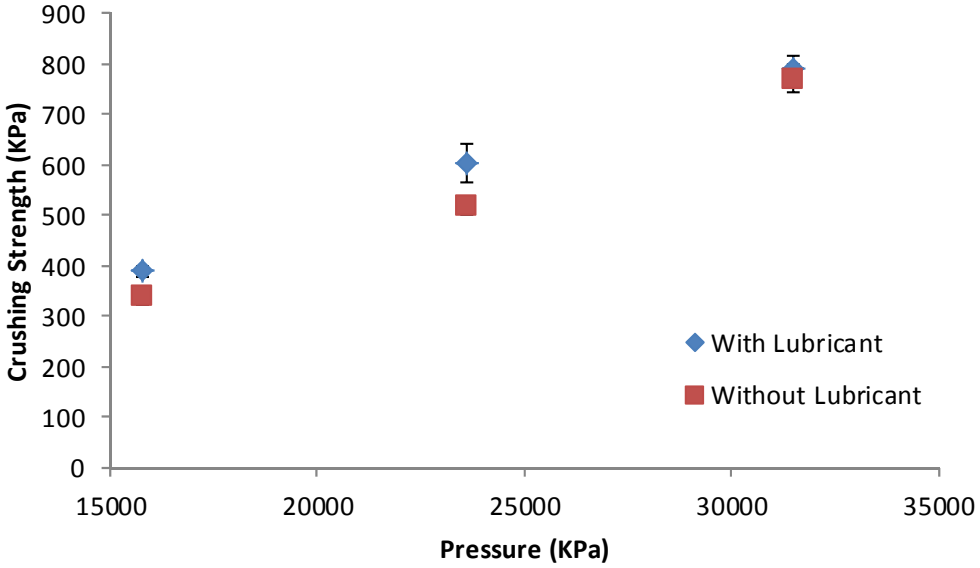

Figure 5.23 Effect of lubricant in crushing strength (magnetite, 25-75µm, 5% moisture).

5.8 Summary

In this chapter, the crushing strength of compacts have been studied. The work is focusing on the effects of variables such as loading force, particle size distribution, moisture content and lubricant on the structure and strength of compacts.

The results show that particle size, maximum load and moisture content increase compact density while lubricant has a minimal effect. The mixture of small and large particles can also increase compact density and has the highest density with 40% small particles and 60% large particles.

On the other hand, increasing particle size decreases compact strength. However, the trend line of 200-280μm particles of hematite in relative density versus crushing strength curve is almost same with the 75-200μm particles. In addition, crushing strengths of magnetite and goethite particles reach the highest point at 5% moisture and 2.5% moisture content for hematite particles. The mixture of 40% small particles with 60% large particles also has a relative high crushing strength. The effect of lubricant on compact strength is minimum.

Chapter 6 Tensile strength of iron ore fine compacts

6.1 Introduction

The tensile strength of compacts is another important measure of compact quality. A compact should have enough tensile strength to avoid breakage in the handling and transportation processes. Tensile strength is also affected by powder properties and characteristics and operation conditions.

While tensile strength is important, it is difficult to measure directly in experiments. The commonly used method to measure tensile strength is through diametrical compression testing. The compressive force is then linked to the tensile strength of the compact (Fell and Newton, 1970).

This chapter is to investigate the effects of consolidation pressure, diameter-height ratio, particle size and distribution, moisture content and lubricant.

6.2 Pressure, relative density and compact strength

In this section, the diametrical compression of a compact of magnetite fines of 25-75 μm formed with 5% moisture and loading pressure of 3000N is analysed. Fig 6.1 shows the sample before, during and after the diametrical compression. Fig 6.1a shows the sample has a cylindrical shape with a diameter-height ratio of 2. During the compression, the sample fractures from the central line as shown in Figure 6.1b. The facture becomes wider and eventually the sample breaks into two pieces (Fig. 6.1c).

(a)

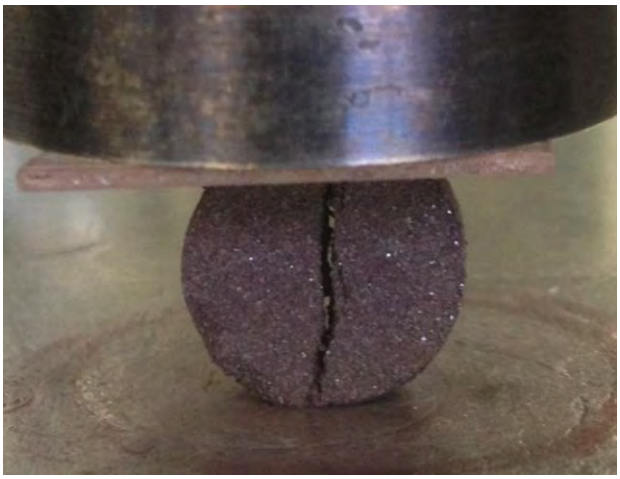

(b)

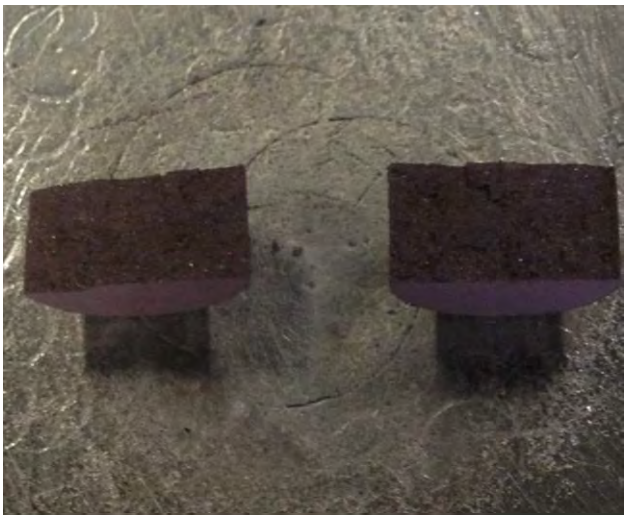

(c)

Figure 6.1 A diametrical compression process showing a compact (a) before; (b) during; and (c) after the compression.

The load-extension data of diametrical compression breakage load is shown in Figure 6.2a. The three curves represent three experimental runs under the same experimental condition. As the graph is plotted as loads versus punch displacement, it is to be changed to tensile stress and strain. The tensile stress (σ_0) of the tablet can be transformed by its breakage stress of diametrical compaction:

$$\sigma_0=\frac{2P}{\pi Dt} \qquad 6.1$$

where P is applied force, D is the sample's diameter and t is the sample's thickness.

Figure 6.2b shows the relationship between the tensile stress as a function of strain. The shapes of the diametrical compaction curves are different from those of the uniaxial unconfined compression curves. The diametrical compression curve increases sharply from the beginning, but fluctuates after reaching the peak. The maximum tensile strength is much lower than that of crushing strength.

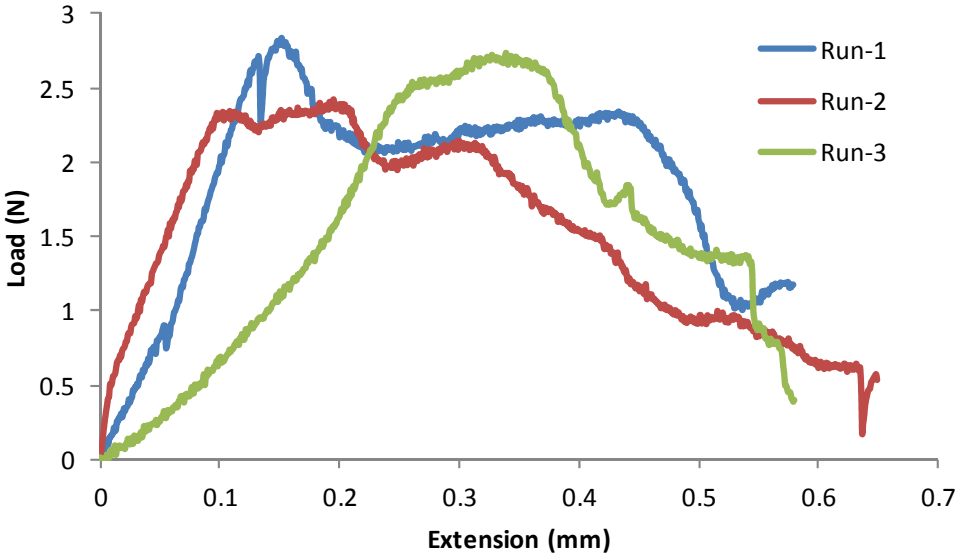

(a)

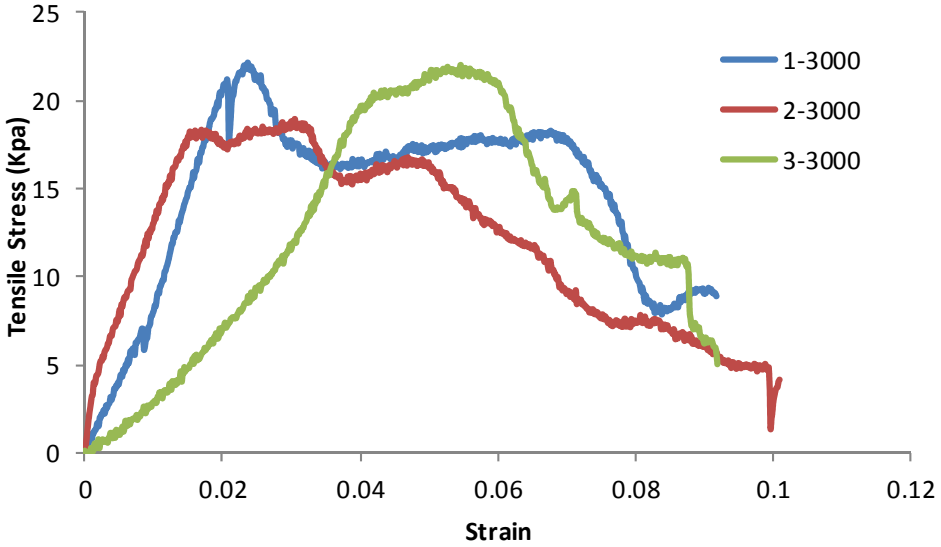

(b)

Figure 6.2 (a) Load-extension graph of the diametrical compression testing and (b) transformed diametrical compression curve (magnetite, 25-75μm, 5% moisture content, 3000N).

Figure 6.4 shows the variation of mean tensile strength with load pressure. The result of

tensile strength of 3000N loading force is the middle point with error bar. Other two points are the average value with the same experiment condition except the loading force is different (4000N, 2000N). It is observed the tensile strength increases almost linearly with consolidation pressure.

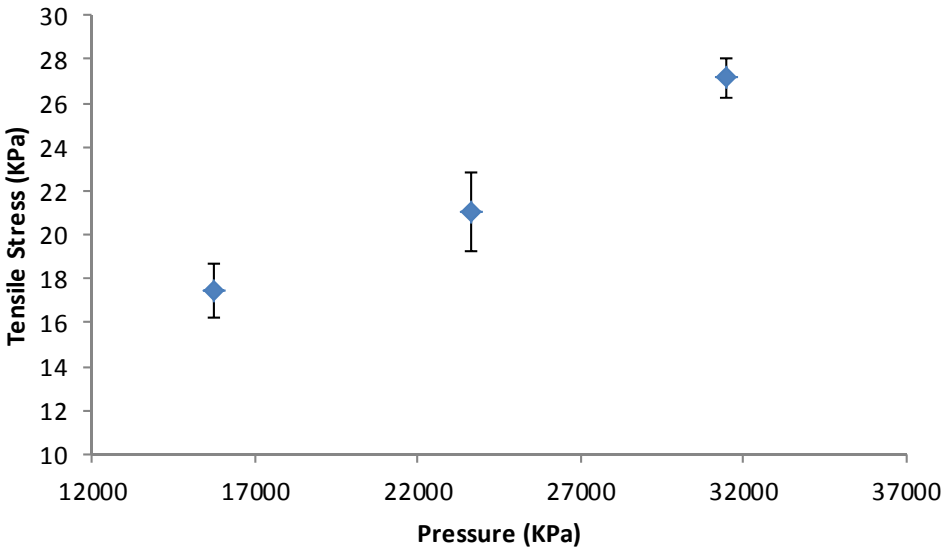

Figure 6.3 Relationship of tensile stress and pressure (magnetite, 25-75μm, 5% moisture content, 3000N)

6.3 Effect of diameter-height ratio

The appropriate adoption of Eq. 6.1 requires proper sample size, in particular the diameter-height ratio. A too large or small ratio may give incorrect tensile strength. Therefore, it is important to exam its effect.

In the experiments, compacts of magnetite fines with different diameter-height ratios ranging from 1 to 3 are tested. The consolidation pressure is 4KN (~32MPa) is used to form the compacts. Different size particles of 25-75μm, 75-200μm and 200-280μm with 5% moisture content (mass ratio) are used.

Figure 6.4 shows the tensile strengths of the compacts. There is only small difference of tensile strength between ratio 1 and ratio 2 while the tensile increases slightly with ratio 3. Because the compact with the ratio of 2 is easier to form and handle in the experiment, all the following studies are based on the samples with diameter-height ratio of 2.

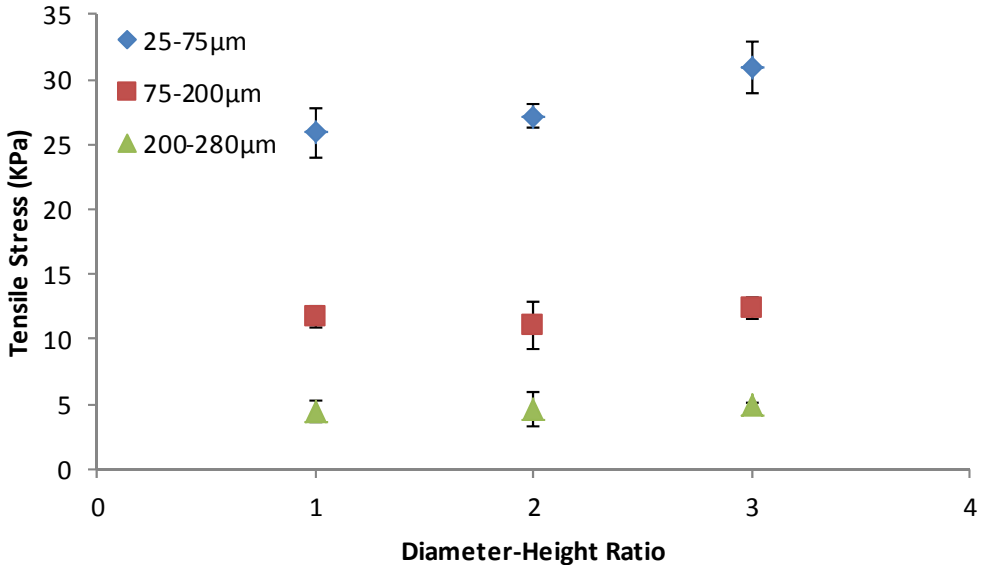

Figure 6.4 Effect of Diameter-Height ratios (4000N, 5% moisture)

6.4 Effect of consolidation pressure

Similar to the uniaxial unconfined compression, consolidation pressure may affect the results of diametrical compression.

The stress-strain relationships with different consolidation pressures is shown Figure 6.5. The compression curves of the diametrical compaction do not have a typical form as the unconfined uniaxial compaction. Most of the curves increase rapidly from beginning, drop after reaching the peaks, and then fluctuates. The typical strain corresponding to the peak points is less than 4% which is much lower than that of uniaxial compression. With increasing pressure, both tensile strength and the critical strain increase. However, the curve of larger particles is relatively unstable, which is due to the weakness of the compacted particles.

Figure 6.6 shows the variation of tensile strength with compact density. It is observed that the tensile strength also increases with the increasing relative density of compacted tablets, and the trend is near linear. However, compared to the crushing strength of the compacts, tensile strength is much lower.

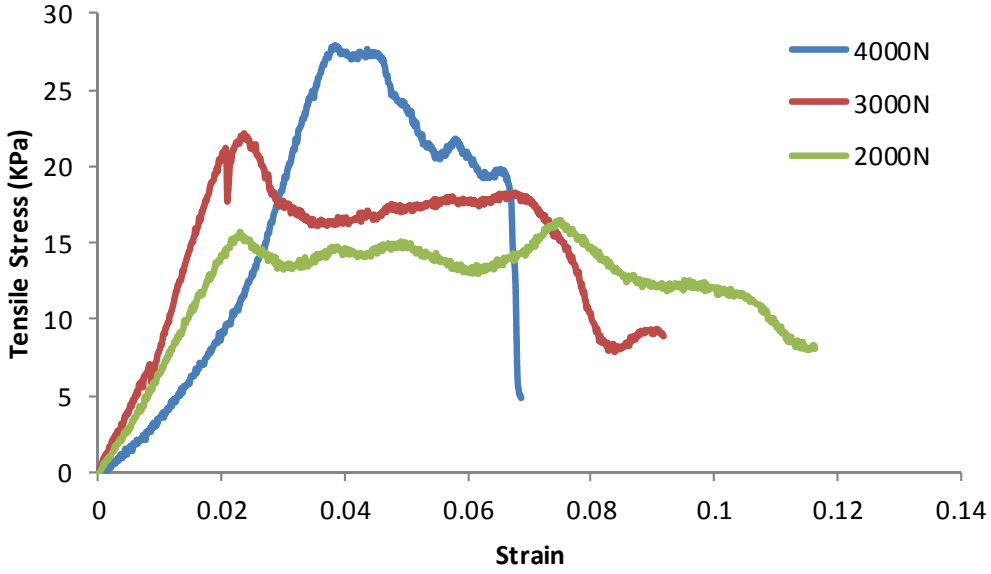

Figure 6.5 Diametrical compression curve of different particle size (25-75 μm, 5% moisture).

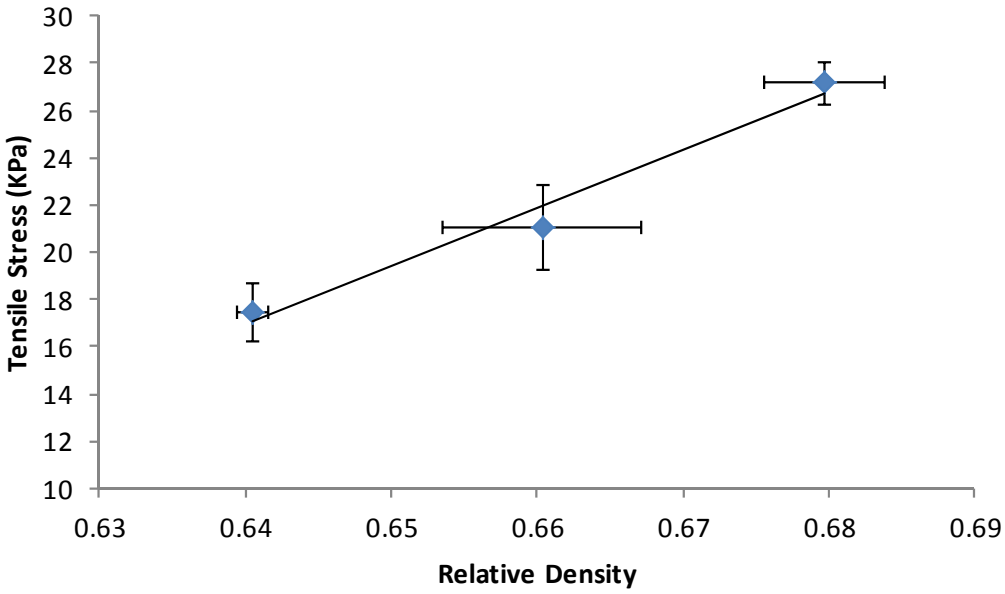

Figure 6.6 Effect of consolidation pressure (5% moisture).

6.5 Effect of particle size

Particle size also may affect the result of tensile strength of compacts. Fig. 6.7 shows the responses of the compacts of different particle sizes during the diametrical compression. The three curves have a similar shape. The strains of 75-200μm particles and 200-280μm particles are similar which are around 0.02, but the strain of 25-75μm particles is much

higher at about 0.04, which is caused by the stronger bonding between the small particles. The peaks also follow a similar trend. The tensile strength of the 25-75μm particle compact is much larger at around 27 KPa while the other two have 11 KPa and 4 KPa for the 75-200μm and 200-280μm particle compacts, respectively. This means compacts of smaller particles have larger strength and can have larger deformation before being fractured.

This is also reflected in Figure 6.8 which plots the tensile strength with compact density. Compacts of larger particle size have lower tensile strength. Compared Figure 5.13a in the uniaxial compression, it is shown that the trends of different particle sizes are similar. The compact of the 25-75 μm particles has the highest tensile and crushing strength and also have the largest slope. And the strength of compacted particles with 75-200μm is greater than that of 200-280μm, but they have similar slopes. In addition, the gap between those two curves is much smaller than the gap between the curve of 75-200μm and the curve of 200-280μm. The slopes of those two curves are also smaller than the curve of 25-75μm.

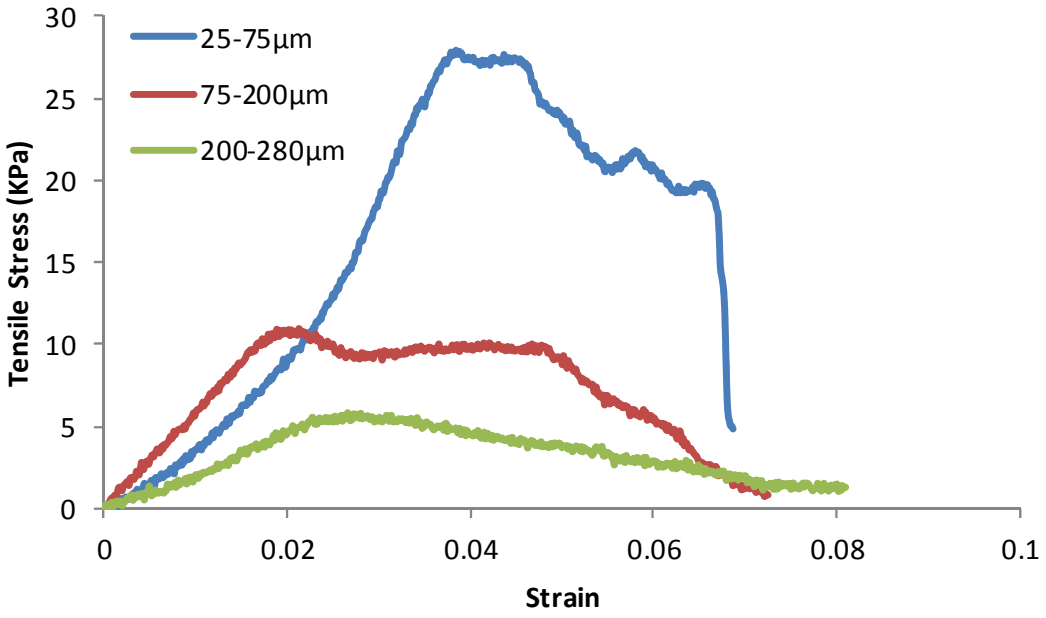

Figure 6.7 Diametrical compression curve of different particle size (4000N 5% moisture).

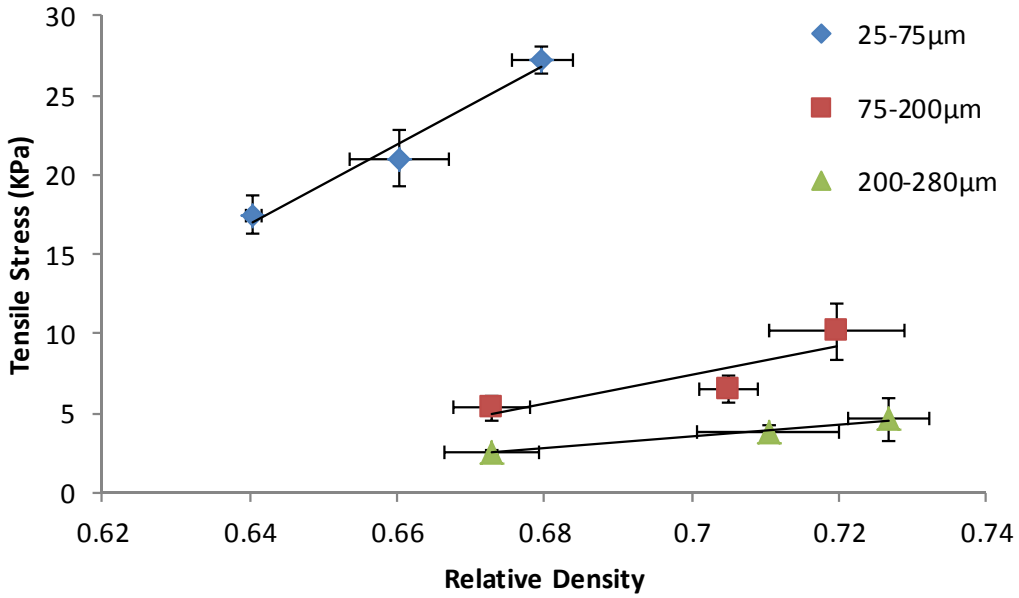

Figure 6.8 Effect of different particle size (5% moisture).

6.6 Effect of particle mixture

Particles of different sizes, 25-75µm and 140-200µm, are mixed at different percentages to identify the effect of particle size.

Fig. 6.9 shows the compression curves of the samples. For the compact consisting of only large particles, the tensile stregth is very low at around 5KPa. For the compact consisting of 100% of small 25-75 µm particles, the tensile strength is much higher at around 25 KPa with a larger critical strain at which the stress reaches a peak. When the large and small particles are mixed at 20%-80%, the compact strength is the highest among the three at around 27 KPa. The critical strain is similar at 5.5%.

Fig. 6.10 shows the variation of the tensile strengths with the percentage of small particles. The tensile strength reaches the highest point at 80% particle with 25-75µm and 20% particle with 140-200µm. Further increase in small particles does not increase the tensile strength much. Compared with the curves of magnetite in Figure 5.16 in the uniaxial compression, the variation of tensile strength has a similar trend. However, the maximum crushing strength occurs with the sample of 40% 25-75µm particles while the maximum tensile strength occurs with the sample of 80% of 25-75 µm particles.

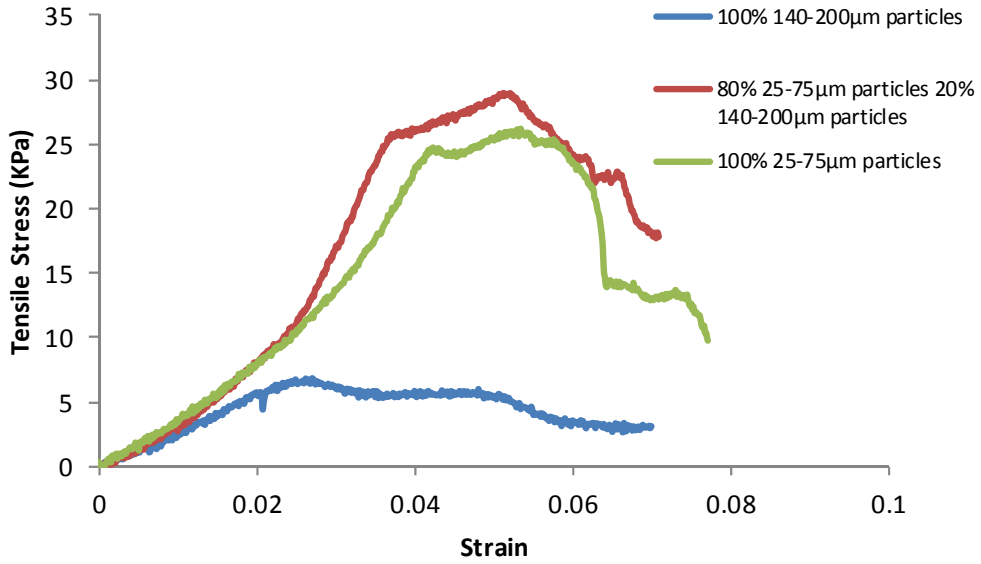

Figure 6.9 Diametrical compression curve of different percentages of 25-75µm particle and 140-200µm particle (4000N 5% moisture).

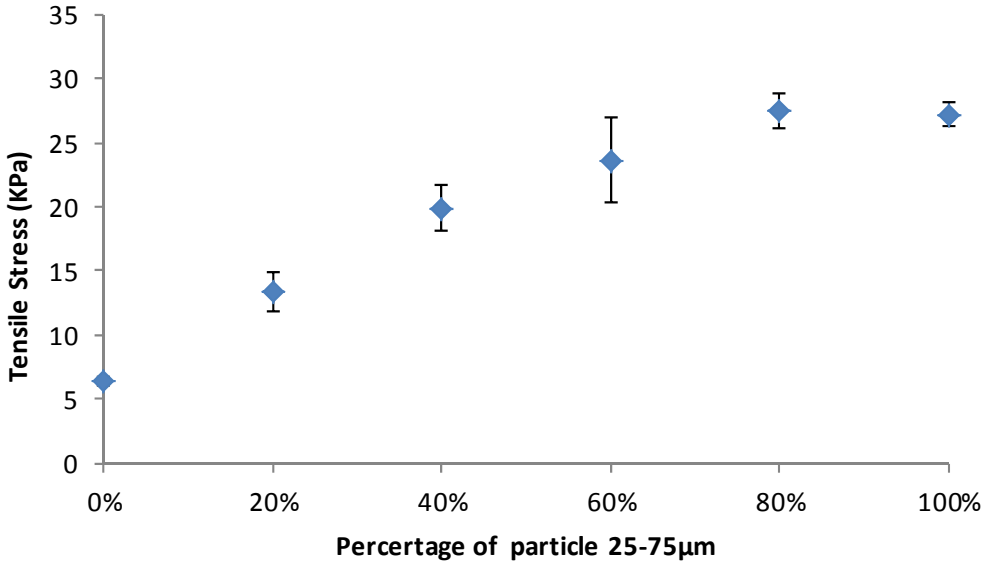

Figure 6.10 Relationship of relative density and different percentages of 25-75µm particle and 140-200µm particle (4000N, 5% moisture).

6.7 Effect of moisture

Moisture content plays an important role in determining the tensile strength of compacts. In the diametrical compression testing, different moisture contents ranging between 2.5%

and 10% were mixed with the particles.

Fig. 6.11 shows the diametrical compression curves of the compacts with different moisture contents. It is the maximum tensile strengths are almost the same, independent of moisture content. However, it is observed that the critical strain increases with moisture content increasing from 2.5% to 5% and 7.5% but decreases with 10% moisture content. This indicate the sample becomes more ductile with increasing moisture content to a certain level. A over saturated sample, however, results in low ductility.

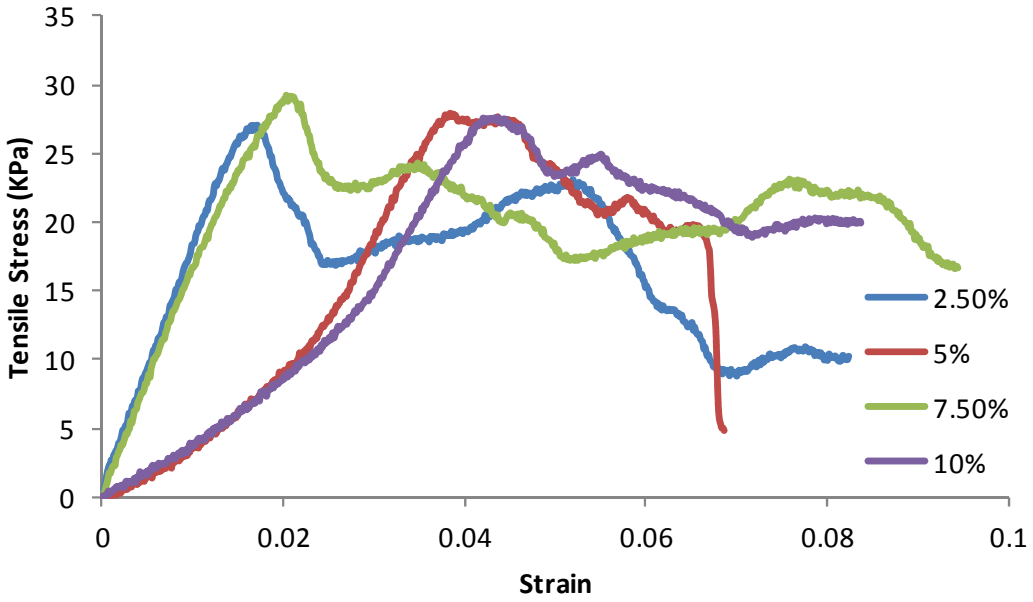

Figure 6.11 Diametrical compression curve of different moisture contents (4000N, 25-75 μm).

The results of different moisture contents are shown in Figure 6.12. It is obvious that there is no much difference of tensile strength between each moisture content. The highest point is around 5%-7.5% moisture content. Compared to Figure 5.20, the trends of two curves are different. The curve of uniaxial compression increases sharply with small addition of moisture content, reaches its peak and decreases with further increase in moisture content. However, the variation of tensile strength is more stable. This indicates that moisture content affects more on crushing strength than tensile strength. At 5% moisture content, both crushing and tensile strengths reaches relatively high values.

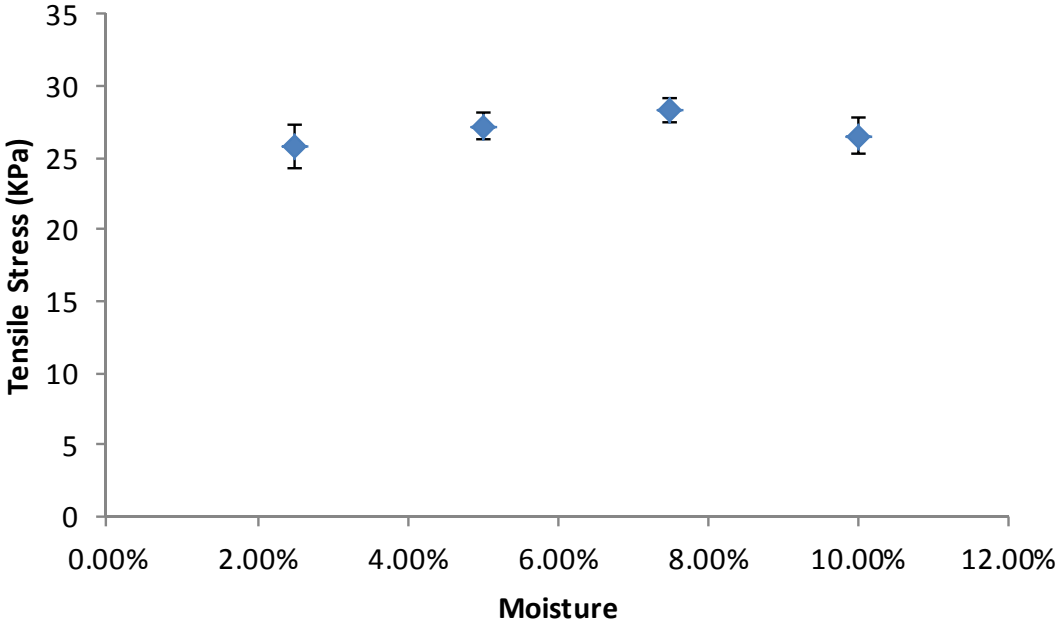

Figure 6.12 Effect of moisture (4000N, 25-75 μm).

6.8 Summary

The tensile strength of compacts is characterised through diametrical compression testing. The effects of consolidation pressure, particle size and moisture content are investigated.

In the testing, the compacts fractured from the central line, which is gradually widened and eventually the compact break into two pieces. The tensile strength increases with increasing consolidation pressure and decreasing particle size, which is similar to the compressive strength. However, the tensile strengths of the samples are not affected much by moisture content.

Chapter 7 Conclusions

Iron ore fines are the products of iron ore mining and processing. Too much fines may affect the handling and transportation process. This work investigated the flowability and compactibility of different types of iron ore fines.

The flowability of iron ore fines was characterised using a Freeman Technology FT4 Rheometer. The yield locus was plotted based on the experimental results which was used to obtain unconfined yield stress, cohesion and flow function of the iron ore fines. The results showed that magnetite fines were more cohesive with larger unconfined yield stress and lower flow function than goethite fines. Therefore, magnetite fines were more difficult achieve the same relative density as goethite fine under the same compaction pressure. As expected, larger particles resulted in higher flow function than smaller particles, indicating they were more free-flowing. The moisture content had similar effects on magnetite and goethite fines: compacts with higher moisture content had higher unconfined yield stress, cohesion and lower flow function. However, the results indicated that the effect of moisture was relatively smaller on magnetite fines than on goethite fines.

The crushing strength of iron ore fines was tested through unconfined uniaxial compression testing. The effects of consolidation pressure, particle size, moisture content and lubricant on compact density and strength were investigated. The results showed that compact density increased with consolidation pressure and moisture. While smaller particles were more difficult to compact, the mixture of small and large particles was able to achieve the highest compact density. The effects of consolidation pressure and moisture content on crushing strength were similar: increasing consolidation pressure or moisture content increased compact strength. However, too much moisture content resulted the decrease in compact strength. A compacts of smaller particles had higher strength, and the mixture of small and larger particles was able to achieve the highest compact strength. The results showed that lubricant did not have a significant effect on compact properties.

The tensile strength of iron ore fines was tested using the diametrical compression. The iron ore fines were compacted to a cylindrical disc with a diameter-height ratio of 2 which was then compressed diametrically. The pressure which fractured the sample was then linked to the tensile strength of the compact. The diametrical compression curve was very different from the unconfined uniaxial compression: the force-displacement curve

increased sharply in the beginning and fluctuated after reaching the peak values. While effects of consolidation pressure, particle size on tensile strength were similar to those on crushing strength, the results showed that the tensile strength of the samples was not influenced much by moisture content. The tensile strength of a compact was also much lower than its crushing strength.

Reference

ABDEL-HAMID, S. & BETZ, G. 2011. Study of radial die-wall pressure changes during pharmaceutical powder compaction. *Drug Development and Industrial Pharmacy,* 37**,** 387-395.

ALMAYA, A. & ABURUB, A. 2008. Effect of particle size on compaction of materials with different deformation mechanisms with and without lubricants. *Aaps Pharmscitech,* 9**,** 414-418.

ANTHONY, J. W., BIDEAUX, R. A., BLADH, K. W. & NICHOLS, M. C. 2011. Handbook of Mineralogy, Mineralogical Society of America, Chantilly, VA 20151-1110, USA.

DANA, E. S. & DANA, J. D. 1883. *A text-book of mineralogy: With an extended treatise on crystallography and physical mineralogy,* J. Wiley & sons.

DAVID, S. & AUGSBURGER, L. 1977. Plastic flow during compression of directly compressible fillers and its effect on tablet strength. *Journal of Pharmaceutical Sciences,* 66**,** 155-159.

DLUBEK, G., REDMANN, F. & KRAUSE-REHBERG, R. 2002. Humidity-induced plasticization and antiplasticization of polyamide 6: A positron lifetime study of the local free volume. *applied polymer science,* 84**,** 244 -255.

ENNETI, R. K., LUSIN, A., KUMAR, S., GERMAN, R. M. & ATRE, S. V. 2013. Effects of lubricant on green strength, compressibility and ejection of parts in die compaction process. *Powder Technology,* 233**,** 22-29.

FELL, J. & NEWTON, J. 1970. Determination of tablet strength by the diametral compression test. *Journal of Pharmaceutical Sciences,* 59**,** 688-691.

FELL, J. & NEWTON, J. 1971. Effect of particle size and speed of compaction on density changes in tablets of crystalline and spray dried lactose. *Journal of Pharmaceutical Sciences,* 60**,** 1866-1869.

FREEMAN, R. & FU, X. 2008. Characterisation of powder bulk, dynamic flow and shear properties in relation to die filling. *Powder Metallurgy,* 51**,** 196-201.

FU, X. W., HUCK, D., MAKEIN, L., ARMSTRONG, B., WILLEN, U. & FREEMAN, T. 2012. Effect of particle shape and size on flow properties of lactose powders. *Particuology,* 10**,** 203-208.

GARCIA-FLORES, R., SINGH, G., ERNST, A. & WELGAMA, P. 2011. Medium-term Rail Planning at Rio Tinto Iron Ore.

HARDMAN, J. & LILLEY, B. 1970. Deformation of particles during briquetting. *Nature*

230.12 (1971): 96-96.

HIRAI, Y. & OKADA, J. 1982. Effect of lubricant on die wall friction during the compaction of pharmaceutical powders. *Chemical & Pharmaceutical Bulletin,* 30**,** 684-694.

KATIKANENI, P., UPADRASHTA, S., ROWLINGS, C., NEAU, S. & HILEMAN, G. 1995. Consolidation of ethylcellulose: effect of particle size, press speed, and lubricants. *International journal of pharmaceutics,* 117**,** 13-21.

LI, S. 2008. *Crystallography and Mineralogy*, Geological Publishing House, China.

LINDBERG, N.-O., PÅLSSON, M., PIHL, A.-C., FREEMAN, R., FREEMAN, T., ZETZENER, H. & ENSTAD, G. 2004. Flowability measurements of pharmaceutical powder mixtures with poor flow using five different techniques. *Drug development and industrial pharmacy,* 30**,** 785-791.

MCKAY, A. D., CARSON, L., HULEATT, M., MIEZITIS, Y. & PORRITT, K. 2012. Australia's identified mineral resources 2011. *Canberra: Australian Government*.

MCKENNA, A. & MCCAFFERTY, D. F. 1982. Effect of particle-size on the compaction mechanism and tensile-strength of tablets. *Journal of Pharmacy and Pharmacology,* 34**,** 347-351.

NOR, S., RAHMAN, M., TARLOCHAN, F., SHAHIDA, B. & ARIFFIN, A. 2008. The effect of lubrication in reducing net friction in warm powder compaction process. *Journal of Materials Processing Technology,* 207**,** 118-124.

O'BRIEN, R. 2009. Australia's iron ore product quality-a report on the quality of iron ore resources in Australia. *Geoscience Australia, Onshore Minerals and Energy Division (*http://www.*australianminesatlas.gov.au/mapping/files/australianironorequality.pdf, accessed on 12/2010*.

POQUILLON, D., LEMAITRE, J., BACO-CARLES, V., TAILHADES, P. & LACAZE, J. 2002. Cold compaction of iron powders - relations between powder morphology and mechanical properties Part 1: Powder preparation and compaction. *Powder Technology,* 126**,** 65-74.

POVEROMO, J. 1999. Iron Ores. *The Aise Steel Foundation.(Ed.)* Ironmaking Volume (1999): 547-5XX.

RUE, P. J. & REES, J. E. 1978. Limitations of Heckel relation for predicting powder compaction mechanisms. *Journal of Pharmacy and Pharmacology,* 30**,** 642-643.

SCHULZE, D. 2008. Powders and bulk solids. *Behaviour, Characterization, Storage and*

Flow. Springer.

SEELIG, R. P. 1947. Introduction to seminar - Review of literature on pressing of metal powders. *Transactions of the American Institute of Mining and Metallurgical Engineers,* 171**,** 506-534.

SHANG, C., SINKA, I. C. & PAN, J. 2012. Constitutive model calibration for powder compaction using instrumented die testing. *Experimental Mechanics,* 52**,** 903-916.

SUN, C. C. 2008. Mechanism of moisture induced variations in true density and mechanism of moisture induced variations in true density and. *International Journal of Pharmaceutics,* 346**,** 93–101.

UPPALAPATI, M. & GREEN, D. J. 2005. Effect of external lubricant on mechanical properties of dry pressed green bodies. *Journal of the American Ceramic Society,* 88**,** 1397-1402.

WARD, M. & BILLINGTON, J. 1979. Effect of zinc stearate on apparent density, mixing, and compaction/ejection of iron powder compacts. *Powder Metallurgy,* 22**,** 201-208.

ZHORNYAK, A. & OLIKER, V. 1981. Pressing behavior of atomized iron powders. *Soviet Powder Metallurgy and Metal Ceramics,* 20**,** 323-328.